12-2021

Deep Learning based Prediction of Clogging Occurrences during Lignocellulosic Biomass Feeding in Screw Conveyors

Yang Li
yli199@vols.utk.edu

To the Graduate Council:

I am submitting herewith a thesis written by Yang Li entitled "Deep Learning based Prediction of Clogging Occurrences during Lignocellulosic Biomass Feeding in Screw Conveyors." I have examined the final electronic copy of this thesis for form and content and recommend that it be accepted in partial fulfillment of the requirements for the degree of Master of Science, with a major in Biosystems Engineering Technology.

Nourredine Abdoulmoumine, Major Professor

We have read this thesis and recommend its acceptance:

Nicole Labbé, Hao Gan

Accepted for the Council:
Dixie L. Thompson

Vice Provost and Dean of the Graduate School

(Original signatures are on file with official student records.)

Deep Learning based Prediction of Clogging Occurrences during Lignocellulosic Biomass Feeding in Screw Conveyors

A Thesis Presented for the

Master of Science

Degree

The University of Tennessee, Knoxville

Yang Li

December 2021

DEDICATION

I dedicate my thesis to my wonderful advisor and colleagues, who offered tremendous help and useful advice. I could not have done this without you. Thank you for all your support along the way.

ABSTRACT

Lignocellulosic biomass is a promising and abundant renewable resource for renewable fuels, materials, and energy production in biorefineries. As demonstration biorefineries are developed, several conveyance issues have been documented, including clogging in conveyors, bridging, and ratholing in silos. These issues are significant because they increase downtime and equipment damage and ultimately reduce the material delivery into conversion systems that transform feedstocks into the intermediates products necessary for fuels, materials, and energy production. The roots of the conveyance failure are diverse and include, but are not limited to, limited knowledge of fundamental biomass mechanics, improperly designed systems, and the immense variability in the composition of lignocellulosic biomass processed in biorefineries.

In biorefineries, especially thermochemical biorefineries, screw conveyors are commonly the last conveyance unit operation connected to the conversion reactors. Therefore, any blockage or clogging in this unit becomes an important issue. In this regard, an automated prediction of conveyor clogging occurrences will be highly beneficial to reduce downtime and increase the efficacy of biomass conversion.

This research project seeks to develop a smart solution that combines sensor technology to monitor the performance of the conveyor in real-time by monitoring its current and vibration signals and an artificial intelligence model to predict the imminence of clogging events for responsive control. Through the specific research objectives in this project, we examine the relationship between clogging events and the mechanical dynamics of the motor that powers the screw. The results suggested motor current and

vibration signals offer an effective way to predict clogging events of lignocellulosic biomass particulates as they unfold in screw conveyors. We validated the prediction performance of selected deep learning models by simulating clogging events in a bench-scale screw conveyor. In addition, we provided various scenarios of input datasets to verify the stability and potential of the proposed deep learning models and both models showed similar performances. Then we investigated the effect of moisture content and particle size on clogging events and the performance of the model for predicting the current signals. The results showed the model can predict eminent clogging events over the varying properties evaluated in this study.

KEYWORDS: *Screw conveyor, auger, fault detection, motor failure, correction.*

TABLE OF CONTENTS

LIST OF TABLES

LIST OF FIGURES

CHAPTER I

INTRODUCTION

1.1 Introduction and Problem Statement

Over the last few decades, substantial government and private sector investments have been made to establish a commercial biorefining industry utilizing lignocellulosic biomass as feedstock to produce fuels, materials, and energy. Significant advancements have been made in developing, demonstrating, and deploying lignocellulosic biomass conversion technologies. It has become evident that significant challenges remain in reliably delivering preprocessed lignocellulosic biomass across several unit operations and to the throat of the conversion reactors inside the biorefinery battery limits. As highlighted in the U.S. Department of Energy (DOE) Bioenergy Technology Office (BETO) 2016 Biorefinery Optimization Workshop Summary Report and corroborated by a discussion with industry partners, many nascent biorefineries have operated below their design capacity or experienced delays in start-up due to challenges related to material conveyance into the reactors (Energy, 2016). In their final report, ClearFuels Technology Inc. and Rentech Inc., two early biomass-to-fuel demonstration plants, reported significant material handling issues at their synthetic gas to liquids (GTL) fuel integrated biorefinery located in Commerce City, Colorado (Pearson, 2014). The gasification process development unit (PDU), which was designed for 20 tons per day (TPD) throughput, never reached more than 35 % of the design capacity.

Similarly, the Renewable Energy Institute International reported feedstock handling challenges at their 25 TPD plant to directly produce premium “drop-in” synthetic fuels in Toledo, Ohio (Schuetzle et al., 2015). Conveyance failures in these demonstration projects implied that an estimated 30 % of the capital investment was underutilized since all systems

downstream of the conveyance and conversion systems operate below capacity. Moreover, operating costs are underestimated, while revenue is overestimated as production rates decrease. These factors, cumulatively, have and still can lead to nascent biorefining projects having lower than planned profitability profiles.

The challenges associated with lignocellulosic biomass conveyance into conversion systems are broad and include material flowability and handling problems (Dai & Grace, 2011; Ma et al., 2021; Miccio, Barletta, & Poletto, 2013). Lignocellulosic biomass flowability is governed by complex multiphysics, which, at present, are not well understood because the fundamental mechanics of these materials are not well understood. The definition of biomass multiphysics is referred to the interaction of various physical aspects of the biomass particles (Pannala, Simunovic, & Frantziskonis, 2010). Besides the limited knowledge of the multiphysics of lignocellulosic biomass materials at scales relevant to biorefineries, the complexity and anisotropic nature of these materials and their natural variability render the daunting task of predicting their flow behaviors even more challenging.

In biorefineries, there are many types of conveyance systems for transporting lignocellulosic biomass, including bucket, belt, chain, pneumatic, and screw conveyors. However, screw and belt conveyors are the most general options for biomass transportation. A screw conveyor provides a unique rotating motion while metering the biomass material that helps to mix up or break down particles (Nachenius, Van De Wardt, Ronsse, & Prins, 2015). One or several inlets and outlets are feasible to the screw conveyors depending on specific operation requirements. Additionally, an outstanding feature of a screw conveyor

is the possibility of heating and drying bulk material while conveying, which makes it preferable over a belt conveyor under certain operations (Chamberlin, Carter, & Jacobson, 2018). A belt conveyor is widely utilized in many industries due to its flexibility in metering materials of various sizes (Havey, 1979). Screw conveyors are commonly the last conveyance unit operation connected to the conversion reactors. Their enclosed configuration prevents potential contamination and provides a good seal between interfaces (Nhuchhen, Basu, & Acharya, 2014), which is particularly important in biorefinery operations. In this system, clogging is an important conveyance fault, although others, e.g., mechanical wear (Sievers et al., 2020), also occur. Clogging in the screw conveyor disturbs the granular or particulate flow, causing higher flow resistance and an increase in the motor horsepower (Mysior, Koziołek, & Rusiński, 2018), low feeding rates (L. Wang, Gong, Shi, & Liu, 2010), disturbance in later dryers or reactors (OSMAN, 2012), and other safety issues (Pezo, Jovanović, Pezo, Čolović, & Lončar, 2015).

There are many approaches to mitigate lignocellulosic biomass clogging in screw conveyors, including increasing the dimension of the discharge port (Zhong & O'Callaghan, 1990) or lengthening the conveyor with a longer mixing procedure for a more uniform and less cohesive flow (Hou, Dong, & Yu, 2014). Additionally, twin screw conveyors can be installed either in co-rotating or counter-rotating motion to enhance the flowability (Minglani et al., 2020). If an intermediate bearing is unavoidable, screw conveyor designers have relied on it to reduce the horizontal dimension of the intermediate suspension bearing as much as possible to eliminate the possibility of material blocking when passing through the intermediate bearing (Patel, Patel, & Patel, 2013; Roberts, 2001).

1.2 Research Proposal and Objectives

One promising and unexplored approach is using sensor systems coupled with artificial intelligence to detect clogging events early to support responsive, automated control. This approach is attractive since there is limited first principle-based knowledge of all the factors that will eliminate clogging events. It is also timely because of renewed interest and significant advancements in the development of artificial intelligence applications for engineering process optimization and decision-making.

Thus, in this project, we propose to develop a sensor and deep learning-based approach to detect the occurrence of lignocellulosic biomass clogging events in screw conveyors. Our proposed approach is to leverage the motor current and vibration signatures of a screw conveyor to develop an intelligent clogging detection system capable of detecting clogging events as they occur. The central hypothesis is that auger conveyance status is directly related to the power drawn by the motor driving the screw and the vibration intensity of the connected components of the screw conveyor. If the central hypothesis underpinning this project is supported by the experimental results, we will also endeavor to establish the relationships between the dynamic current and vibration signatures of the system and the conveyance status of the screw conveyor. Additionally, we will evaluate the impact of important properties of lignocellulosic biomass, e.g., moisture content and particle size, on the relationship between dynamic current and vibration signatures and conveyance status. In the end, we expect to develop a strategy for identifying clogging scenarios, which will allow the biorefining industry to monitor their screw conveyance processes easily and

make corrections immediately. The research activities of this project are organized around the following research objectives, questions, and supporting hypotheses.

Objective 1

To examine the relationship between the occurrence of clogging in a benchtop screw conveyor and the current and vibration signals of herbaceous (switchgrass), softwood (loblolly pine), and hardwood (hybrid poplar) feedstocks.

Hypothesis: The current flow in the motor driving a screw conveyor will increase in the event of clogging during switchgrass, loblolly pine, and hybrid poplar feeding. Similarly, the vibration signals of the screw conveyor system will decrease in the event of clogging during switchgrass, loblolly pine, and hybrid poplar feeding.

Research questions, rationale, and justification: There are two research questions associated with this objective and hypothesis: (i) Will the current drawn by the motor driving a screw conveyor show any changes in amplitude in the event of an imminent clogging during switchgrass, loblolly pine, and hybrid poplar feeding? and (ii) Will the vibration of the connected components of the screw conveyor show any changes in amplitude in the event of an imminent clogging during switchgrass, loblolly pine, and hybrid poplar feeding?

The current signature of an induction motor of a screw conveyor is one of the most convenient and most direct diagnostic signals that can be extracted compared to acoustic,

thermal, or vibration signals (Glowacz et al., 2017). We expect a relationship between the current signature of the motor and the performance of the conveyor connected to the motor because the speed of the rotor is greatly affected by the load in the screw conveyor. When the load increases in the screw, the speed of the rotor decreases, which leads to a drop in the revolutions per minute (RPM) of the motor. Generally, for an induction motor, a reduction in RPM indicates that fewer lines of force are being cut between the rotor and the windings of the motor. This phenomenon decreases the voltage produced by the interaction between the armature and the magnetic field in electric motors, which is opposed to the supply voltage. This self-induced voltage is often referred to as counter electromagnetic force (CEMF), which decreases the inductive reactance of the motor. Since the inductive reactance is a type of resistance and the voltage supply is constant, the current signature should theoretically increase based on Ohm's Law.

The vibration signal is another diagnostic signal that is analyzed by researchers for fault diagnostics in mechanical or electromechanical systems, including motors and motor-driven systems (Alameh, Hoblos, & Barakat, 2018; Long et al., 2021; Panigrahy & Chattopadhyay, 2021). Conventionally, an abnormal vibration signal is an indicator of damaged parts inside the motor, including broken bars (Panigrahy & Chattopadhyay, 2021), worn bearings (Z. Yang, Merrild, Runge, Pedersen, & Børsting, 2009), and other rotor related faults (Gandhi, Turk, & Dahiya, 2020; Y. Yang, Liu, Jiang, & Behdinan, 2020). Most rotor-related faults result in an unbalanced rotor that causes an abrupt vibration, and the severity of this unusual conduct is directly reflected by the load (Panigrahy & Chattopadhyay, 2021). The application of vibration analysis for rotor-related fault

diagnostics suggests, by extension, that this same approach could be applicable to biomass screw conveyance fault diagnostics. Screw conveyors, like most moving mechanical systems, have distinct vibration profiles that could potentially be harnessed to gain insights into the operational status of the system. In recent years, the complexity of motor-based conveyor systems has increased, necessitating the use of two or more signals to refine the diagnostic process and provide solutions applicable to various industrial processes (Panigrahy & Chattopadhyay, 2021; Z. Yang et al., 2009). The combination of the current and vibration analysis follows this trend.

Objective 2

To implement deep learning based current and vibration signature analysis approaches to predict the imminent occurrence of clogging in a benchtop screw conveyor during the conveyance of herbaceous (switchgrass), softwood (loblolly pine), and hardwood (hybrid poplar) feedstocks.

Hypothesis: We hypothesize that the current signal drawn from the motor powering the conveyor will be a better input signal than using vibration input signal or current and vibration combined input signal for selected deep learning models for predicting an imminent clogging event. Among two selected deep learning approaches, namely Convolutional Neural Network (CNN) and Gated Recurrent Unit (GRU), GRU will have a better prediction performance over CNN.

Research questions, rationale, and justification: This research objective has two research questions: 1) Which signal is better as the input data for deep learning models to analyze and predict an imminent clogging event? 2) What deep learning-based approach is best suited to predict a clogging event in a screw conveyor?

Biomass particle mechanics is a young but rapidly growing subfield of the general field of granular mechanics. This growth stems from significant biomass flow challenges encountered by early biorefineries (Crawford, Ray, Yancey, & Nagle, 2015; Kumar, Bhardwaj, Agrawal, Chaturvedi, & Verma, 2020). These challenges have prompted researchers, national laboratories, and prominent funding agencies to examine the fundamental mechanics that govern particulate biomass flows. Consequently, at the moment, it is difficult to make predictions on biomass particulate flowability based solely on first principles. With the recent rapid development of data mining, computing power, and new algorithms, machine learning has gradually become a key method for realizing artificial intelligence (AI). AI methods generally treat a process generating data for its analysis as a 'black-box.' Given the lack of fundamental knowledge on particulate mechanics phenomena that affect biomass flow, it is reasonable to treat biomass conveyance systems as black boxes. Following this logic, applying AI-based approaches to biomass conveyance fault detection is compelling for monitoring conveyance health. Deep learning algorithms are more advanced and sophisticated algorithms derived from conventional machine learning. They are widely used in the field of mechanical automation for mechanical structure analysis and strain measurement analysis (Lee, Jo, & Hwang, 2017; Yi Lu, Masrur, ZhiHang, & Baifang, 2006). The main advantages of employing a

deep learning approach instead of machine learning include: more similar "learning" process to the human brain that achieves more flexibility to derive the hierarchy in data (Dong, Wen, Lei, & Zhang, 2020), extraction of distinctive features that eliminates white noise from raw data (Geng, Wang, Jia, Qin, & Chen, 2020), and exceptional performance compared to conventional machine learning with unstructured data, which is the dominant data type in the real world (C. Li, Zhang, Qin, & Estupinan, 2020). Deep learning methods have already been used for motor fault diagnosis, providing early evidence of their applicability to this current research problem (Konar & Chattopadhyay, 2011; Xiang Li, Li, & Ma, 2020; Lu, Li, Ren, & Miao, 2016). Additionally, Convolutional Neural Network (CNN) is proven to be one of the deep learning approaches that have the most potential to tackle motor fault diagnosis (Guo, Zhou, & Zhang, 2021; He, Shao, Zhong, & Zhao, 2020). However, CNN is more frequently connected to examining visual representations such as image recognition and analysis instead of mechanical signals (Ince, Kiranyaz, Eren, Askar, & Gabbouj, 2016; Y. Wang, Zhang, & Zhang, 2019). Yet, Gated Recurrent Unit (GRU) is more applied in long sequences analysis, especially time-series data (Yamak, Yujian, & Gadosey, 2019). Recent studies have developed GRU models for speech recognition (Zhu, Dai, Hu, & Li, 2020), soil moisture prediction (Yu, Zhang, Xu, Dong, & Zhangzhong, 2021), as well as rotating machinery diagnosis (Mao, Zhang, Wang, Chu, & Yuan, 2021; Zhang, Zhou, Huang, Cao, & Zhou, 2021). Since many of the input datasets are time-dependent sequences, this method is potentially more competitive than CNN, considering both current and vibration signals are time series data. Moreover, we previously tested both CNN and GRU models in comparison with multiple machine learning models with the

result of both deep learning models overperformed all machine learning models, thereforem we only present deep learning models in this paper.

Objective 3

To analyze the effect of varying moisture content and particle size distribution on the current signature and vibration signatures and the predictive ability of the deep learning models.

Hypothesis: The deep learning models developed in Objective 2 are robust and will predict imminent clogging occurrences for feedstock with varying moisture contents and particle size distributions without additional training.

Research questions, rationale, and justification: This objective has two research questions: 1) Is there any significant impact of varied feedstock properties (moisture content and particle size distribution) on the current signals and the occurrence of clogging events? 2) Are the deep learning models developed, trained, and optimized in Objective 2 able to predict clogging occurrences on a feedstock with varying moisture contents and particle size distributions?

During biorefinery operations, one of the critical challenges is getting biomass into the reactor without interruption while dealing with variability in the biomass properties (Dai, Cui, & Grace, 2012). The varying properties of biomass directly impact the material flow performance and production efficiency of biorefinery (Cuenca & Anthony, 2012; Cummer & Brown, 2002; XT Li et al., 2004). Generally, size distribution, particle shape, moisture

content, bulk and particle density, compressibility, possible contaminants, and other particle properties such as particle surface roughness and hardness play an important role in biomass conveyance in biorefinery and are frequently considered while designing and operating the feeding systems (Dai et al., 2012; Wu, Schott, & Lodewijks, 2011). However, moisture content and particle size distribution are the two major causes that impede the smooth conveying process in biomass handling (Miao, Grift, Hansen, & Ting, 2014). High moisture increases the cohesiveness of the particulate biomass and increases the potential for bridging, ratholing, and clogging effects, which decrease the flowing tendency in the system (Mattsson, 1990, 1997). On the other hand, biomass materials in biorefineries have irregular shapes and broad distribution of size depending on the type of size reduction equipment such as hammer milling and knife milling (Himmel et al., 1986). This irregularity in sizes and size distribution has a negative impact on material flow because it directly increases the particle-to-particle (internal) and particle-to-wall (external) friction effects (Mattsson, 1990). Therefore, these two properties are suspected of having significant impacts on the occurrence of clogging events and were selected as important properties for the investigation in this objective.

1.3 Organization of the Thesis

In this thesis, the style guide of the American Psychological Association (APA) technical publications will be used in the text as well for the bibliographies. The organization of this thesis is divided into five chapters. Chapter I presents a brief statement of the problem tackled in this project. Further, it also outlines the research proposal, the specific research objectives, and the rationale behind the specific objectives. Chapter II presents background

information on lignocellulosic biomass composition and discusses its potential for renewable energy. This same chapter introduces screw conveyor systems and typical conveyance issues encountered in the biorefinery. Each section in this chapter provides detailed foundational knowledge necessary to grasp the specific problems tackled in this thesis. Chapter III examines the relationship between the conveyor clogging event and the current and vibration signals of a benchtop screw conveyor system for lignocellulosic biomass materials: loblolly pine, switchgrass, and poplar. We first describe our benchtop screw conveyor system and provide a breakdown view on how data flow through this system. We then present our data collection and analysis strategies before discussing our results. In Chapter IV, we present the different statistical and artificial intelligence methodological approaches we will use to develop our clogging recognition system. We first outline all our data processing steps. Then we focus on reviewing other related machine learning models and show how our work is distinguished from other works. In the last section of Chapter IV, a robust deep learning model is constructed to realize the second objective of this thesis and compare the performance of the deep learning model against conventional machine learning models. Chapter V provides a brief description of the variation in lignocellulosic biomass physical characteristics. Then, we vary the moisture content and size distribution of switchgrass and conduct similar analyses in Objective 1 and Objective 2. Using these analyses, we will explore the impact of the feedstock size and the moisture content on the predictive accuracy of the model. These two steps serve to validate the robustness and generalizability of our model over those two parameters.

References

Alameh, K., Hoblos, G., & Barakat, G. (2018). Statistical Vibration-Based Fault Diagnosis Approach Applied To Brushless DC Motors. *IFAC-PapersOnLine, 51*(24), 338-345. doi:https://doi.org/10.1016/j.ifacol.2018.09.599

Chamberlin, C., Carter, D., & Jacobson, A. (2018). Measuring residence time distributions of wood chips in a screw conveyor reactor. *Fuel Processing Technology, 178*, 271-282.

Crawford, N. C., Ray, A. E., Yancey, N. A., & Nagle, N. (2015). Evaluating the pelletization of "pure" and blended lignocellulosic biomass feedstocks. *Fuel Processing Technology, 140*, 46-56.

Cuenca, M. A., & Anthony, E. J. (2012). *Pressurized fluidized bed combustion*: Springer Science & Business Media.

Cummer, K. R., & Brown, R. C. (2002). Ancillary equipment for biomass gasification. *Biomass and Bioenergy, 23*(2), 113-128.

Dai, J., Cui, H., & Grace, J. R. (2012). Biomass feeding for thermochemical reactors. *Progress in Energy and Combustion Science, 38*(5), 716-736. doi:https://doi.org/10.1016/j.pecs.2012.04.002

Dai, J., & Grace, J. R. (2011). Biomass granular screw feeding: An experimental investigation. *Biomass and Bioenergy, 35*(2), 942-955.

Dong, S., Wen, G., Lei, Z., & Zhang, Z. (2020). Transfer learning for bearing performance degradation assessment based on deep hierarchical features. *ISA Transactions*. doi:https://doi.org/10.1016/j.isatra.2020.09.004

Energy, U. D. o. (2016). Biorefinery Optimization Workshop Summary Report. In: Report, Office of Energy Efficiency and Renewable Energy, Bioenergy ….

Gandhi, P., Turk, D. N., & Dahiya, D. R. (2020). Health monitoring of induction motors through embedded systems-simulation of broker rotor bar fault and abnormal gear teeth fault. *Microprocessors and Microsystems, 76*, 103077. doi:https://doi.org/10.1016/j.micpro.2020.103077

Geng, Y., Wang, Z., Jia, L., Qin, Y., & Chen, X. (2020). Bogie fault diagnosis under variable operating conditions based on fast kurtogram and deep residual learning towards imbalanced data. *Measurement, 166*, 108191. doi:https://doi.org/10.1016/j.measurement.2020.108191

Glowacz, A., Glowacz, W., Glowacz, Z., Kozik, J., Gutten, M., Korenciak, D., . . . Carletti, E. (2017). Fault diagnosis of three phase induction motor using current signal, MSAF-Ratio15 and selected classifiers. *Archives of Metallurgy and Materials*.

Guo, Y., Zhou, Y., & Zhang, Z. (2021). Fault diagnosis of multi-channel data by the CNN with the multilinear principal component analysis. *Measurement, 171*, 108513. doi:https://doi.org/10.1016/j.measurement.2020.108513

Havey, C. (1979). Belt conveyors for bulk materials.

He, Z., Shao, H., Zhong, X., & Zhao, X. (2020). Ensemble transfer CNNs driven by multi-channel signals for fault diagnosis of rotating machinery cross working conditions. *Knowledge-Based Systems, 207*, 106396. doi:https://doi.org/10.1016/j.knosys.2020.106396

Himmel, M., Tucker, M., Baker, J., Rivard, C., Oh, K., & Grohmann, K. (1986). *Comminution of biomass: hammer and knife mills.* Paper presented at the Proceedings of the 7th Symposium on Biotechnology for Fuels and Chemicals, Gatlinburg, Tennessee, 14-17 May, 1985.

Hou, Q. F., Dong, K. J., & Yu, A. B. (2014). DEM study of the flow of cohesive particles in a screw feeder. *Powder Technology, 256*, 529-539. doi:https://doi.org/10.1016/j.powtec.2014.01.062

Ince, T., Kiranyaz, S., Eren, L., Askar, M., & Gabbouj, M. (2016). Real-Time Motor Fault Detection by 1-D Convolutional Neural Networks. *IEEE Transactions on Industrial Electronics, 63*(11), 7067-7075. doi:10.1109/TIE.2016.2582729

Konar, P., & Chattopadhyay, P. (2011). Bearing fault detection of induction motor using wavelet and Support Vector Machines (SVMs). *Applied Soft Computing, 11*(6), 4203-4211. doi:https://doi.org/10.1016/j.asoc.2011.03.014

Kumar, B., Bhardwaj, N., Agrawal, K., Chaturvedi, V., & Verma, P. (2020). Current perspective on pretreatment technologies using lignocellulosic biomass: An emerging biorefinery concept. *Fuel Processing Technology, 199*, 106244.

Lee, Y. O., Jo, J., & Hwang, J. (2017, 11-14 Dec. 2017). *Application of deep neural network and generative adversarial network to industrial maintenance: A case study of induction motor fault detection.* Paper presented at the 2017 IEEE International Conference on Big Data (Big Data).

Li, C., Zhang, S., Qin, Y., & Estupinan, E. (2020). A systematic review of deep transfer learning for machinery fault diagnosis. *Neurocomputing, 407*, 121-135. doi:https://doi.org/10.1016/j.neucom.2020.04.045

Li, X., Grace, J., Lim, C., Watkinson, A., Chen, H., & Kim, J. (2004). Biomass gasification in a circulating fluidized bed. *Biomass and Bioenergy, 26*(2), 171-193.

Li, X., Li, X., & Ma, H. (2020). Deep representation clustering-based fault diagnosis method with unsupervised data applied to rotating machinery. *Mechanical Systems and Signal Processing, 143*, 106825. doi:https://doi.org/10.1016/j.ymssp.2020.106825

Long, Z., Zhang, X., Zhang, L., Qin, G., Huang, S., Song, D., . . . Wu, G. (2021). Motor fault diagnosis using attention mechanism and improved adaboost driven by multi-sensor information. *Measurement, 170*, 108718. doi:https://doi.org/10.1016/j.measurement.2020.108718

Lu, N., Li, T., Ren, X., & Miao, H. (2016). A deep learning scheme for motor imagery classification based on restricted boltzmann machines. *IEEE transactions on neural systems and rehabilitation engineering, 25*(6), 566-576.

Ma, C., Christianson, L., Huang, X., Christianson, R., Cooke, R. A., Bhattarai, R., & Li, S. (2021). Efficacy of heated tourmaline in reducing biomass clogging within woodchip bioreactors. *Science of The Total Environment, 755*, 142401.

Mao, X., Zhang, F., Wang, G., Chu, Y., & Yuan, K. (2021). Semi-random subspace with Bi-GRU: Fusing statistical and deep representation features for bearing fault diagnosis. *Measurement, 173*, 108603. doi:https://doi.org/10.1016/j.measurement.2020.108603

Mattsson, J. E. (1990). Basic handling characteristics of wood fuels: angle of repose, friction against surfaces and tendency to bridge for different assortments. *Scandinavian Journal of Forest Research, 5*(1-4), 583-597.

Mattsson, J. E. (1997). Tendency to bridge over openings for chopped Phalaris and straw of Triticum mixed in different proportions with wood chips. *Biomass and Bioenergy, 12*(3), 199-210. doi:https://doi.org/10.1016/S0961-9534(96)00048-7

Miao, Z., Grift, T. E., Hansen, A. C., & Ting, K. C. (2014). Flow performance of ground biomass in a commercial auger. *Powder Technology, 267*, 354-361. doi:https://doi.org/10.1016/j.powtec.2014.07.038

Miccio, F., Barletta, D., & Poletto, M. (2013). Flow properties and arching behavior of biomass particulate solids. *Powder Technology, 235*, 312-321.

Minglani, D., Sharma, A., Pandey, H., Dayal, R., Joshi, J. B., & Subramaniam, S. (2020). A review of granular flow in screw feeders and conveyors. *Powder Technology, 366*, 369-381. doi:https://doi.org/10.1016/j.powtec.2020.02.066

Mysior, M., Koziołek, S., & Rusiński, E. (2018). Problem formulation of screw feeding system of fibrous materials using TRIZ. In *Advances and Impacts of the Theory of Inventive Problem Solving* (pp. 57-64): Springer.

Nachenius, R., Van De Wardt, T., Ronsse, F., & Prins, W. (2015). Residence time distributions of coarse biomass particles in a screw conveyor reactor. *Fuel Processing Technology, 130*, 87-95.

Nhuchhen, D. R., Basu, P., & Acharya, B. (2014). A comprehensive review on biomass torrefaction. *International Journal of Renewable Energy & Biofuels, 2014*, 1-56.

OSMAN, H. B. (2012). *Granular flow and heat transfer in a screw conveyor heater: a discrete element modeling study.*

Panigrahy, P. S., & Chattopadhyay, P. (2021). Tri-axial vibration based collective feature analysis for decent fault classification of VFD fed induction motor. *Measurement, 168*, 108460. doi:https://doi.org/10.1016/j.measurement.2020.108460

Pannala, S., Simunovic, S., & Frantziskonis, G. (2010). Multiscale/Multiphysics Modeling of Biomass Thermochemical Processes. In *Computational Modeling in Lignocellulosic Biofuel Production* (Vol. 1052, pp. 245-271): American Chemical Society.

Patel, J. N., Patel, S. P., & Patel, S. S. (2013). Productivity Improvement of Screw Conveyor by Modified Design. *International Journal of Emerging Technology and Advanced Engineering, 3*(1), 492-496.

Pearson, J. (2014). *ClearFuels-Rentech Integrated Biorefinery Final Report*. Retrieved from

Pezo, L., Jovanović, A., Pezo, M., Čolović, R., & Lončar, B. (2015). Modified screw conveyor-mixers – Discrete element modeling approach. *Advanced Powder Technology, 26*(5), 1391-1399. doi:https://doi.org/10.1016/j.apt.2015.07.016

Roberts, A. W. (2001). Design considerations and performance evaluation of screw conveyors. *Proceedings of the BELTCON, 11*(11), 263-270.

Schuetzle, D., Tamblyn, G., Caldwell, M., Hanbury, O., Schuetzle, R., Rodriguez, R., . . . Struble, D. (2015). *Recovery Act. Demonstration of a Pilot Integrated Biorefinery for the Efficient, Direct Conversion of Biomass to Diesel Fuel*. Retrieved from

Sievers, D. A., Kuhn, E. M., Thompson, V. S., Yancey, N. A., Hoover, A. N., Resch, M. G., & Wolfrum, E. J. (2020). Throughput, reliability, and yields of a pilot-scale conversion process for production of fermentable sugars from lignocellulosic biomass: a study on feedstock ash and moisture. *ACS Sustainable Chemistry & Engineering, 8*(4), 2008-2015.

Wang, L., Gong, G., Shi, H., & Liu, H. (2010). *Rotation and gate movement compound control of screw conveyor hydraulic system with disturbance compensation.* Paper presented at the International Conference on Intelligent Robotics and Applications.

Wang, Y., Zhang, H., & Zhang, G. (2019). cPSO-CNN: An efficient PSO-based algorithm for fine-tuning hyper-parameters of convolutional neural networks. *Swarm and Evolutionary Computation, 49*, 114-123. doi:https://doi.org/10.1016/j.swevo.2019.06.002

Wu, M., Schott, D., & Lodewijks, G. (2011). Physical properties of solid biomass. *Biomass and Bioenergy, 35*(5), 2093-2105.

Yamak, P. T., Yujian, L., & Gadosey, P. K. (2019). *A comparison between arima, lstm, and gru for time series forecasting.* Paper presented at the Proceedings of the 2019 2nd International Conference on Algorithms, Computing and Artificial Intelligence.

Yang, Y., Liu, C., Jiang, D., & Behdinan, K. (2020). Nonlinear vibration signatures for localized fault of rolling element bearing in rotor-bearing-casing system. *International Journal of Mechanical Sciences, 173*, 105449. doi:https://doi.org/10.1016/j.ijmecsci.2020.105449

Yang, Z., Merrild, U. C., Runge, M. T., Pedersen, G., & Børsting, H. (2009). A Study of Rolling-Element Bearing Fault Diagnosis Using Motor's Vibration and Current Signatures. *IFAC Proceedings Volumes, 42*(8), 354-359. doi:https://doi.org/10.3182/20090630-4-ES-2003.00059

Yi Lu, M., Masrur, M. A., ZhiHang, C., & Baifang, Z. (2006). Model-based fault diagnosis in electric drives using machine learning. *IEEE/ASME Transactions on Mechatronics, 11*(3), 290-303. doi:10.1109/TMECH.2006.875568

Yu, J., Zhang, X., Xu, L., Dong, J., & Zhangzhong, L. (2021). A hybrid CNN-GRU model for predicting soil moisture in maize root zone. *Agricultural Water Management, 245*, 106649. doi:https://doi.org/10.1016/j.agwat.2020.106649

Zhang, Y., Zhou, T., Huang, X., Cao, L., & Zhou, Q. (2021). Fault diagnosis of rotating machinery based on recurrent neural networks. *Measurement, 171*, 108774. doi:https://doi.org/10.1016/j.measurement.2020.108774

Zhong, Z., & O'Callaghan, J. (1990). The effect of the shape of the feed opening on the performance of a horizontal screw conveyor. *Journal of Agricultural Engineering Research, 46*, 125-128.

Zhu, Z., Dai, W., Hu, Y., & Li, J. (2020). Speech emotion recognition model based on Bi-GRU and Focal Loss. *Pattern Recognition Letters, 140*, 358-365. doi:https://doi.org/10.1016/j.patrec.2020.11.009

CHAPTER II

BACKGROUND

Abstract

Over the last decades, there have been substantial government and private sector investments to establish a commercial biorefining industry that uses lignocellulosic biomass as feedstock to produce fuels, chemicals, and other products. However, several biorefining plants experienced material conveyance problems due to the variability and complexity of the biomass feedstock. While the problems were reported in most conveyance unit operations in the biorefining plants, screw conveyors merit special attention because they are the most common conveyors used in biomass conveyance and typically function as the last conveyance unit connected to the conversion reactors. Thus, their operating status affects the plant production rate. Therefore, detecting emerging clogging events and, ultimately, proactively adjusting operating conditions to avoid downtime is crucial to improving overall plant economics. One promising solution is the development of sensor systems to detect clogging to support automated decision-making and process control.

2.1 Introduction

At present, the world is heavily dependent on fossil fuels, including non-renewable energy sources such as petroleum oil and natural gas. In addition to the fact that such resources are being consumed more rapidly than they can regenerate, the consumption of fossil fuels also leads to greenhouse gas (GHGs) emissions, e.g., CO_2, CH_4, and N_2O (Hitchon, Gunter, Gentzis, & Bailey, 1999). In 2008, the IPCC Fourth Assessment Report *"Climate Change 2007*" has identified CO_2 as the most troubling anthropogenic GHG and accounted for

approximately 77% of the total GHG emissions (Pachauri & Reisinger, 2008). Besides the fact that CO_2 contributes to global warming (Norby & Luo, 2004), burning fossil fuels also releases huge amounts of aerosols (Liu et al., 2021), such as sulfides (Brühl, Lelieveld, Crutzen, Tost, & Stier, 2012), which cools the ground by blocking sunlight.

There are many potential renewable energy sources. However, biomass is the only renewable energy source that can substitute for chemicals or petroleum (Ibarra-Gonzalez & Rong, 2019; Owusu & Asumadu-Sarkodie, 2016). Other renewable energy sources, such as solar, wind, hydropower, and nuclear energy, are all non-carbon-based fuels and are mainly used for heat and electricity (Owusu & Asumadu-Sarkodie, 2016). Since the industrial revolution, the world has relied heavily on carbon-containing fossil fuels such as petroleum oil, natural gas, and coal for transportation fuel production and the manufacture of numerous everyday materials and products. Unlike fossil fuels, which are generated over centuries and are thus not renewable, biomass is synthesized photosynthetically from carbon dioxide and is an attractive CO_2 neutral and renewable alternative for fossil fuels (Field, Campbell, & Lobell, 2008; Jaiswal, Dutta, Banerjee, Pohrmen, & Kumar, 2021; Klass, 1998).

The exploitation of biomass as an energy source for humankind can trace back millennia ago when humans burned or consumed it as fuel or food (McKendry, 2002). However, the utilization of biomass for renewable energy production has been relatively recent and dramatically increased over the last hundred years (Field et al., 2008). In 2007, the Energy Information Administration (EIA) reported that only 3.7% of total energy consumption in the US comes from biomass energy. In 2020, the energy consumption that

using biomass has increased to approximately 5% of total primary energy consumption in the US by EIA. However, biomass-based energy production continued to grow in the renewable energy field and accounted for about 53% of total renewable energy consumption in 2007 (Payne, 2011). In recent years, the global demand for energy crops increased tremendously, which means many countries are enlarging their renewable energy production (Langholtz, Stokes, & Eaton, 2016). In the United States, the Renewable Fuel Standard (RFS) program was launched from the Energy Policy Act of 2005 that requires a minimum amount of renewable fuels to reduce GHGs emissions and the amount of petroleum-based transportation fuels. A minimum amount of renewable fuels must be added to the normal use of petroleum fuels to reduce GHGs emissions and the use of non-renewable energy. Moreover, to phase in the use of renewable fuels, the Energy Independence and Security Act of 2007 (EISA) expanded renewable energy standards. The standards scale up the use of renewable energy and increase mandatory biofuel production to 36 billion gallons; A maximum of 15 billion gallons of corn-based bioethanol can be produced, while cellulosic biofuels are required to produce a minimum of 16 billion gallons.

Conveyance systems have become an indispensable part of the mechanization and automation of the material handling system, including bulk biomass material transport in biorefineries (Garcia-Nunez et al., 2016; Kamm, Hille, Schönicke, & Dautzenberg, 2010; Amit Kumar & Sokhansanj, 2007; Nitzsche, Budzinski, & Gröngröft, 2016). For metering particulate materials such as biomass particles, belt conveyor and screw conveyors are the most general types of machinery employed. Belt conveyors are favored because of advantages like low cost (Grujić & Erdeljan, 2014; Lieberwirth, 1994), low maintenance

(Jeftenić, Ristić, Bebić, & Štatkić, 2009), large capacity (Król, Kisielewski, Kaszuba, & Gładysiewicz, 2017), and flexible to topographic condition (Wang & Zhigang, 2012). On the other hand, screw conveyors offer not only similar benefits such as low cost (Chang & Steele, 1997; Hu, Chen, Jian, Wan, & Liu, 2010) and low maintenance (Hu et al., 2010), but also provide additional benefits like minimized environmental pollution and material contamination (Wable & Kurkute, 2015), which makes it preferable for conveying grain and feed (Chang & Steele, 1997), bulk material (Roberts, 2015), and especially dusty material with high volatility (Wable & Kurkute, 2015) such as refined lignocellulosic biomass (Sievers, Kuhn, Stickel, Tucker, & Wolfrum, 2016; Sievers & Stickel, 2018). Screw conveyors are also known as auger screw conveyors (Ye, Wang, Yu, Luo, & Cen, 2018), rotating screw conveyors (Nachenius, Van De Wardt, Ronsse, & Prins, 2015), or pitch spiral conveyors (Jiang et al., 2013). This type of conveyor is suitable and versatile for horizontal transport (Nachenius et al., 2015), incline transport (McDonough et al., 2011), or vertical transport (Owen & Cleary, 2009) of granular, powdery, and small materials. Screw conveyor is widely used in all walks of life because of its simple structure and convenient intermediate loading and unloading (McClaren, 1982). In the process of conveying materials, it can also be used for mixing (Pezo, Jovanović, Pezo, Čolović, & Lončar, 2015a), heating (Nachenius et al., 2015), and cooling (Hain, Wulff, & Stacheter, 1981) the materials. Blockage or clogging is a common and serious operational problem in lignocellulosic biomass conveyance (Dai & Grace, 2011). Generally, a clogging event is mainly created by the bridging effect take place at the outlet of the screw conveyor (Dai, 2007; Dai, Cui, & Grace, 2012; Dai & Grace, 2008). The occurrence of the bridging effect

creates a “net” of the biomass material and blocks the effluent feed, which eventually generates a compacted plug as the finalized blockage (Dai, 2007; Dai & Grace, 2008).

In recent years, research efforts on smart process control have been intensified, especially in machinery fault diagnosis based on artificial intelligence (Carbonell, Michalski, & Mitchell, 1983; Filippetti, Franceschini, Tassoni, & Vas, 2000). Based on the developing computation capacity of artificial intelligence and machine learning, the machinery fault diagnosis system needs not only strong learning ability for computers, but also algorithms that flexibly match the characteristics of the mechanical application system and combine with strong operational and maintenance fault handling experience (Awadallah & Morcos, 2003; Siddique, Yadava, & Singh, 2003). Through a continuous and iterative learning process, the fault diagnosis system based on artificial intelligence is realized to improve the identification of the overall operation and maintenance failure rate and fully realize automatic processing (Siddique et al., 2003). The achievement is fundamentally based on the application architecture design (Awadallah & Morcos, 2003), knowledge base data acquisition (Peters, 2008), data preprocessing (Parnandi, Wade, & Matarić, 2010), operational instance modeling (Martin-Diaz, Morinigo-Sotelo, Duque-Perez, & Romero-Troncoso, 2018), dependent variable and independent variable filtering (Sun, Zhao, Yan, Shao, & Chen, 2017; Wu, Gao, Hong, & Gao, 2008), fault identification library establishment and process automation (Ishibashi, Han, & Kawai, 2017; Kankar, Sharma, & Harsha, 2011).

2.1.1 Lignocellulosic Biomass

Lignocellulosic biomass is one of the most abundant biomass resources on the earth and is mainly composed of cellulose, hemicellulose, and lignin with 30-50, 20-40, and 15-25% on a dry, extractive free basis, respectively (Fengel & Wegener, 2011). Figure 2-1 shows some typical lignocellulosic biomass materials.

In addition, lignocellulosic biomass contains small amounts of extractives as well as structural proteins, lipids, and ash (Fengel & Wegener, 2011). Cellulose is a homogenous linear polymer with an ether linkage between C_1 and C_4 of connecting glucose monomers with β stereochemistry as shown in Figure 2-2. This ether linkage is hence called β-(1,4)-glycosidic bond (Fengel & Wegener, 2011; Hendriks & Zeeman, 2009). Cellulose fibers interact with each other and other biomass constituents through hydrogen bonds and can form crystalline and amorphous regions. The ratio between the materials in the crystalline and amorphous regions is defined as the crystallinity of cellulose, which is an important parameter to characterize cellulose properties. Higher crystallinity reflects better dimensional stability, material strength, and heat resistance.

Hemicellulose is a heteropolysaccharide composed of different types of monosaccharides, including five and six-carbon sugars, with the proportion of xylan being approximately 50% for all types of biomass materials. Hemicellulose runs through the cellulose fibers and lignin and acts a bridge connecting the two polymers polymers (Xu, Yu, Tesso, Dowell, & Wang, 2013). Lignin is an amorphous aromatic heteropolymer formed through radical polymerization coupling of 4-hydroxycinnamyl alcohol monomers, primarily through endwise coupling (Ralph, Lapierre, & Boerjan, 2019). The aromatic

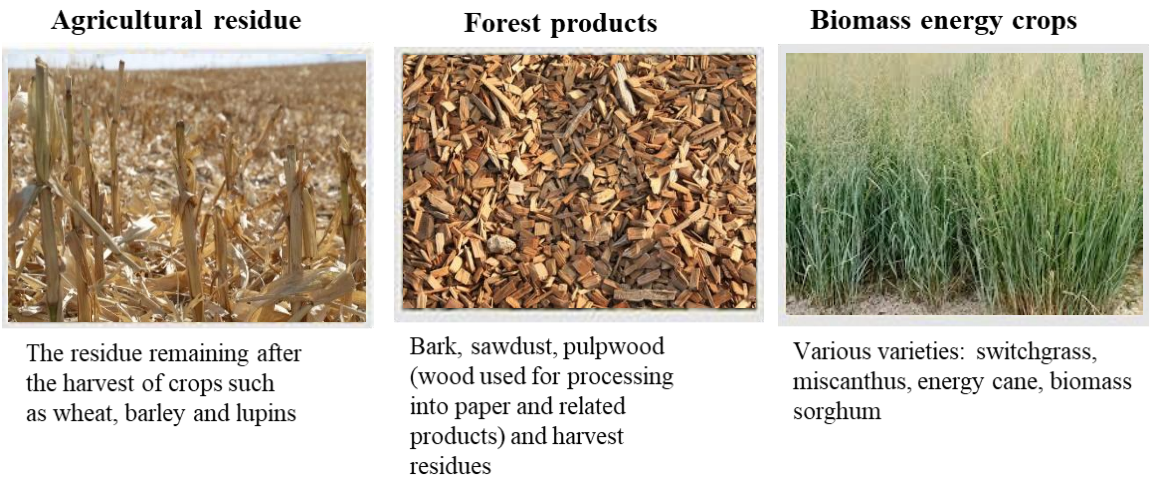

Figure 2-1. Typical lignocellulosic biomass (Balin, 2020; Rinkesh).

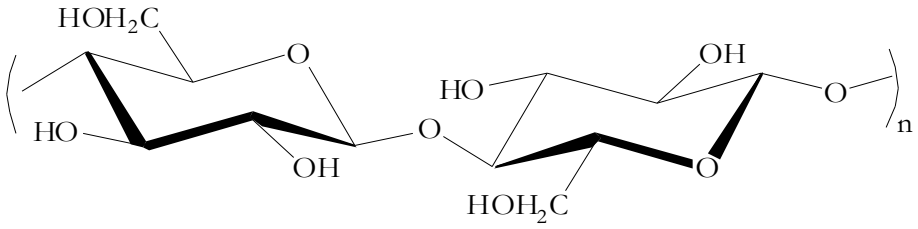

Figure 2-2. The repeat unit of cellulose, cellobiose, is repeated n^{th} time in the cellulose polymer. Cellobiose is made of two glucose units linked through $\beta 1-4$ glycosidic bond.

units of lignin are further classified into three groups: p-hydroxyphenyl (H), guaiacyl (G), and syringyl (S), depending on the level of methoxylation at the C_3 and C_5 positions[59] as shown in Figure 2-3.

Lignin is dispersed between cellulose fibers and provides compressive resistance (Ghaffar & Fan, 2013; Renders, Van den Bosch, Koelewijn, Schutyser, & Sels, 2017). Combined, cellulose, hemicellulose, and lignin play distinctive structural roles that create a unique structure. This lignocellulosic biomass structure results from natural selection in the long-term evolution of plants and provides resistance to both biological and non-biological agents for protection (Xu, Shi, & Wang, 2013; Xu, Yu, et al., 2013).

As previously mentioned, lignocellulosic biomass contains a variety of structural units such as five-carbon sugar, six-carbon sugar, and aromatic compounds. Cellulose and hemicellulose are high molecular polymers connected by glycoside bonds, while lignin is a three-dimensional biological macromolecule composed of many benzene rings. Hemicellulose and lignin are covalently linked to form a network structure in which cellulose is embedded, resulting in high tensile and mechanical strength in lignocellulose biomass. The tensile and mechanical strengths are material properties that play important roles in granular mechanics and, thus, affect the lignocellulosic biomass particulate flow. However, the relationship between biomass composition and structure and their roles on the mechanical properties that dictate flow are not well understood.

Lignocellulosic biomass has garnered significant attention in the last several decades because of the possibility of using it as renewable feedstock to produce alternative products currently delivered by fossil fuels such as petroleum and coal. The chemical diversity

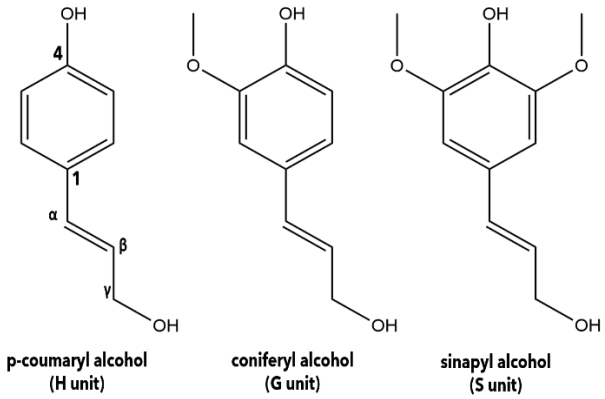

Figure 2-3. Chemical structures of the building blocks of native lignin.

of lignocellulosic biomass structural components makes it possible to produce a wide array of products, including combined heat and power (CHP), liquid transportation fuels, and commodity chemicals. These product groups can be obtained through two technology platforms: the thermochemical technology platform and the biochemical technology (Anil Kumar, Kumar, Baredar, & Shukla, 2015). The thermochemical technology platform involves three central processes, which are combustion, gasification, and pyrolysis. Using these processes, raw renewable materials, e.g., lignocellulosic biomass, are converted into gaseous, liquid, and solid intermediate products, which can be utilized to produce CHP, liquid transportation fuels, or chemicals (Anil Kumar et al., 2015).

2.1.2 Bulk Handling in Lignocellulosic Biorefineries

A lignocellulosic biorefinery is defined as a facility that integrates biomass conversion processes and equipment to produce CHP, fuels, and value-added chemicals from lignocellulosic biomass. The term biorefinery emerged to emphasize the analogy between integrated facilities that process lignocellulosic biomass into various products and petroleum refineries, which also produce various products except for crude petroleum. Like industrial facilities that handle solid feeds, lignocellulosic biorefineries rely heavily on conventional bulk solid handling systems to hold, discharge, and convey biomass particulates throughout the plant. Bulk solid handling systems include about 80 different types of conveyors for bulk transport according to the Conveyor Equipment Manufacturers Association (CEMA), including the most common and frequently used ones, such as belt, screw, chain, and vibratory conveyors (Waje, Thorat, & Mujumdar, 2007). Additionally, bulk handling systems include bins, silos, and hoppers for holding and dispensing solid

materials. In the context of the lignocellulosic biorefinery, other bulk handling systems include communication or size reduction, screening, filtering, and solid separation systems.

The reliable and consistent operations of bulk handling systems have been recognized as a trouble area in early biorefining demonstration facilities. Specific challenges associated with bulk handling include unexpected equipment wear due to high ash and other contaminants, ratholing, bridging, and suboptimal feeding rates. Ratholing is an effect that some of the feeding materials form into a narrower channel above the outlet hopper while the remaining material maintain stationary against the hopper wall. Bridging is a case that the material forms into a bridge or arch based on the edges of the discharge point and blocks incoming materials. Both effects have the result in the materials not flowing as desired. These challenges collectively result in lower throughput rates, often far below the biorefinery plant design throughput, and increased capital and operating costs due to the need for frequent shutdown and equipment replacement. While challenges have been reported with all bulk handling systems in biorefineries, challenges associated with screw conveyors deserves special attention because:

- They are widely used in both biochemical and thermochemical biorefineries as well as other in agricultural (grain transport), biological (pharmaceutical powder and pellet transport) or chemical (catalyst and solid residue transport) industries because of their simpler design and structure, the possibility of designing them with good sealing thereby enabling the introduction of fluids in the housing, their low cost, their convenient loading and unloading characteristics, and the ability to blend materials (Dai & Grace, 2011);

- They are the most typical bulk transport system connected to conversion reactors and, consequently, their failure or suboptimal performance has an outsized impact on the biorefinery plant operations;
- They are closed systems and, thus, it is difficult to notice and detect suboptimal operations;
- They are commonly motor-driven and present unique safety concerns if biomass material accumulates without detection, especially given their proximity to conversion reactors, often operated at high temperature and pressure. The blockage or clogging phenomenon not only affects the conveyance efficiency or electricity consumption but more seriously, can cause motor burnout, explosion, mangle the shaft, and other industrial accidents (Dai & Grace, 2011).

Screw conveyors, or auger conveyors, have been the workhorse of bulk solid transport for decades. They can be divided into two types: shafted and shaftless screw conveyors. The working principle of the screw conveyor is the rotation of the screw shaft with spiral blades to push the substances that are relative to the conveyor surface. The material rotates with the screw by friction from the inner surface of the screw conveyor housing, which pushes the material forward axially while simultaneously accomplishing metering. Screw conveyors are divided into the horizontal screw conveyor and the vertical screw conveyor, which are mainly used for horizontal transportation and vertical lifting of various loose materials such as powder, particle, and small blocks. In the horizontal screw conveyor, the friction force is caused by the gravity of the material; and in the vertical spiral conveyer,

the friction is due to the centrifugal force of material rotation. The screw conveyor has several advantages over the belt conveyor, the second most common conveyor in bulk solid transport according to CEMA. The advantages of a screw conveyor include the capability for conveying various bulk materials from a sluggish to a quick flow, a no return section compared to the belt conveyor, and an enclosed environment that eliminates contamination and prevents spillage and losses. However, several disadvantages such as wearing issues, transport capacity decline with the conveyor angle of inclination, and blockage in the conveyor can significantly affect the performance of the screw conveyor (Owen & Cleary, 2009).

2.1.3 Clogging in Screw Conveyor

Despite all its advantages, screw conveyors have shortcomings. For example, they are more prone to faults or suboptimal operations when transporting materials that are cohesive or sticky, highly compressible, lumpy, fibrous, or stringy, and susceptible to deterioration. These material characteristics, many associated with lignocellulosic biomass particulates, and the small conveyance space are some of the causes of the development of clogging or jamming in screw conveyors. These conditions make it easy to produce particle-particle entanglements when the screw shaft rotates, which leads to gradual agglomeration and the development of a clog which ultimately results in a blockage that impedes bulk flow. Figure 2-4 shows the final stage of the process described earlier.

Clogging in screw conveyors has been recognized as an important challenge. Although comprehensive studies focused on elucidating this phenomenon are not available at the moment, few researchers have tangentially investigated the phenomena and mitigation

strategies. Lato et al. (Pezo, Jovanović, Pezo, Čolović, & Lončar, 2015b) implemented a discrete element modeling (DEM) approach to identify a method for reducing the blockage occurrences induced by interparticle cohesion. The main idea was to improve the mixing quality and homogeneity by inserting an additional screw or spiral strip on the periphery of the screw before entering the main mixer in the same or opposite direction of the material flow. Bowens et al. (Bowens, Owoc, & Hendrick, 2003) invented a new wear-resistant extruder screw which includes a base alloy body with a plurality of flights, a major outer diameter, and a minor inner diameter. Three coating layers on a significant portion of the screw body could provide sufficient wear resistance. The efficiency of screw conveyance decreases when the conveying angle increases. The capacity in the auger reduces to 70% and 45% while inclination is 15° and 25° (Bucklin, Thompson, Montross, & Abdel-Hadi, 2013). Shimizu et al. (Shimizu & Cundall, 2001) simulated the horizontal and vertical screw conveyor configuration at the initial and final stages. However, the modeling operation employed the number of particles as variability and excluded different inclinations.

Figure 2-4. Clogging event for lignocellulosic biomass in a bench-scale reactor.

References

Awadallah, M. A., & Morcos, M. M. (2003). Application of AI tools in fault diagnosis of electrical machines and drives-an overview. *IEEE Transactions on Energy Conversion, 18*(2), 245-251.

Balin, E. (2020). Soil experts recommend leaving crop residue in their fields. Retrieved from https://starherald.com/agriculture/soil-experts-recommend-leaving-crop-residue-in-their-fields/article_ee22864d-3a4b-5c98-8976-01ba8d4493ca.html

Bowens, S. H., Owoc, A. L., & Hendrick, A. A. (2003). Wear Resistant Extruder Screw. In: Google Patents.

Brühl, C., Lelieveld, J., Crutzen, P., Tost, H., & Stier, P. (2012). The role of carbonyl sulphide as a source of stratospheric sulphate aerosol and its impact on climate. *Atmospheric Chemistry & Physics, 12*(3).

Bucklin, R., Thompson, S., Montross, M., & Abdel-Hadi, A. (2013). Chapter 7 - Grain Storage Systems Design. In M. Kutz (Ed.), *Handbook of Farm, Dairy and Food Machinery Engineering (Second Edition)* (pp. 123-175). San Diego: Academic Press.

Carbonell, J. G., Michalski, R. S., & Mitchell, T. M. (1983). An overview of machine learning. In *Machine learning* (pp. 3-23): Elsevier.

Chang, C., & Steele, J. (1997). Performance characteristics of the inlet section of a screw conveyor. *Applied Engineering in Agriculture, 13*(5), 627-630.

Dai, J. (2007). *Biomass granular feeding for gasification and combustion.* University of British Columbia,

Dai, J., Cui, H., & Grace, J. R. (2012). Biomass feeding for thermochemical reactors. *Progress in Energy and Combustion Science, 38*(5), 716-736. doi:https://doi.org/10.1016/j.pecs.2012.04.002

Dai, J., & Grace, J. R. (2008). Biomass screw feeding with tapered and extended sections. *Powder Technology, 186*(1), 56-64. doi:https://doi.org/10.1016/j.powtec.2007.10.033

Dai, J., & Grace, J. R. (2011). Biomass granular screw feeding: An experimental investigation. *Biomass and Bioenergy, 35*(2), 942-955. doi:https://doi.org/10.1016/j.biombioe.2010.11.026

Fengel, D., & Wegener, G. (2011). *Wood: chemistry, ultrastructure, reactions*: Walter de Gruyter.

Field, C. B., Campbell, J. E., & Lobell, D. B. (2008). Biomass energy: the scale of the potential resource. *Trends in Ecology & Evolution, 23*(2), 65-72. doi:https://doi.org/10.1016/j.tree.2007.12.001

Filippetti, F., Franceschini, G., Tassoni, C., & Vas, P. (2000). Recent developments of induction motor drives fault diagnosis using AI techniques. *IEEE Transactions on Industrial Electronics, 47*(5), 994-1004.

Garcia-Nunez, J. A., Rodriguez, D. T., Fontanilla, C. A., Ramirez, N. E., Lora, E. E. S., Frear, C. S., . . . Garcia-Perez, M. (2016). Evaluation of alternatives for the evolution of palm oil mills into biorefineries. *Biomass and Bioenergy, 95*, 310-329.

Ghaffar, S. H., & Fan, M. (2013). Structural analysis for lignin characteristics in biomass straw. *Biomass and Bioenergy, 57*, 264-279.

Grujić, M., & Erdeljan, D. (2014). *Advantages of high angle belt conveyors (hac) in mining.* Paper presented at the Applied Mechanics and Materials.

Hain, G., Wulff, B., & Stacheter, J. (1981). Device for washing and cooling the granulate of cottage cheese, curd or the like. In: Google Patents.

Hendriks, A. T. W. M., & Zeeman, G. (2009). Pretreatments to enhance the digestibility of lignocellulosic biomass. *Bioresource Technology, 100*(1), 10-18. doi:https://doi.org/10.1016/j.biortech.2008.05.027

Hitchon, B., Gunter, W., Gentzis, T., & Bailey, R. (1999). Sedimentary basins and greenhouse gases: a serendipitous association. *Energy Conversion and Management, 40*(8), 825-843.

Hu, G., Chen, J., Jian, B., Wan, H., & Liu, L. (2010). *Modeling and simulation of transportation system of screw conveyors by the discrete element method.* Paper presented at the 2010 International Conference on Mechanic Automation and Control Engineering.

Ibarra-Gonzalez, P., & Rong, B.-G. (2019). A review of the current state of biofuels production from lignocellulosic biomass using thermochemical conversion routes. *Chinese Journal of Chemical Engineering, 27*(7), 1523-1535. doi:https://doi.org/10.1016/j.cjche.2018.09.018

Ishibashi, T., Han, B., & Kawai, T. (2017). *Rotating machinery library for diagnosis.* Paper presented at the Proceedings of the 12th International Modelica Conference, Prague, Czech Republic, May 15-17, 2017.

Jaiswal, K. K., Dutta, S., Banerjee, I., Pohrmen, C. B., & Kumar, V. (2021). Photosynthetic microalgae–based carbon sequestration and generation of biomass in biorefinery approach for renewable biofuels for a cleaner environment. *Biomass Conversion and Biorefinery*, 1-19.

Jeftenić, B., Ristić, L., Bebić, M., & Štatkić, S. (2009). *Controlled induction motor drives supplied by frequency converters on belt conveyors—Modeling and commissioning.* Paper presented at the 2009 35th Annual Conference of IEEE Industrial Electronics.

Jiang, E., Su, X., Wang, M., Xiong, L., Zhao, C., & Xu, X. (2013). Design of variable pitch spiral conveyor for biomass continual pyrolysis reactor. *Nongye Jixie Xuebao= Transactions of the Chinese Society for Agricultural Machinery, 44*(2), 121-124.

Kamm, B., Hille, C., Schönicke, P., & Dautzenberg, G. (2010). Green biorefinery demonstration plant in Havelland (Germany). *Biofuels, Bioproducts and Biorefining: Innovation for a sustainable economy, 4*(3), 253-262.

Kankar, P. K., Sharma, S. C., & Harsha, S. P. (2011). Fault diagnosis of ball bearings using machine learning methods. *Expert Systems with Applications, 38*(3), 1876-1886. doi:https://doi.org/10.1016/j.eswa.2010.07.119

Klass, D. L. (1998). *Biomass for renewable energy, fuels, and chemicals*: Elsevier.

Król, R., Kisielewski, W., Kaszuba, D., & Gładysiewicz, L. (2017). Testing belt conveyor resistance to motion in underground mine conditions. *International Journal of Mining, Reclamation and Environment, 31*(1), 78-90.

Kumar, A., Kumar, N., Baredar, P., & Shukla, A. (2015). A review on biomass energy resources, potential, conversion and policy in India. *Renewable and Sustainable Energy Reviews, 45*, 530-539. doi:https://doi.org/10.1016/j.rser.2015.02.007

Kumar, A., & Sokhansanj, S. (2007). Switchgrass (Panicum vigratum, L.) delivery to a biorefinery using integrated biomass supply analysis and logistics (IBSAL) model. *Bioresource Technology, 98*(5), 1033-1044.

Langholtz, M., Stokes, B., & Eaton, L. (2016). 2016 Billion-ton report: Advancing domestic resources for a thriving bioeconomy, Volume 1: Economic availability of feedstock. *Oak Ridge National Laboratory, Oak Ridge, Tennessee, managed by UT-Battelle, LLC for the US Department of Energy, 2016*, 1-411.

Lieberwirth, H. (1994). Economic advantages of belt conveying in open-pit mining. In *Mining Latin America/Minería Latinoamericana* (pp. 279-295): Springer.

Liu, H., Wang, Q., Xing, L., Zhang, Y., Zhang, T., Ran, W., & Cao, J. (2021). Measurement report: quantifying source contribution of fossil fuels and biomass-burning black carbon aerosol in the southeastern margin of the Tibetan Plateau. *Atmospheric Chemistry and Physics, 21*(2), 973-987.

Martin-Diaz, I., Morinigo-Sotelo, D., Duque-Perez, O., & Romero-Troncoso, R. J. (2018). An experimental comparative evaluation of machine learning techniques for motor fault diagnosis under various operating conditions. *IEEE Transactions on Industry Applications, 54*(3), 2215-2224.

McClaren, J. L. (1982). Grain bin and truck loading and unloading system. In: Google Patents.

McDonough, M. X., Campabadal, C. A., Mason, L. J., Maier, D. E., Denvir, A., & Woloshuk, C. (2011). Ozone application in a modified screw conveyor to treat grain for insect pests, fungal contaminants, and mycotoxins. *Journal of Stored Products Research, 47*(3), 249-254.

McKendry, P. (2002). Energy production from biomass (part 1): overview of biomass. *Bioresource Technology, 83*(1), 37-46. doi:https://doi.org/10.1016/S0960-8524(01)00118-3

Nachenius, R., Van De Wardt, T., Ronsse, F., & Prins, W. (2015). Residence time distributions of coarse biomass particles in a screw conveyor reactor. *Fuel Processing Technology, 130*, 87-95.

Nitzsche, R., Budzinski, M., & Gröngröft, A. (2016). Techno-economic assessment of a wood-based biorefinery concept for the production of polymer-grade ethylene, organosolv lignin and fuel. *Bioresource Technology, 200*, 928-939.

Norby, R. J., & Luo, Y. (2004). Evaluating ecosystem responses to rising atmospheric CO2 and global warming in a multi-factor world. *New phytologist, 162*(2), 281-293.

Owen, P., & Cleary, P. (2009). Prediction of screw conveyor performance using the Discrete Element Method (DEM). *Powder Technology, 193*(3), 274-288.

Owusu, P. A., & Asumadu-Sarkodie, S. (2016). A review of renewable energy sources, sustainability issues and climate change mitigation. *Cogent Engineering, 3*(1), 1167990.

Pachauri, R., & Reisinger, A. (2008). Climate change 2007. Synthesis report. Contribution of Working Groups I, II and III to the fourth assessment report. *Cambridge University Press, Cambridge*.

Parnandi, A., Wade, E., & Matarić, M. (2010). *Motor function assessment using wearable inertial sensors.* Paper presented at the 2010 Annual International Conference of the IEEE Engineering in Medicine and Biology.

Payne, J. E. (2011). On Biomass Energy Consumption and Real Output in the US. *Energy Sources, Part B: Economics, Planning, and Policy, 6*(1), 47-52. doi:10.1080/15567240903160906

Peters, J. (2008). Machine learning for motor skills in robotics. *KI-Künstliche Intelligenz, 2008*(4), 41-43.

Pezo, L., Jovanović, A., Pezo, M., Čolović, R., & Lončar, B. (2015a). Modified screw conveyor-mixers–Discrete element modeling approach. *Advanced Powder Technology, 26*(5), 1391-1399.

Pezo, L., Jovanović, A., Pezo, M., Čolović, R., & Lončar, B. (2015b). Modified screw conveyor-mixers – Discrete element modeling approach. *Advanced Powder Technology, 26*(5), 1391-1399. doi:https://doi.org/10.1016/j.apt.2015.07.016

Ralph, J., Lapierre, C., & Boerjan, W. (2019). Lignin structure and its engineering. *Current opinion in biotechnology, 56*, 240-249.

Renders, T., Van den Bosch, S., Koelewijn, S.-F., Schutyser, W., & Sels, B. (2017). Lignin-first biomass fractionation: the advent of active stabilisation strategies. *Energy & environmental science, 10*(7), 1551-1557.

Rinkesh. What is Biomass Energy? Retrieved from https://www.conserve-energy-future.com/biomassenergy.php

Roberts, A. W. (2015). Bulk solids: optimizing screw conveyors. *Chemical engineering, 122*(2), 62.

Shimizu, Y., & Cundall, P. A. J. J. o. e. m. (2001). Three-dimensional DEM Simulations of Bulk Handling by Screw Conveyors. *127*(9), 864-872.

Siddique, A., Yadava, G., & Singh, B. (2003). *Applications of artificial intelligence techniques for induction machine stator fault diagnostics.* Paper presented at the 4th IEEE International Symposium on Diagnostics for Electric Machines, Power Electronics and Drives, 2003. SDEMPED 2003.

Sievers, D. A., Kuhn, E. M., Stickel, J. J., Tucker, M. P., & Wolfrum, E. J. (2016). Online residence time distribution measurement of thermochemical biomass pretreatment reactors. *Chemical Engineering Science, 140*, 330-336.

Sievers, D. A., & Stickel, J. J. (2018). Modeling residence-time distribution in horizontal screw hydrolysis reactors. *Chemical Engineering Science, 175*, 396-404.

Sun, W., Zhao, R., Yan, R., Shao, S., & Chen, X. (2017). Convolutional discriminative feature learning for induction motor fault diagnosis. *IEEE Transactions on Industrial Informatics, 13*(3), 1350-1359.

Wable, M. M., & Kurkute, V. K. (2015). Design and Analysis of Screw Conveyor at Inlet of Ash/Dust Conditioner. *International Journal of Emerging Technology and Advanced Engineering, 5*(5).

Waje, S., Thorat, B., & Mujumdar, A. J. D. T. (2007). Screw Conveyor Dryer: Process and Equipment Design. *25*(1), 241-247.

Wang, L., & Zhigang, L. (2012). Research on control system of belt conveyor in coal mine. In *Electrical, Information Engineering and Mechatronics 2011* (pp. 885-891): Springer.

Wu, W., Gao, X., Hong, B., & Gao, S. (2008). Classifying single-trial EEG during motor imagery by iterative spatio-spectral patterns learning (ISSPL). *IEEE Transactions on Biomedical Engineering, 55*(6), 1733-1743.

Xu, F., Shi, Y.-C., & Wang, D. (2013). X-ray scattering studies of lignocellulosic biomass: a review. *Carbohydrate polymers, 94*(2), 904-917.

Xu, F., Yu, J., Tesso, T., Dowell, F., & Wang, D. (2013). Qualitative and quantitative analysis of lignocellulosic biomass using infrared techniques: a mini-review. *Applied energy, 104*, 801-809.

Ye, C., Wang, Q., Yu, L., Luo, Z., & Cen, K. (2018). Characteristics of coal partial gasification experiments on a circulating fluidized bed reactor under CO2O2 atmosphere. *Applied Thermal Engineering, 130*, 814-821.

CHAPTER III

EXAMINATION OF THE RELATIONSHIP BETWEEN SWITCHGRASS, HYBRID POPLAR, AND LOBLOLLY PINE AND THE MOTOR CURRENT AND VIBRATION SIGNATURES ON CLOGGING EVENTS IN A SCREW CONVEYORS

Abstract

Lignocellulosic biomass, e.g., switchgrass, hybrid poplar, and loblolly pine, are available feedstocks in the Southeastern United States and have been relied upon by biorefineries as the primary feedstock for renewable fuel and chemicals production. Screw conveyors are one of the primary methods of lignocellulosic biomass bulk transport in biorefineries and are often the conveyance method of choice at the throat of the conversion reactors. Therefore, flow problems in this unit are concerning for biorefineries as they can result in downtime, safety issues, and reduce the plant throughput, which ultimately adversely affects the plant economics. It is therefore important to identify predictors of potential flow challenges to develop mitigation strategies. The goal of the study in this chapter is to examine the relationship between the current and the vibration of the motor powering the screw conveyor on the flow or conveyance status of a bench-scale screw conveyor. This investigation focuses on three bioenergy relevant feedstocks: switchgrass (herbaceous), hybrid poplar (hardwood), and loblolly pine (softwood).

In this study, three feedstocks are hammermilled and sieved into mesh 20 to 40, which has a particle size range of 0.425 – 0.850 mm. Then 10g of each feedstock is fed into a customized bench-scale conveyor with the outlet in absentia to secure a clogging event. From the beginning of each feeding process to 30s after motor shaft is fully stopped due to clogging, current and vibration signals are collected constantly and simultaneously for the analysis of the relationship of both signals and flow conditions in the conveyor and the effect of different feedstocks on clogging event occurrence timing. The results of original signals show that a clogging event in the conveyor has a clear impact on both signals. For example, switchgrass and hybrid poplar feedstocks caused a clogging event to occur at approximately 20s after the feeding process starts and approximately

16s for loblolly pine. The current signal showed obvious alteration at the same time stamp, and vibration showed slightly delayed (1-1.5s) alteration to the time stamp. Additionally, by applying the first derivative transformation on both signals, the transformed data shows the distinguished region between the region represents normal feeding process, and the region represents motor shaft fully stopped region, which is defined as the clogging developing region.

3.1. Introduction

Lignocellulosic biomass materials are heterogeneous plant materials that are primarily composed of cellulose, hemicellulose, and lignin and secondarily of extractives and inorganic elements collectively called ash (Cai et al., 2017). These materials are abundant and renewable and have consequently emerged as essential feedstocks to reduce our overdependence on fossil fuels for producing chemicals, fuels, and materials (Cai et al., 2017; M. H. Langholtz, B. J. Stokes, & L. M. Eaton, 2016; Vassilev, Vassileva, & Vassilev, 2015). In biorefineries where these materials are chemically or biologically transformed to the products mentioned above, significant conveyance issues have been reported in early process plants leading to a renewed research focus on developing suitable engineering solutions(G et al., 2021; Minglani et al., 2020). Conveyance issues are related to the nature of lignocellulosic biomass materials, which, unlike other natural solid materials that require conveyance in various industries, complicate the development of generalized solutions.

First, lignocellulosic biomass materials have varying composition and properties by biomass plant types, regions where the materials are grown, harvest practices, and preprocessing approaches that affect their conveyance in biorefineries (Cai et al., 2017; M. Langholtz, B. Stokes, & L. Eaton, 2016). Biorefineries are anticipated to rely on a broad portfolio of feedstocks leading to feedstock and flow governing properties variability. Flow governing properties are

physiomechanical properties that dictate flow behaviors. For example, polydispersity, non-ideal particle shapes, low moisture content, compressibility, elasticity, and cohesiveness are all properties that vary widely in processed biomass materials and influence flow performance in systems (Lei et al., 2018; Pachón-Morales et al., 2020; Saidur, Abdelaziz, Demirbas, Hossain, & Mekhilef, 2011). Thus, the variability of lignocellulosic biomass, combined with its difficult flow characteristics compared to particles from other particulate processes (Cui & Grace, 2008), significantly complicates the prospect of developing generalizable solutions.

With the improvement of technologies to convert lignocellulosic biomass into fuels, intermediates upgradable to fuels (e.g., bio-oil, hydrogen, synthesis gas, etc.), and products (e.g., biochar, bioplastics, etc.), plant biomass sources have a huge potential to replace depleting fossil fuels (Wicker, Kumar, Khan, & Bhatnagar, 2021). Flow-related issues are considered one of the major challenges of utilizing lignocellulosic biomass as a feedstock in a biorefinery. Unsatisfactory feeding rates in biorefinery have been reported due to bridging (Prescott & Barnum, 2000), ratholing (Johanson, 2004), or clogging (Miao, Grift, Hansen, & Ting, 2014), which negatively impacts biorefinery economics. For example, Merrow et al. (Merrow, Phillips, & Myers, 1981) reported that typically only 20-50% of the designed production rate is achieved during biorefinery operations due to, among other reasons, feedstock transport issues. Despite the documented challenges of meeting adequate production rates due to conveyance issues, investigations focused on identifying biomass flow issues are limited, if not non-existent.

In this chapter, we examine the relationship between the current and vibration signatures of a bench-scale screw conveyor's motor during the conveyance of three lignocellulosic biomass materials (switchgrass, pine, and poplar) with the goal of understanding if these signatures could

be predictors of the clogging events, one of the most common and negative failures in biomass conveyance in screw feeders Motors are commonly relied upon to drive screw conveyors and transfer biomass materials into subsequent systems making them an ideal sensing point to monitor for abnormal operations, failures, or eminent failures. Generally, motor failures take place on the stator, rotor, bearings, or shaft of the motor (Bonnett, 2000; García-Escudero, Duque-Perez, Morinigo-Sotelo, & Perez-Alonso, 2011; Kankar, Sharma, & Harsha, 2011; Pires, Kadivonga, Martins, & Pires, 2013) and are commonly detected by vibration and thermal sensing (García-Escudero et al., 2011; Kankar et al., 2011; Konar & Chattopadhyay, 2011), as well as other sensing approaches including electrodynamic, optical, microwave, acoustic, ultrasonic, and resonance-based sensing (Pires et al., 2013; Yan, 1996). One common technique for detecting motor failures in recent years is Motor Current Signature Analysis (MCSA) (Cameron, Thomson, & Dow, 1986; Kankar et al., 2011; Pires et al., 2013; Somayajula, Sanchez-Sinencio, & Gyvez, 1996). Although previously untried in the context of lignocellulosic biomass conveyance status analysis, we posit that the motor current and the conveyor vibration signatures will show distinct patterns that capture the progress of clogging as it unfolds in a screw conveyor. Specifically, we hypothesize that the conveyor motor current will increase as clogging occurs. Similarly, we also hypothesize that the vibration signature will exhibit differences between the normal and abnormal, i.e., clogging, conveyance status and that these differences are statistically significant to be exploited for early detection of eminent clogging events.

3.2. Background

The vibration signal has been used as an indication of the running condition of the motor (Alameh, Hoblos, & Barakat, 2018). When the electrical load is unbalanced, or the motor has been running

for a great amount of time, the vibrational amplitude is expected to gradually increase because of the bearing damages (Yang, Merrild, Runge, Pedersen, & Børsting, 2009). The air gaps in the machinery affect the vibration frequencies, which will reflect any damaged parts inside, especially the stator and bearing for a motor (Schoen, Habetler, Kamran, & Bartfield, 1995). Additionally, motor vibration will accelerate the motor bearing wearing process, making the anticipated service life of the bearing significantly shorter and generating an immense amount of noise. At the same time, the motor vibration leads to a reduction of the winding insulation, which has the potential for health risks. Traditionally, vibration sensors have been widely used to predict any motor faults during industrial operations (Benbouzid, 1999). However, it is well-known that monitoring the vibration signal of the motor cannot effectively check the current working state of the motor and evaluate the working performance of the motor (Rações, Ferreira, Pires, & Damásio, 2019). This is due to the complications of extracting reproducible diagnostic results while accounting for the noise created by the joint sensors to the motor and the surrounding environment (Xiang-Qun, Hong-Yue, Jun, & Jing, 2000). Tsypkin et al. debated the conventional opinion that vibration signal analysis does not serve as a limited technology for motor fault diagnosis (Tsypkin, 2011). However, Gangsar et al. reported in their state-of-art review that vibration signal analysis can still apply to most mechanical faults of the induction motor (Gangsar & Tiwari, 2020).

Another well-known method for the identification of rotor conditions is thermal sensing. Temperature is one of the most important indices for the normal operation of the motor. When the actual temperature exceeds the rated temperature, the validated usage of the motor will be greatly reduced. The most common technique in thermal sensing is infrared thermal image analysis (Glowacz & Glowacz, 2017; Younus & Yang, 2012). By establishing such an infrared

thermography foundation, many researchers in the field have attempted to implement thermal condition monitoring techniques to detect and identify faults in the motor (Al-Musawi, Anayi, & Packianather, 2020; Glowacz & Glowacz, 2017). The advantages of utilizing thermal imagery as an indicator of motor abnormal working condition, especially overheating, include nonintrusive layout (Kral, Haumer, & Lee, 2013), flexibility on how to set up a thermal camera (Gangsar & Tiwari, 2020), and the absence of electromagnetic relation to the motor (Smolyanov, Sarapulov, & Tarasov, 2019). One meritorious study from Adam Glowacz and Zygfryd Glowacz should be acknowledged, as they analyzed the thermal picture pixels to detect rotor faults in induction motors, achieving 100% detection accuracy and motivated Orhan Yaman to include thermal image analysis in the study to develop an automated motor fault detection system based on binary patter (Glowacz & Glowacz, 2017; Yaman, 2021). Sdid et al. presented an online method based on an H-G diagram that uses the rotor slip frequency to represent the motor active power consumption (G) and reactive power consumption (H), which identifies motor state saturation from temperature; however, the paper concluded that this method needs further refinement to confirm its reliability (Sdid & Benbouzid, 2000). Another publication proposed a thermographic method based on image segmentation to analyze five conditions on a typical induction motor. The authors recommended additional monitoring for voltage imbalance and automation for image segmentation (Garcia-Ramirez et al., 2014). Other previously mentioned monitoring techniques were also determined as too costly or requiring further improvements or observers (Gangsar & Tiwari, 2020; Yaman, 2021).

Back in the 1980s, several researchers had already discovered the technique of extracting features from the current signal to reveal abnormal machinery behaviors (Cameron et al., 1986;

Martins, Pires, & Amaral, 2011; Ruey-Wen & Visvanathan, 1979). The relationship between the current signature from the motor and the machinery that is driven by the motor has been well-proven as direct and efficient (M. E. Benbouzid, 2000; Thomson & Fenger, 2001). Other advantages that magnified its functionality were also reported, including simple and inexpensive measurement and storage of the electrical signal (Kalaskar & Gond, 2014; Ukil, Chen, & Andenna, 2011), easy online monitoring (M. E. H. Benbouzid, 2000), and early identification or prediction of potential failure (Kalaskar & Gond, 2014). For this reason, MCSA has become more prevalent in recent years (Nandi, Toliyat, & Li, 2005). For example, Jung et al. (Jung, Lee, & Kwon, 2006) proposed an advanced algorithm that processes signals and data using MCSA. Modern researchers improved this technique by implementing additional steps such as the multiresolution (MRA) approach (García-Escudero et al., 2011), preprocess current signals (De Santis, Livi, Sadeghian, & Rizzi, 2015; Lee, Jo, & Hwang, 2017), or refinement of traditional analysis steps (Pires et al., 2013). Pires et al. (Pires et al., 2013) pointed out the limitations of conventional MCSA for rotor diagnosis and presented a novel MCSA technique called Motor Square Current Signature Analysis (MSCSA) to extract more information from the motor and identify specific fault information, such as broken bars or rotor eccentricity. Other researchers altered the traditional 2D current signature to a 3D stator current state for pattern recognition (Martins et al., 2011). These revolutionary approaches greatly enhanced the performance of MCSA and laid the foundation for making MCSA the standardized preventive maintenance methodology (M. E. Benbouzid, 2000; García-Escudero et al., 2011).In this chapter, the conventional vibration signal monitoring and MCSA approaches were employed to observe the consequences of screw conveyor clogging event to current signature and vibration dynamics similar to the preliminary steps of the previous researches (Cameron et al.,

1986; García-Escudero et al., 2011; Martins et al., 2011; Ukil et al., 2011). The monitoring software for vibration signals comes directly with the vibration sensor. A simple Python algorithm was implemented for visualizing the current signature extracted from an induction motor that empowers a screw conveyor for metering switchgrass.

3.3. Materials and Methods

Figure 3-1 outlines the overall experimental plan adopted in the study. Briefly, our plan consists of acquiring, preparing, and characterizing our materials. We then feed the materials through our

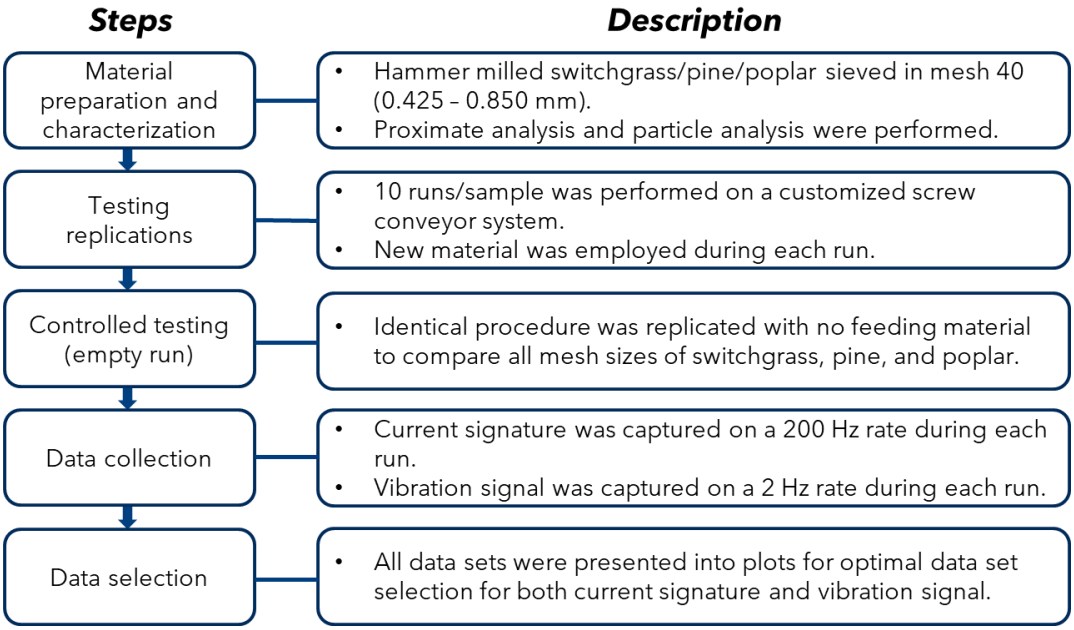

Figure 3-1. Overview of the experimental plan for clogging simulation.

experimental setup to generate current and vibration feedback signals during the feeding process. Finally, we process and analyze the acquired data. These steps are outlined in greater detail in the subsequent sections.

3.3.1. Material Preparation and Characterization

Three biomass materials were used, including switchgrass, hybrid poplar, and loblolly pine. Alamo switchgrass variant was obtained from Genera Energy Inc. in Vonore, TN, which we received in dried condition. We obtained hybrid poplar and loblolly pine materials from trees harvested from the Cumberland Forest Unit of the University of Tennessee, Institute of Agriculture's Forest Resources Research and Education Center in Oliver Springs, TN. The trees were approximately 20-25 and 10 years old for hybrid poplar and loblolly pine, respectively, and were felled, delimbed, and cut into logs at the harvest site. The logs were then debarked using a draw knife and subsequently dried in a large kiln at 48 °C for 10 days to begin removing a portion of the water contained within their fibers. At the end of the drying period, we chipped the logs in a chipper and then placed them back in a large kiln to continue drying at 48 °C for another 10 days. Subsequently, the switchgrass and the dried chips were hammermilled through a 1 mm screen to create starter batches which were further sieved between sieve mesh size 20 – 40 (0.425 – 0.85 mm) for the experiments in this chapter.

We conducted proximate analysis on the sieved samples to quantify the moisture (E871-82), ash (E1755-01), and volatile matter (E872-82) contents following the American Society for Testing and Materials (ASTM) standards (Brian Stanton, 2018; Lyzun; Magzine, MAY 16, 2017). Fixed carbon content is also calculated based on acquired data. It is noteworthy to point out that

the proximate analysis is a common procedure to provide general information on the biomass properties since they can be highly variable during material preprocessing and preparation (Nimmanterdwong, Chalermsinsuwan, & Piumsomboon, 2021). Nonetheless, these properties are reported in this chapter because they are routinely used to define lignocellulosic biomass. Additionally, we performed particle size analysis using Microtrack 3D particle size analyzer to acquire information of size range, mean particle size, and difference volume percentage, which means the percentage of total particles fall into each defined size rage.

3.3.2. Experimental Setup

We designed and fabricated a customized lignocellulosic biomass screw conveyor with a motor and data collection hardware to investigate the relation between clogging events and the dynamic current and vibration signals. Figure 3-2 shows the overall experimental apparatus, which consists of a screw conveyor system and a sensor and data acquisition platform. A picture of the conveyor is included in Figure A-1, Appendix A. The screw conveyor consists of a screw auger with a 15/16 in. (23.8 mm) flight diameter and a 1/2 in. (12.7 mm) shaft diameter housed in 1 in. (25.4 mm) long 12-1/8 in. (308 mm) schedule 80 clear PVC pipe supported on two legs.

The screw conveyor housing is terminated by two 3-15/16 in. (diameter = 100 mm) flanges coupled to a similarly sized circular four-bolt flange with mounted ball bearings (KML Bearing USA, Model #UCFC 201-8). The screw shaft is coupled to and powered by an induction motor (Dayton, Model #453R96) using a rigid clamping shaft coupling. The sensor and data acquisition platform includes a current sensor (CR Magnetics, Model #CR4120S), a data acquisition (DAQ) system (Measurement Computing, Model #USB-1208FS-Plus), a vibration data logger (EXTECH

VB300) attached to the upper motor housing by a magnet, and a number of computer software (MATLAB R2019b, EXTECH VB300 software, Spyder 4.1.5) as terminal emulators.

First, before conducting any runs with the three biomass materials, we ran the conveyor 20 times while empty to obtain our current and vibration baselines. The curves representing these

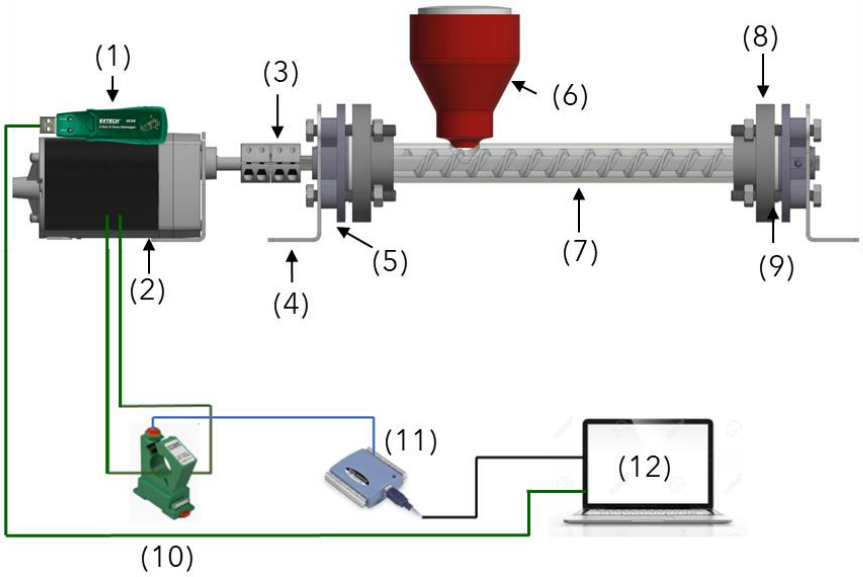

Figure 3-2. Experimental setup for the current and vibration analysis of the motor. (1) Vibration datalogger; (2) Motor; (3) Coupling; (4) Supporting feet; (5) Flange bearing; (6) Feed hopper; (7) Pipe with the screw inside; (8) Housing flange; (9) Gasket; (10); Current transducer; (11) Data acquisition device; (12) Computing software.

signals are labeled "baseline" in the results. Then, we ran the conveyor with approximately 20 g of each material charged into the hopper without any flow obstruction at the outlet of the conveyor to mimic a normal conveyance status. The curves representing these signals are labeled "normal" in the results. Finally, we ran the conveyor with approximately 20 g of the biomass material charged into the feed hopper with flow obstruction at the outlet of the conveyor to mimic an abnormal conveyance status. The curves representing these signals are labeled "abnormal" in the results. A flow obstruction is mimicked by closing the outlet of the conveyor with a blind flange to guarantee that a plug will be formed. In all three cases, the screw motor is turned on, and the biomass in the feed hopper, if any, gradually drops onto the screw as the material is positively displaced toward the outlet. In the case of the abnormal conveyance status runs, as the material is unable to exit the screw conveyor housing, a plug begins to form, usually within 20-30 s after the motor is started. We used a constant motor speed of 105 rpm without any load resulting in a biomass feeding rate of approximately 2 g/s in the normal conveyance status. Simultaneously, as the motor starts, the current and vibration sensors acquire and send their respective signals to the computer. A new biomass sample is used for each run during the normal and abnormal conveyance status runs. Furthermore, in the abnormal conveyance status scenario, the conveying process terminates when the conveyor shaft completely stops rotating, usually around 60 s. We cleaned the conveyor housing between each run.

3.3.3. Data Collection, Processing, and Analysis

We collected two types of datasets during each run. The first dataset comes from the current sensor hardware (Figure 3-2, parts 10, and 11) and consists of 12,000 current data points per run. It is worth noticing that the motor current signature has a unit of milliamps (mA) because the power

source is a low voltage AC induction motor. The second dataset comes from the vibration sensor hardware (Figure 3-2., part 1) and consists of 120 acceleration data points of the three-dimensional vibration signal in the motor space with an additional summed-up variable to represent the total vibration, and the unit for vibration signal is the gravitational acceleration (m/s^2) (Rigacci, Sato, & Shirase, 2021). The datasets are then directly plotted with no interference with a statistical calculation on standard deviation. Additionally, we transformed the data using the first derivative transformation to reveal the specific abnormal region in extracted signals(Azzoug et al., 2021). In both datasets, time series signals start to deviate while a clogging event occurs and then reach a plateau when the conveyor's clogging is fully formed. The precise time interval from signal starts to deviate to reach a plateau is difficult to conclude based on raw datasets. Alternatively, the first derivative transformed datasets can be used to easily distinguish the region of clogging event under development to the normal operating region and clogging event fully formed region, which is both relatively steady regions but on different levels, compared to the development region.

3.4. Results

3.4.1. Material Characteristics and Properties

We selected the three materials (switchgrass, loblolly pine, and hybrid poplar) since they represent three bioenergy relevant feedstocks commonly used in lignocellulosic biorefineries. While the proximate properties of these materials are expected to vary, we do not anticipate that this variability will influence their flowability. Therefore, the proximate analysis is primarily conducted in this study to provide a record of the materials. The results of the proximate analysis data are shown in Table 3-1. Each mean value with standard deviation was calculated based on three replications.

The highest mean moisture content in weight percentage is hybrid poplar that is 7.4 wt. %, wet basis followed by switchgrass that is 7.16wt. %, wet basis. The lowest moisture mean is loblolly

Table 3-1. Proximate analysis of switchgrass (SG), loblolly pine (LP), and hybrid poplar (HP).

	Mean (SD)		
	SG	LP	HP
Moisture (wt.% wet basis)	7.16 (0.22)	5.35 (0.13)	7.40 (0.62)
Proximate analysis, (wt.% dry basis)			
Ash	0.90 (0.08)	0.16 (0.04)	0.61 (0.05)
Volatiles	90.70 (0.69)	85.57 (0.36)	87.12 (0.53)
Fixed Carbon	9.43 (0.42)	14.27 (0.34)	11.48 (0.39)

SD stands for standard deviation based on three replicates.

pine with a lower value, 5.35 wt. %, wet basis. Switchgrass has the highest ash content (0.9 wt. %, dry basis) and volatile matter (90.7 wt. %, dry basis), and lowest fixed carbon (9.43 wt. %, dry basis). Loblolly pine has the lowest ash content (0.16 wt. %, dry basis), the lowest volatile content (85.57 wt. %, dry basis), and the highest fixed carbon (14.27 wt. %, dry basis). Hybrid poplar has middle values of all three materials for all three characteristics. The proximate analysis results of switchgrass, loblolly pine, and hybrid poplar are consistent with the results reported in other studies(Lemus et al., 2002; Lindsey, Johnson, Kim, Jackson, & Labbé, 2013; Sanchez-Silva, López-González, Villaseñor, Sánchez, & Valverde, 2012).

Figure 3-3 shows the particle size distribution determined using a quasi 3D particle image analyzer based on dynamic image analysis (PartAn3D Pro, Microtrac, York, PA, USA). By capturing images of every particle that falls through the measurement field of high-resolution digital cameras, the particle image analyzer calculated the particle size information. We then reported different percentages in volume (Diff Volume %) of total particles being analyzed based on D_p intervals, which means p% of total particles have an approximate size to somewhat Diff Volume %. Based on the D_{50} results in millimeters, which indicates 50% of particles from the original sample have the approximated size, all biomass materials showed appropriate sizes within the mesh 40 range.

3.4.2. Current and Vibration Signatures

Switchgrass, loblolly pine, and hybrid poplar with particle sizes ranging between 0.425 and 0.850 mm are used for conveyance status runs with 20 replications for each material. During each run, both current and vibration data are collected.

Figure 3-4 shows the current and vibration signals of the three biomass materials. In the baseline and normal conveyance status runs, the current and vibration signals reach a steady state

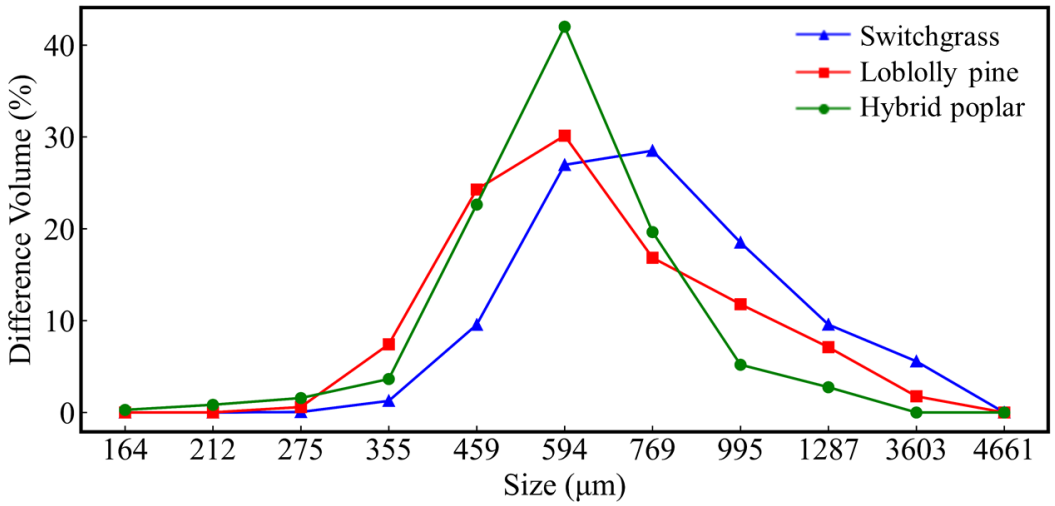

Figure 3-3. Size distribution of three biomass materials.

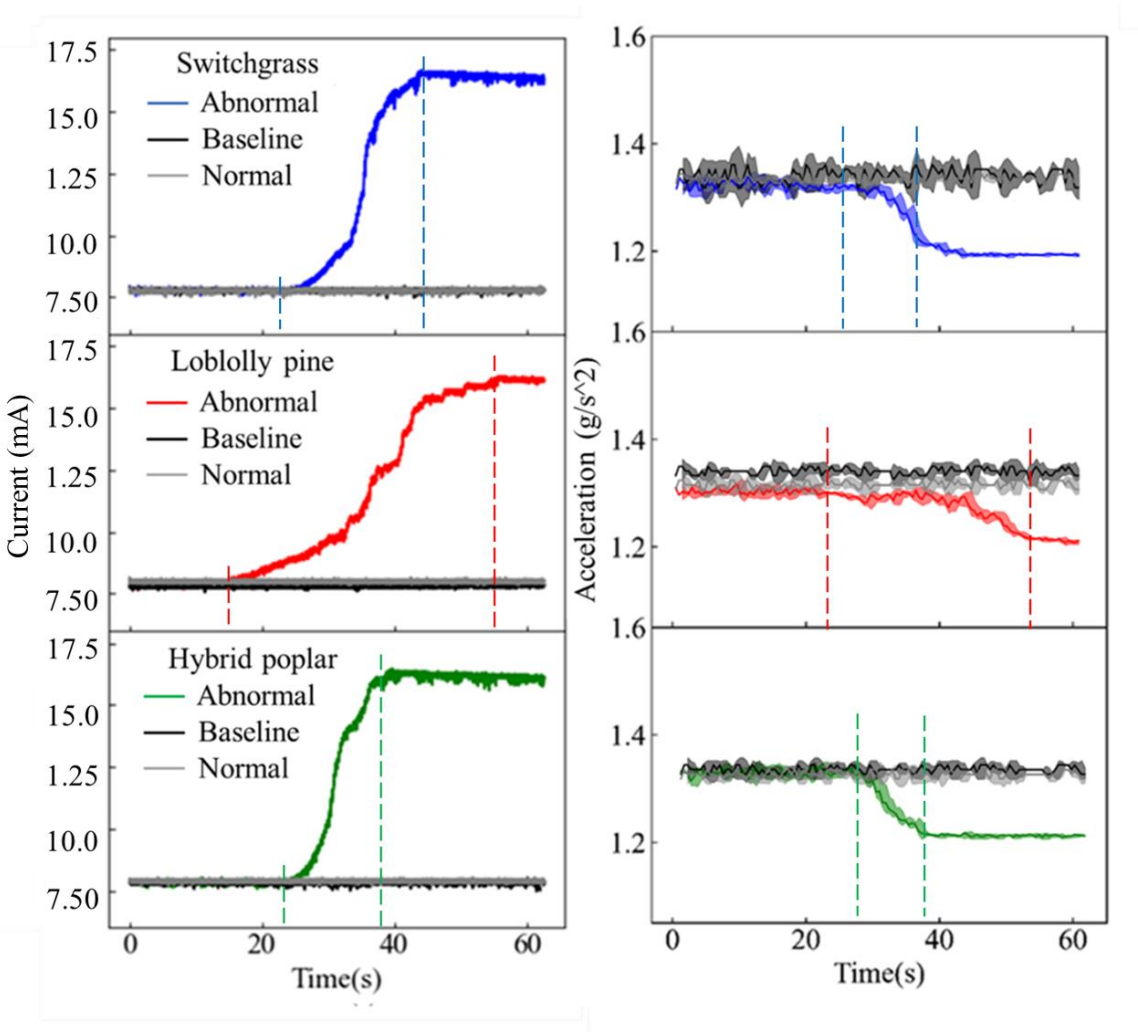

Figure 3-4. Current (left) and vibration (right) mean signals of switchgrass, loblolly pine, and hybrid poplar with particle sizes between 0.425 and 0.85 mm. Each mean is displayed as a thick line and was derived from 20 individual runs. The standard deviation of the runs is represented by the overlayed semi-transparent shaded regions with the same color as the mean. Note: One the current signals, the standard deviation regions are plotting but are not easily discerned.

for all three materials in contrast to abnormal conveyance status runs. In the baseline conveyance status runs, the current signal remains relatively flat for all of the runs with steady state means of 7.82, 7.81, and 7.84 mA and standard deviations of 0.04, 0.04, and 0.05 mA, and vibration signal with means of 1.229, 1.321, and 1.238 m/s^2 and standard deviations of 0.017, 0.016, and 0.019 m/s^2 for switchgrass, loblolly pine, and hybrid poplar, respectively. In the normal conveyance status runs, we observed similar behavior for the current and vibration signals of the three materials with near-identical steady state means and standard deviations. In the abnormal conveyance status runs, the current and vibration signals first start at the baseline steady state positions previously observed for the baseline and normal conveyance status runs. In the case of the current signal, it gradually increases as the clogging builds until reaching a plateau around 16.62, 16.59, and 16.71 mA for switchgrass, loblolly pine, and hybrid poplar, respectively. In contrast, the vibration signal decreases in amplitude as the clogging build until the signal reaches and persists at the minima around 1.189, 1.193, and 1.205 m/s^2 with the same order as the current. Such decrease in vibration signal is due to the reduction in rpm of the motor from elevated resistance to motor shaft by the clogging event. Switchgrass and hybrid poplar's both current and vibration signals were relatively flat between t = 0 s to t = 20 s. Afterward, the current signal quickly increased at an approximate rate of 1.13 mA/s for switchgrass and 1.19 mA/s for hybrid poplar. A similar signal increase was also observed for the loblolly pine, although the increase occurred the earliest with pine (~ t = 16 s) compared to switchgrass (~ t = 20s) and loblolly pine (~ t = 20s). Switchgrass and hybrid poplar had steeper current and vibration signature slopes after the signal began to increase. Additionally, the signal trend for loblolly pine had a relatively gradual signal alternation compared to switchgrass and hybrid poplar; this behavior can also be observed in the vibration plots. Poplar

had the highest value in current and lowest in vibration when the signals reached their extreme values. For more information, the raw data of all replications can be found in Appendix, Figure A-1 for current signal and Figure A-2 for vibration signal.

Since the increase in the current and vibration signals is attributed to the development of clogging in the conveyor, we define the flat region in both current and vibration signals before they begin to alter as normal operation region, indicates a clogging event is not happening yet, and later region as clogging event region. More specifically, for the clogging event region, we define the signal altering region in both current and vibration signals as clogging development region, and the later flat region as the full clogging region. Since the clogging development region is the target region for this paper, we decided to use the first derivative transformation on both current and vibration raw signals because the normal operation and full clogging regions are both relatively flat compared to the development region, and we anticipate that the regions that capture the increase in the signals would protrude when the data is transformed using the first-derivative. The first-derivative transformed data could then be leveraged to identify the onset of a clogging event, i.e., transition from the normal to abnormal conveyance status. Figure 3-5 shows the first derivative transformed current and vibration signals of the same datasets used in Figure 3-4.

Using the first-derivative transformed data, we defined the onset of a clogging event using two criteria: (1) a threshold first-derivative value of 0.3 mA/s and -0.02 m/s^2 for the current and vibration signals, respectively (criteria #1); and (2) 90% of signal data points maintaining the selected threshold values over a 5 s window (criteria #2). These criteria were selected arbitrarily since there is no precedent that we could use for guidance and could be easily changed depending on the needs of specific applications. Based on the first derivative transformation and standard

deviation in Figure 3-5, we observe that the signal altering region, where current increases and vibration decreases, can be easily singularized from normal operation and fully clogging regions.

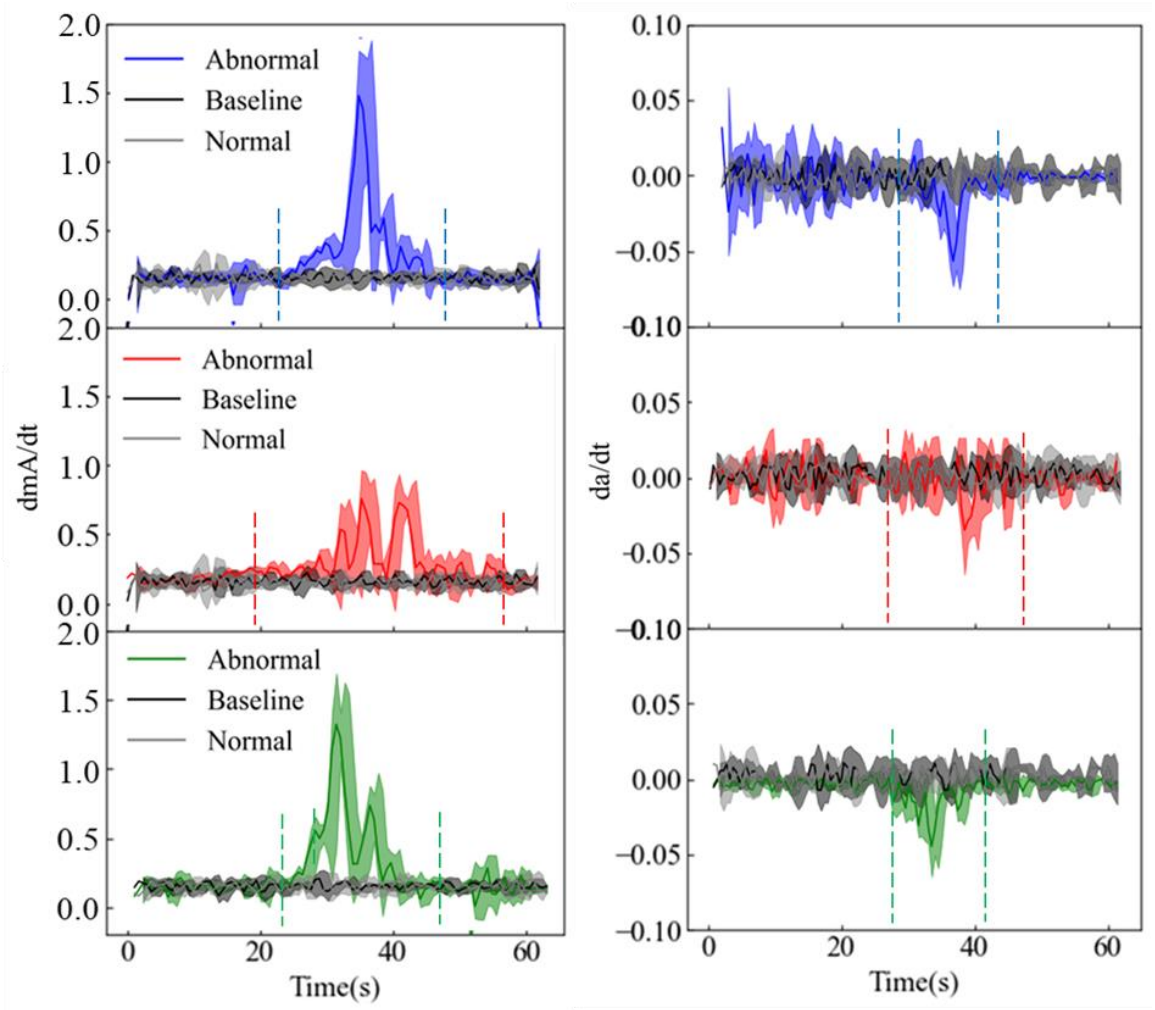

Figure 3-5. The mean first-derivative of the current (left) and vibration (right) signals of switchgrass, loblolly pine, and hybrid poplar. Each mean is displayed as a thick line and was derived from 20 individual runs. The standard deviation of the runs is represented by the overlayed semi-transparent shaded regions with the same color as the mean.

More specifically, for switchgrass and hybrid poplar, the starting points of signal alteration agree with the approximated time stamps from Figure 3-4 with the consideration of white noise being considered, whereas the white noise is represented by the standard deviation for each type of dataset. As shown in the figure, the starting points defined by the two criteria are t = 22 s for switchgrass and t = 21.5 s for hybrid poplar. For loblolly pine, the starting point, t = 18 s, is slightly delayed compared to the approximated time stamp. However, the result still agrees with the inspection from Figure 3-4 that loblolly pine showed earlier signal alteration.

3.5. Discussion

This study investigates the relationship between clogging event occurrences and two mechanical signals extracted from a bench-scale screw conveyor system. Switchgrass and hybrid poplar signals showed obvious alteration at the onset of clogging (~ t>22s), where loblolly pine showed earlier alteration (~ t>16s). Hybrid poplar and switchgrass signals reached their peak value (~ t>37s and ~ t>40s, respectively) prior to the loblolly pine signal (~ t>53s). Similarly, the onset of clogging occurred earlier with switchgrass and hybrid poplar compared to loblolly pine. This phenomenon has validated the relationship between clogging events and current and vibration signals, which is related to the study of Gudavalli et al. that the mechanical signals, such as torque, of the motor that functions as a power source of conveyor, have a relationship to the biomass flowing conditions during conveyance (Gudavalli, Bose, Donohoe, & Sievers, 2020). During the development of a clogging event, the abnormal behavior will also be reflected on both signals and reach the highest and lowest peak values from current and vibration signals, respectively. This relationship can be found in other motor fault diagnosis using mechanical signals (Rações et al., 2019; Somayajula et al., 1996).

By comparing three curves in each figure, the slope of each curve is directly related to the development of a clogging event, where the slopes are positive in current signals and negative in vibration signals. Loblolly pine had the overall lowest absolute slope values in both figures, which indicates a longer clogging development. On the other hand, switchgrass and hybrid poplar showed similar clogging development initiation, but hybrid poplar had the highest absolute slope values, which indicates a faster clogging development. Therefore, the total duration of clogging development from hybrid poplar is the shortest (t = 15s) compared to switchgrass (t = 21s) and loblolly pine (t = 36s). Similar relationship of motor signals and flowing condition in the conveyor are also demonstrated in other studies (Konar & Chattopadhyay, 2011; Rações et al., 2019). We can easily pick up signal alterations and slopes under clogging development based on the first derivative data transformation of the same dataset. The first derivative transformed curves show the same characteristics with more obvious divergences, such as the onset of clogging and slope, identified previously on the untransformed data, albeit at a higher magnitude. Additionally, both current and vibration signals using loblolly pine showed dissimilar behaviors to switchgrass and hybrid poplar, such as the turning point of abnormal signal and the slope of signal changing region. This observation may be related to the physicalchemical property differences among these feedstocks. Additional studies in the future will be helpful to investigate on how the property differences of the feedstocks affect flow behavior as well as corresponded current and vibration signals.

3.6 Conclusions

Motor current and vibration signals offer an effective way to monitor and diagnose clogging events of lignocellulosic biomass particulates as they unfold in screw conveyors. In this study, the

clogging event is monitored and investigated by using vibration and the current measurements, respectively. All of the flowing conditions defined in the study can be diagnosed via both signals analyses. The time-varying motor current and vibration signals are derived, showing that clogging events in screw conveyors can be diagnosed by detecting a series of abnormal current and vibration signal sidebands around the power supply frequency component in the time-frequency domain. This finding has the potential utilization for conveyance clogging detection related and motor fault diagnosis related subjects, as well as extends the use of artificial intelligence techniques to analyze current and vibration signals to reveal the flowing conditions in the conveyor in a more sophisticated way. Nevertheless, this technique is quite convenient to configure in industries. Therefore, our work exhibits a huge potential to use simple current and vibration signal analyses to diagnose industrial screw conveyor clogging events.

References

Al-Musawi, A. K., Anayi, F., & Packianather, M. (2020). Three-phase induction motor fault detection based on thermal image segmentation. *Infrared Physics & Technology, 104*, 103140. doi:https://doi.org/10.1016/j.infrared.2019.103140

Alameh, K., Hoblos, G., & Barakat, G. (2018). Statistical Vibration-Based Fault Diagnosis Approach Applied To Brushless DC Motors. *IFAC-PapersOnLine, 51*(24), 338-345. doi:https://doi.org/10.1016/j.ifacol.2018.09.599

Azzoug, Y., Sahraoui, M., Pusca, R., Ameid, T., Romary, R., & Cardoso, A. J. M. (2021). High-performance vector control without AC phase current sensors for induction motor drives: Simulation and real-time implementation. *ISA Transactions, 109*, 295-306. doi:https://doi.org/10.1016/j.isatra.2020.09.021

Benbouzid, M. E. (2000). A review of induction motors signature analysis as a medium for faults detection. *IEEE Transactions on Industrial Electronics, 47*(5), 984-993. doi:Doi 10.1109/41.873206

Benbouzid, M. E. H. (1999). Bibliography on induction motors faults detection and diagnosis. *IEEE Transactions on Energy Conversion, 14*(4), 1065-1074. doi:10.1109/60.815029

Benbouzid, M. E. H. (2000). A review of induction motors signature analysis as a medium for faults detection. *IEEE Transactions on Industrial Electronics, 47*(5), 984-993. doi:10.1109/41.873206

Bonnett, A. H. (2000). Root cause AC motor failure analysis with a focus on shaft failures. *IEEE Transactions on Industry Applications, 36*(5), 1435-1448. doi:10.1109/28.871294

Brian Stanton, B. O. N., Renata Bura, Rachel Emerson, and Jeff Kallestad. (2018). The Devil is in the Details: Understanding Poplar's True Potential as an Energy Feedstock through Biomass Studies. Retrieved from https://hardwoodbiofuels.org/resources/newsletter-archive/winter2017/biomass-studies/

Cai, J., He, Y., Yu, X., Banks, S. W., Yang, Y., Zhang, X., . . . Bridgwater, A. V. (2017). Review of physicochemical properties and analytical characterization of lignocellulosic biomass. *Renewable and Sustainable Energy Reviews, 76*, 309-322.

Cameron, J. R., Thomson, W. T., & Dow, A. B. (1986). Vibration and current monitoring for detecting airgap eccentricity in large induction motors. *IEE Proceedings B - Electric Power Applications, 133*(3), 155-163. doi:10.1049/ip-b.1986.0022

Cui, H., & Grace, J. R. (2008). Spouting of biomass particles: A review. *Bioresource Technology, 99*(10), 4008-4020. doi:https://doi.org/10.1016/j.biortech.2007.04.048

De Santis, E., Livi, L., Sadeghian, A., & Rizzi, A. (2015). Modeling and recognition of smart grid faults by a combined approach of dissimilarity learning and one-class classification. *Neurocomputing, 170*, 368-383. doi:https://doi.org/10.1016/j.neucom.2015.05.112

G, G., S, K., R, Y. K., Bhatia, S. K., S, A. K., M, R., . . . J, R. B. (2021). Valorization of agricultural residues: Different biorefinery routes. *Journal of Environmental Chemical Engineering, 9*(4), 105435. doi:https://doi.org/10.1016/j.jece.2021.105435

Gangsar, P., & Tiwari, R. (2020). Signal based condition monitoring techniques for fault detection and diagnosis of induction motors: A state-of-the-art review. *Mechanical Systems and Signal Processing, 144*, 106908. doi:https://doi.org/10.1016/j.ymssp.2020.106908

García-Escudero, L. A., Duque-Perez, O., Morinigo-Sotelo, D., & Perez-Alonso, M. (2011). Robust condition monitoring for early detection of broken rotor bars in induction motors. *Expert Systems with Applications*, *38*(3), 2653-2660. doi:https://doi.org/10.1016/j.eswa.2010.08.055

Garcia-Ramirez, A. G., Morales-Hernandez, L. A., Osornio-Rios, R. A., Benitez-Rangel, J. P., Garcia-Perez, A., & Romero-Troncoso, R. d. J. (2014). Fault detection in induction motors and the impact on the kinematic chain through thermographic analysis. *Electric Power Systems Research*, *114*, 1-9. doi:https://doi.org/10.1016/j.epsr.2014.03.031

Glowacz, A., & Glowacz, Z. (2017). Diagnosis of the three-phase induction motor using thermal imaging. *Infrared Physics & Technology*, *81*, 7-16. doi:https://doi.org/10.1016/j.infrared.2016.12.003

Gudavalli, C., Bose, E., Donohoe, B. S., & Sievers, D. A. (2020). Real-time biomass feedstock particle quality detection using image analysis and machine vision. *Biomass Conversion and Biorefinery*, 1-12.

Johanson, K. (2004). Rathole stability analysis for aerated powder materials. *Powder Technology*, *141*(1), 161-170. doi:https://doi.org/10.1016/j.powtec.2004.02.004

Jung, J., Lee, J., & Kwon, B. (2006). Online Diagnosis of Induction Motors Using MCSA. *IEEE Transactions on Industrial Electronics*, *53*(6), 1842-1852. doi:10.1109/TIE.2006.885131

Kalaskar, C. S., & Gond, V. J. (2014). Motor current signature analysis to detect the fault in induction motor. *International Journal of Engineering Research and Applications*, *4*(6), 58-61.

Kankar, P. K., Sharma, S. C., & Harsha, S. P. (2011). Fault diagnosis of ball bearings using machine learning methods. *Expert Systems with Applications*, *38*(3), 1876-1886. doi:https://doi.org/10.1016/j.eswa.2010.07.119

Konar, P., & Chattopadhyay, P. (2011). Bearing fault detection of induction motor using wavelet and Support Vector Machines (SVMs). *Applied Soft Computing*, *11*(6), 4203-4211. doi:https://doi.org/10.1016/j.asoc.2011.03.014

Kral, C., Haumer, A., & Lee, S. B. (2013). A practical thermal model for the estimation of permanent magnet and stator winding temperatures. *IEEE Transactions on Power Electronics*, *29*(1), 455-464.

Langholtz, M., Stokes, B., & Eaton, L. (2016). 2016 Billion-ton report: Advancing domestic resources for a thriving bioeconomy, Volume 1: Economic availability of feedstock. *Oak Ridge National Laboratory, Oak Ridge, Tennessee, managed by UT-Battelle, LLC for the US Department of Energy*, *2016*, 1-411.

Langholtz, M. H., Stokes, B. J., & Eaton, L. M. (2016). 2016 Billion-ton report: Advancing domestic resources for a thriving bioeconomy, Volume 1: Economic availability of feedstock. *Oak Ridge National Laboratory, Oak Ridge, Tennessee, managed by UT-Battelle, LLC for the US Department of Energy*, *2016*, 1-411.

Lee, Y. O., Jo, J., & Hwang, J. (2017, 11-14 Dec. 2017). *Application of deep neural network and generative adversarial network to industrial maintenance: A case study of induction motor fault detection.* Paper presented at the 2017 IEEE International Conference on Big Data (Big Data).

Lei, T., Zuend, A., Cheng, Y., Su, H., Wang, W., & Ge, M. (2018). Hygroscopicity of organic surrogate compounds from biomass burning and their effect on the efflorescence of

ammonium sulfate in mixed aerosol particles. *Atmospheric Chemistry and Physics, 18*(2), 1045-1064.

Lemus, R., Brummer, E. C., Moore, K. J., Molstad, N. E., Burras, C. L., & Barker, M. F. (2002). Biomass yield and quality of 20 switchgrass populations in southern Iowa, USA. *Biomass and Bioenergy, 23*(6), 433-442. doi:https://doi.org/10.1016/S0961-9534(02)00073-9

Lindsey, K., Johnson, A., Kim, P., Jackson, S., & Labbé, N. (2013). Monitoring switchgrass composition to optimize harvesting periods for bioenergy and value-added products. *Biomass and Bioenergy, 56*, 29-37. doi:https://doi.org/10.1016/j.biombioe.2013.04.023

Lyzun, A. Stock Photo - Pine wood chips on the ground. Retrieved from https://www.123rf.com/photo_37775941_pine-wood-chips-on-the-ground.html

Magzine, B. I. (MAY 16, 2017). Efficiency boost for straw based biofuel production. Retrieved from https://biofuels-news.com/news/efficiency-boost-for-straw-based-biofuel-production/

Martins, J. F., Pires, V. F., & Amaral, T. (2011). Induction motor fault detection and diagnosis using a current state space pattern recognition. *Pattern Recognition Letters, 32*(2), 321-328. doi:https://doi.org/10.1016/j.patrec.2010.09.010

Merrow, E. W., Phillips, K., & Myers, C. W. (1981). *Understanding Cost Growth and Performance Shortfalls in Pioneer Process Plants*: RAND Corporation.

Miao, Z., Grift, T. E., Hansen, A. C., & Ting, K. C. (2014). Flow performance of ground biomass in a commercial auger. *Powder Technology, 267*, 354-361. doi:https://doi.org/10.1016/j.powtec.2014.07.038

Minglani, D., Sharma, A., Pandey, H., Dayal, R., Joshi, J. B., & Subramaniam, S. (2020). A review of granular flow in screw feeders and conveyors. *Powder Technology, 366*, 369-381. doi:https://doi.org/10.1016/j.powtec.2020.02.066

Nandi, S., Toliyat, H. A., & Li, X. (2005). Condition Monitoring and Fault Diagnosis of Electrical Motors—A Review. *IEEE Transactions on Energy Conversion, 20*(4), 719-729. doi:10.1109/TEC.2005.847955

Nimmanterdwong, P., Chalermsinsuwan, B., & Piumsomboon, P. (2021). Prediction of lignocellulosic biomass structural components from ultimate/proximate analysis. *Energy, 222*, 119945. doi:https://doi.org/10.1016/j.energy.2021.119945

Pachón-Morales, J., Perré, P., Casalinho, J., Do, H., Schott, D., Puel, F., & Colin, J. (2020). Potential of DEM for investigation of non-consolidated flow of cohesive and elongated biomass particles. *Advanced Powder Technology, 31*(4), 1500-1515. doi:https://doi.org/10.1016/j.apt.2020.01.023

Pires, V. F., Kadivonga, M., Martins, J. F., & Pires, A. J. (2013). Motor square current signature analysis for induction motor rotor diagnosis. *Measurement, 46*(2), 942-948. doi:https://doi.org/10.1016/j.measurement.2012.10.008

Prescott, J. K., & Barnum, R. A. (2000). On powder flowability. *Pharmaceutical technology, 24*(10), 60-85.

Rações, H. D., Ferreira, F. J., Pires, J. M., & Damásio, C. V. (2019). *Application of Different Machine Learning Strategies for Current-and Vibration-based Motor Bearing Fault Detection in Induction Motors.* Paper presented at the IECON 2019-45th Annual Conference of the IEEE Industrial Electronics Society.

Rigacci, M., Sato, R., & Shirase, K. (2021). Evaluating the influence of mechanical system vibration characteristics on servo motor efficiency. *Precision Engineering, 72*, 680-689. doi:https://doi.org/10.1016/j.precisioneng.2021.07.012

Ruey-Wen, L., & Visvanathan, V. (1979). Sequentially linear fault diagnosis: Part I-Theory. *IEEE Transactions on Circuits and Systems, 26*(7), 490-496. doi:10.1109/TCS.1979.1084663

Saidur, R., Abdelaziz, E. A., Demirbas, A., Hossain, M. S., & Mekhilef, S. (2011). A review on biomass as a fuel for boilers. *Renewable and Sustainable Energy Reviews, 15*(5), 2262-2289. doi:https://doi.org/10.1016/j.rser.2011.02.015

Sanchez-Silva, L., López-González, D., Villaseñor, J., Sánchez, P., & Valverde, J. L. (2012). Thermogravimetric–mass spectrometric analysis of lignocellulosic and marine biomass pyrolysis. *Bioresource Technology, 109*, 163-172. doi:https://doi.org/10.1016/j.biortech.2012.01.001

Schoen, R. R., Habetler, T. G., Kamran, F., & Bartfield, R. G. (1995). Motor bearing damage detection using stator current monitoring. *IEEE Transactions on Industry Applications, 31*(6), 1274-1279. doi:10.1109/28.475697

Sdid, M. S. N., & Benbouzid, M. E. H. (2000). H-G diagram based rotor parameters identification for induction motors thermal monitoring. *IEEE Transactions on Energy Conversion, 15*(1), 14-18. doi:10.1109/60.849110

Smolyanov, I., Sarapulov, F., & Tarasov, F. (2019). Calculation of linear induction motor features by detailed equivalent circuit method taking into account non-linear electromagnetic and thermal properties. *Computers & Mathematics with Applications, 78*(9), 3187-3199. doi:https://doi.org/10.1016/j.camwa.2019.05.015

Somayajula, S. A. S., Sanchez-Sinencio, E., & Gyvez, J. P. d. (1996). Analog fault diagnosis based on ramping power supply current signature clusters. *IEEE Transactions on Circuits and Systems II: Analog and Digital Signal Processing, 43*(10), 703-712. doi:10.1109/82.539002

Thomson, W. T., & Fenger, M. (2001). Current signature analysis to detect induction motor faults. *Ieee Industry Applications Magazine, 7*(4), 26-34. doi:Doi 10.1109/2943.930988

Tsypkin, M. (2011, 15-18 May 2011). *Induction motor condition monitoring: Vibration analysis technique - A practical implementation.* Paper presented at the 2011 IEEE International Electric Machines & Drives Conference (IEMDC).

Ukil, A., Chen, S., & Andenna, A. (2011). Detection of stator short circuit faults in three-phase induction motors using motor current zero crossing instants. *Electric Power Systems Research, 81*(4), 1036-1044. doi:https://doi.org/10.1016/j.epsr.2010.12.003

Vassilev, S. V., Vassileva, C. G., & Vassilev, V. S. (2015). Advantages and disadvantages of composition and properties of biomass in comparison with coal: An overview. *Fuel, 158*, 330-350. doi:https://doi.org/10.1016/j.fuel.2015.05.050

Wicker, R. J., Kumar, G., Khan, E., & Bhatnagar, A. (2021). Emergent green technologies for cost-effective valorization of microalgal biomass to renewable fuel products under a biorefinery scheme. *Chemical Engineering Journal, 415*, 128932. doi:https://doi.org/10.1016/j.cej.2021.128932

Xiang-Qun, L., Hong-Yue, Z., Jun, L., & Jing, Y. (2000). Fault detection and diagnosis of permanent-magnet DC motor based on parameter estimation and neural network. *IEEE Transactions on Industrial Electronics, 47*(5), 1021-1030. doi:10.1109/41.873210

Yaman, O. (2021). An automated faults classification method based on binary pattern and neighborhood component analysis using induction motor. *Measurement, 168*, 108323. doi:https://doi.org/10.1016/j.measurement.2020.108323

Yan, Y. (1996). REVIEW ARTICLE: Mass flow measurement of bulk solids in pneumatic pipelines. *Measurement Science and Technology, 7*, 1687-1706.

Yang, Z., Merrild, U. C., Runge, M. T., Pedersen, G., & Børsting, H. (2009). A Study of Rolling-Element Bearing Fault Diagnosis Using Motor's Vibration and Current Signatures. *IFAC Proceedings Volumes, 42*(8), 354-359. doi:https://doi.org/10.3182/20090630-4-ES-2003.00059

Younus, A. M. D., & Yang, B.-S. (2012). Intelligent fault diagnosis of rotating machinery using infrared thermal image. *Expert Systems with Applications, 39*(2), 2082-2091. doi:https://doi.org/10.1016/j.eswa.2011.08.004

CHAPTER IV

DEEP LEARNING BASED PREDICTION OF CLOGGING OCCURRENCES DURING LIGNOCELLULOSIC BIOMASS FEEDING IN SCREW CONVEYORS

Abstract

Efficient biorefinery operations require trouble-free and steady conveyance of lignocellulosic biomass materials in and out conversion systems. The partial or full blockage of biomass transport is a common feeding problem encountered in lignocellulosic biomass screw conveyors and is typically referred to as clogging. The occurrence of clogging is associated with distinct changes in the mechanical signals of a screw conveyor power source, which is usually an induction motor. It is beneficial to leverage these changes in the time sequence signals to proactively predict imminent clogging occurrence for process control decision-making. In this chapter, we present a deep learning-based framework for predicting biomass clogging in screw conveyors using two deep learning approaches: Convolutional Neural Network (CNN) and Gated Recurrent Unit (GRU).

First, we collected the current and vibration signals generated during the conveyance of switchgrass, hybrid poplar, and loblolly pine. Second, the input signals were analyzed to determine the clogging region using the first derivative transformation and assign different labels to distinguish normal region and clogging region. Then, we created multiple types of input data based on various combinations of both signals for finding the optimal input signal type by subjecting each type to selected deep learning models to predict the incoming clogging event based on normal region signals beforehand. The prediction logic follows by employing any 20 data points in the input signal with both signal value and labels to predict the signal value and labeling information for the next 10 data points. A sensitivity analysis is performed based on the coefficient of determination (R^2) calculated between the original and predicted signal values. The predicted labels are plotted into a feature map to visualize the predicted normal region and clogging region, and a loss function based on mean squared error is used to reveal the model forecasting procedure. A prediction accuracy in percentage is calculated based on how well the models correctly predicted

the labeling information. Last, an optimization analysis is used by tuning selected model parameters to improve the mean square error (MSE) during model training process and find a local optimal parameter combination that produces the lowest error. We observed that using current signal only as input data for signal predicting can achieve a high R^2 value (0.993, 0.949, 0.985) for switchgrass, loblolly pine, and hybrid poplar, respectively). The proposed GRU method achieved slightly higher labeling accuracy compared to the CNN model but CNN had a better clogging prediction. Model optimization results showed an optimal parameter combination could further reduce the local MSE for both CNN and GRU and slightly improve the clogging prediction.

4.1.Introduction

One of the leading limitations of using lignocellulosic biomass as feedstock in biorefineries is the flow issues encountered by these materials in different conveyance systems, such as bridging (Prescott & Barnum, 2000), ratholing (Johanson, 2004), and clogging (Miao, Grift, Hansen, & Ting, 2014). These flow issues have a detrimental effect on biorefinery economics, resulting in lower plant profitability (Dutta et al., 2015). The roots of the conveyance failure are diverse and include, but are not limited to, limited knowledge of fundamental biomass mechanics, improper system design, and the immense variability in the composition of lignocellulosic biomass processed in biorefineries (Yan et al., 2020).

Among the different conveyance systems prevalent in biorefineries, the screw conveyor provides a unique rotating motion while metering the biomass material that helps to mix up or break down particles (Nachenius, van de Wardt, Ronsse, & Prins, 2015). Screw conveyors are commonly the last conveyance unit operation connected to the conversion reactors because their enclosed configuration prevents potential contamination and provides a good seal between interfaces, which is particularly important in biorefinery operations (Nhuchhen, Basu, & Acharya,

2014). Clogging is a critical conveyance fault in screw conveyors, although others, e.g., mechanical wear (Sievers et al., 2020), also occur. Clogging in the screw conveyor disturbs the granular or particulate flow, provides higher flow resistance and leads to increased motor horsepower (Mysior, Koziołek, & Rusiński, 2018), low feeding rate (L. Wang, Gong, Shi, & Liu, 2010), disturbance in later dryers or reactors (OSMAN, 2012), and other safety issues (Pezo, Jovanović, Pezo, Čolović, & Lončar, 2015).

There are many approaches to mitigate lignocellulosic biomass clogging in screw conveyors, including increasing the dimension of the discharge port (Zhong & O'Callaghan, 1990), lengthening the conveyor with a longer mixing procedure (Pezo et al., 2015) for a more uniform and less cohesive flow (Hou, Dong, & Yu, 2014), or using twin-screw conveyors in co-rotating or counter-rotating motion to enhance the flowability (Minglani et al., 2020). If an intermediate bearing is unavoidable, screw conveyor designers have to reduce the horizontal dimension of the intermediate suspension bearing as much as possible to eliminate the possibility of material blocking when passing through the intermediate bearing (Patel, Patel, & Patel, 2013; Roberts, 2001).

One promising and unexplored approach is using sensor systems coupled with artificial intelligence for the early detection of clogging events to support responsive, automated control. This approach is attractive since there is limited first principle-based knowledge of all the factors to eliminate clogging events. It is also timely because of renewed interest and significant advancements in artificial intelligence applications for engineering process optimization and decision-making (Jha, Bilalovic, Jha, Patel, & Zhang, 2017; Mutlu & Yucel, 2018).

In recent years, researchers have sought to employ deep learning techniques to improve the data analysis for engineering processes and construct an algorithm for motor fault diagnosis (Altug,

Mo-Yuen, & Trussell, 1999; Chow, Sharpe, & Hung, 1993; Fuessel & Isermann, 2000; Glowacz, Glowacz, Glowacz, & Kozik, 2018; Hu, Si, Zhang, & Qin, 2020; Ince, Kiranyaz, Eren, Askar, & Gabbouj, 2016; Konar & Chattopadhyay, 2011; Ye & Wu, 2000). Deep learning algorithms have become increasingly feasible and extensively used in motor signal analysis processes under the growing influence of computing power and sensing technology (Azamfar, Singh, Bravo-Imaz, & Lee, 2020). By reducing the possibility of overfitting, deep learning methods provide more elegant performance and often have more rigorous classification and prediction accuracy than conventional machine learning methods (Avci et al., 2021). Convolutional Neural Networks (CNNs), a class of Feedforward Neural Networks (FNNs) that contains a complex structure and convolutional operationality, is one of the representative deep learning algorithms (Kalchbrenner, Grefenstette, & Blunsom, 2014; Lawrence, Giles, Tsoi, & Back, 1997; Simard, Steinkraus, & Platt, 2003). A CNN can conduct representation learning and classify input information according to its hierarchical structure with shift invariance (Falcon et al., 2016). CNNs have shown outstanding results in motor condition monitoring, especially for high dimensional data analysis (Azamfar et al., 2020; Ince et al., 2016; F. Wang, Liu, Hu, & Chen, 2020). Another widely used deep learning algorithm is the Gated Recurrent Unit (GRU), which is a special type of recurrent neural network (RNN) with an optimized long short-term memory (LSTM) (Hochreiter & Schmidhuber, 1997). GRU combines the input gate and forgetting gate in the LSTM into a single update gate, resulting in fewer training parameters and a faster convergence during training (Chung, Gulcehre, Cho, & Bengio, 2014). GRU method is especially useful for processing time sequence data (Deng, Wang, Jia, Tong, & Li, 2019). Therefore, depending on the type of the data and number of data points, a carefully selected deep learning technique can be applied and optimized to monitor a screw conveyor operation process and detect flow issues like clogging of the lignocellulosic biomass

material. In this project, we propose to develop a sensor and deep learning-based approach to predict the occurrence of lignocellulosic biomass clogging events in a benchtop screw conveyor.

4.2.Background

Deep learning as a new objective in machine learning has been introduced in many industrial fields such as image recognition, bioinformatics, autopilot, machinery diagnosis, and others (Yanming Guo et al., 2016). Most deep learning methods, including the widely used CNN and GRU can learn to extract "optimized" features directly from the original data to maximize the classification or prediction accuracy (Avci et al., 2021). These features include shape and impulse indicators, skewness, and kurtosis of the time series data. The features are normalized to a normal distribution of zero mean and unit variance (Yu, Liu, Zhu, Zhang, & Zhao, 2020). In the next section, we will discuss the basic operating principles of the CNN and GRU methods that will be utilized for clogging detection in our screw conveyor system.

CNN is an artificial neural network that can process high-dimensional data. It is typically applied for highly correlated local data, such as visual image, video prediction, and text categorization (Aloysius & Geetha, 2017). CNN can capture the same patterns across different regions and requires a minimal amount of preprocessing. CNN uses a variant of the multilayer perceptron (MLP) to deal with high-dimensional data based on their shared-weight structure and translation invariance features (Alzubaidi et al., 2021).

Typically, CNN consists of three types of layers: convolutional, pooling, and fully connected. In the convolutional layer, different features of the input data are extracted using a convolution process, and additional layers can extract complex features from the last feature using iterative methods. Each convolutional layer consists of multiple convolutional units, and their parameters

are optimized using a back propagation algorithm. The features extracted in the convolutional layer have high dimensions and are downsized to a lower dimension. In the pooling layer, the outputs of the neuron clusters in one layer are combined into a single neuron for the next layer. Finally, the local features are combined in the fully connected layer to form the global features and compute the final result. Figure 4-1 shows the principle of a one-dimensional CNN system.

GRU is an optimized version of the recurrent neural network (RNN), a widely used artificial neural network algorithm that utilizes hidden layers to preserve information from the previous moment (Yu et al., 2020). The output of RNN is a function of both the current state and prior memories and thus makes it suitable for handling time sequence data. However, when the input information is increased to a certain length, the RNN cannot connect to the relevant information. GRU was developed to address the issues inherent in traditional RNN, especially gradient vanishing and simple hidden layer structure problems. GRU consists of a gated RNN structure, consisting of an update gate and a rest gate. Compared to the long short-term memory (LSTM) (Hochreiter & Schmidhuber, 1997), the other commonly used variant of RNN, GRU, has fewer training parameter requirements and converges quicker. Figure 4-2 shows the expanded model of an RNN system with GRU implementation.

4.3.Materials and Methods

4.3.1. Biomass Preparation and Characterization

The biomass preparation and characterization are identical to Chapter III with the same biomass materials and processing methodology.

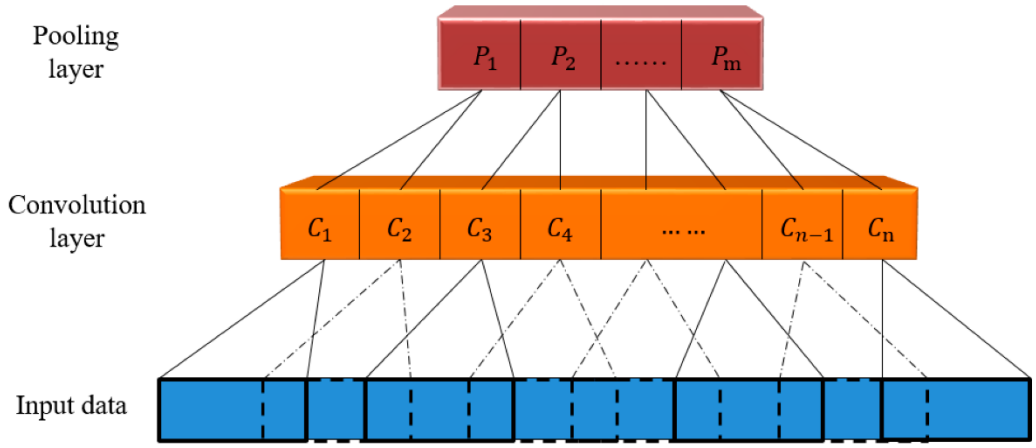

Figure 4-1. Schematic diagram of one-dimensional CNN (X. Li, Li, Qu, & He, 2019).

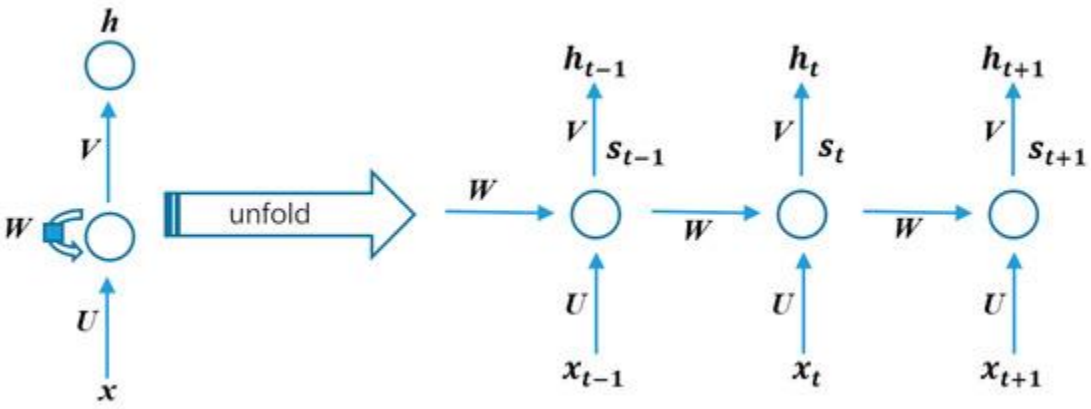

Figure 4-2. Schematic diagram of GRU system. x, h, and s represent the input, output, and hidden states, respectively. U, V, and W represent the weight matrix between the input and hidden layers, hidden layers and outputs, and the hidden layers, respectively (X. Li et al., 2019).

4.3.2. Data Collection and Preparation

The data collection and preparation follow the same methodology that is introduced in Chapter III. We collected two types of datasets during each run. The first dataset comes from the current transducer hardware and consists of 12,000 current data points per run. The second dataset comes from the vibration sensor hardware and consists of 120 acceleration data points of the three-dimensional (x, y, z) vibration signal in the motor space with an additional summed-up variable representing the total vibration.

After the two sets of signals are collected, the frequencies are different in current signal and vibration signal (200 Hz and 2 Hz, respectively) due to the specifically selected sensors easily accessible to us. Therefore, for each testing dataset where both current and vibration signals are present, the combined input data result in uneven data size; that is, the vibration signals are present, the combined input data result in uneven data size; that is, the vibration signal has less data than the current signal with an established frequency ratio of 100:1. However, by the operating principle of the deep learning algorithms we chose in this study, all variables in one dataset should have the same size; thereby, the algorithm can compare all data points and learn from them. Consequently, the current and vibration signals need to be unisized to the same frequency for the deep learning algorithmic analysis. We employed two data transformation strategies to unisize current and vibration signals. The first approach is to reduce the frequency of the current signal to the same as the vibration signal. We used the decimation of the current signal to dilute its high sampling frequency to match the low sampling frequency of the vibration signal without interfering with the original time sequencing features(Sokolovic, Jovanovic, & Damnjanovic, 2004). The second approach is to magnify the frequency of a vibration signal to the same frequency as the current signal. We conducted the unisizing process through data interpolation on vibration signal using

the spline interpolation method (Ouamane, Boutellaa, Bengherabi, Taleb-Ahmed, & Hadid, 2017; Sencer, Dumanli, & Yamada, 2018). The univariate spline method creates a function between fixed data points and places in a judicious selection of additional points that can fit a smooth curve passing through all data points. As a result, the interpolated vibration data has an equally high frequency to current data and comparatively higher similarity than linear data interpolation (Butzer, Fischer, & Stens, 1990). Subsequently, the two approaches are utilized in two out of four input datasets that combine current and vibration signals to generate two sub-datasets each.

Therefore, we finalized a total of six types of input datasets after data transformation: (1) current signal, (2) vibration signal, (3) current and three-dimensional vibration signal with low frequency, (4) current and three-dimensional vibration signal with high frequency, (5) current and summed vibration signal with low frequency, and (6) current and summed vibration signal with high frequency. The output from selected deep learning models using each type of input dataset has similar format to the input dataset. For example, the outcome, which is predicted signal, using input type (1), also is a time series dataset of current signal with high frequency.

4.3.3. Deep Learning Model Development and Training

After the transformation of the datasets, each dataset is further processed by the first-derivative method. Using the first-derivative transformed data and the criteria first introduced in Chapter III, we assigned “normal operation” or “clogging event” labels to each data point. Briefly, the two criteria are: (1) a threshold first-derivative value of 0.05 mA/s and -0.02 m/s2 for the current and vibration signals, respectively (criteria #1); and (2) 90% of signal data points maintaining the selected threshold values over a 5 s window (criteria #2). If a data point satisfies both criteria, it is labeled as a “clogging event”. If a data point does not satisfy both criteria, it is labeled as “normal

operation". Using the two criteria, we can differentiate the normal operation and clogging event regions in the datasets and assign contrasting labels for the deep learning model's training processes. To achieve the goal of predicting a clogging event, we defined the prediction logic of forecasting the conveyance conditions for the next 10 data points based on the previous 20 points of all signals. Generally, labeling is necessary for deep learning models for data classification and prediction (Q. Zhu, Du, Turkbey, Choyke, & Yan, 2017; Z. Zhu, Su, & Zhou, 2019). Subsequently, we individually applied two deep learning approaches, Convolutional Neural Networks (CNNs) and Gated Recurrent Unit (GRU), to grasp the unique features represented by a clogging event and evaluate how well the two approaches perform in classifying and predicting clogging events based on current and vibration signals. The reason we chose these two models are: for CNN, although it is more commonly used for spatial or 2D image analysis, but it also can be applied for 1D data to extract information along the time domain with cheaper computational cost to RNNs and independent to the learning history from previous time series data (Selvin, Vinayakumar, Gopalakrishnan, Menon, & Soman, 2017); for GRU, it is similar to LSTM, which is a special kind of RNNs that well-suited for processing, classifying, and predicting on time series data, with simpler structure (Yamak, Yujian, & Gadosey, 2019). These approaches are different in how they internally carry out classification or prediction, but their analytical logic is somewhat similar (Garcia-Ramirez et al., 2014; Yanming Guo et al., 2016; Lu, Li, Ren, & Miao, 2016). The analytical logic essentially consists of two parts, the model training part and the model testing part (Yanming Guo et al., 2016). The model testing is discussed in the next section. In the model training part, the deep learning model utilizes all the data fed into the model and "learn" from differences between data points with different labels (Goodfellow, Bengio, & Courville, 2016). Then, in the model testing part, the trained model utilizes a new dataset that is called testing data

and consists of predefined labels to validate the model classification and prediction ability by comparing the predefined labels as well as the future predicted current and vibration signals (Goodfellow et al., 2016).

Initially, the continuous time-series data obtained from the conveyor system is randomly split into two groups called training dataset and testing dataset with a ratio of 9:1, which is an intermediate value from similar studies (El-Kenawy et al., 2021; Guimarães & Shiguemori, 2019; Nguyen et al., 2021). The training dataset with its predefined labels is fed into each selected deep learning algorithm to carry out the mean, standard deviation, variance, and amplitude calculation from each status for comparison and to construct classification and prediction rules. Afterward, the testing dataset is employed to ascertain how well the model classified each data point by comparing the predefined and the model's assigned labels on the data points during the training process. By comparing the model's assigned labels as it learns and the predefined labeling information in the input training data, we can determine the labeling accuracy, indicating how well the algorithm is trained. Typically, principal component analysis (PCA) is used to assess data suitability by selecting the most relevant variables (Yang, Li, Wang, Ainapure, & Lee, 2020). However, the datasets used in this experiment only contain two variables, current and vibration. Therefore, we omitted PCA in this experiment. Figure B-1 in Appendix B shows the steps involved in the clogging prediction based on deep learning algorithms.

Additionally, a loss function helps evaluate the performance of the selected models during the training process (Voulodimos, Doulamis, Doulamis, & Protopapadakis, 2018). In the context of machine learning or deep learning, the loss function is essentially the optimization objective function that must be minimized through iterative training cycles or epochs. In this study, we used

the Mean Squared Error (MSE) for the CNN and GRU models as the governing function to generate the loss function matrix. The mean squared error is defined with Equation 4.1:

$$MSE = \frac{1}{n}\sum_{l=1}^{n}\left(\widehat{Y}_l - Y_l\right)^2, \tag{4.1}$$

where n is the size of training samples, and $\widehat{Y}_l$ and Y_l are the model's assigned and analyzed labels based on model training, respectively. The MSE value is calculated after each training iteration by CNN and GRU model, and eventually, a loss function map is constructed that depicts how well each model minimized the MSE over several epochs.

4.3.3.1. Model Testing and Clogging Prediction

After the CNN and GRU models have been trained, we assessed their clogging prediction ability. We used two approaches in the deep learning realm that are commonly use in time series data analysis (Adams, Rahmim, & Tang, 2021; Gao et al., 2020; Yiming Guo, Zhou, & Zhang, 2021; Mao, Zhang, Wang, Chu, & Yuan, 2021), to forecast or predict conveyance conditions for the next 10 data points based on the previous 20 points of all signals. The underlying assumption for the forecasting method is that the time sequence in a defined future time has the same condition as the current time sequence condition (Qiu, Ren, Suganthan, & Amaratunga, 2017; Shi, Xu, & Li, 2017). This method provides an ideal solution to short-term time series data forecasting and aligns well with our research goal (Qiu et al., 2017). Specifically, the 20 data points are equivalent to a 10 s time interval of signal for the low-frequency input data and a 0.1 s time interval for the high-frequency input data. By the same logic, the 10 forecasted data points are equivalent to half of the time intervals or 5 s for the low-frequency data and 0.05 s for the high-frequency data. We used a feature map to better visualize the forecasted data and the assignment of normal and clogging

labels (Al-Saffar, Tao, & Talab, 2017). After data forecasting by the deep learning models, the forecasted data contains numerical values of current or vibration signals and the labels associated with each data point. Using the forecasted model output data, we marked the data points representing each region (i.e., normal operation and clogging event regions) and assigned different colors to each label on the feature map to make it easier to visualize the two regions. We calculated the coefficient of determination (R^2) based on the numerical values of signals between the forecasted data and original datasets. We also calculated the labeling accuracy as the number of labels that the models correctly forecast compared to the labels in the original input datasets as a percentage value. The labeling accuracy is defined by Equation 4.2.

$$\text{Labeling accuracy (\%)} = \frac{\text{Number of correct labels}}{\text{Number of all labels}} \times 100, \tag{4.2}$$

4.3.3.2. Model Optimization

We used common values of the CNN and GRU model parameters in the previous section based on our literature survey. However, to further refine and optimize the forecasting power of the proposed CNN and GRU models, we selected a set of model parameters for sensitivity analysis to determine the model parameters that strongly influence performance. The parameters identified through the sensitivity analysis are then further evaluated to rationally select the appropriate values of those parameters to optimize each model's performance. These parameters are common parameters that define the selected deep learning models and can be manipulated in the algorithm to influence the model performance (İnik, Altıok, Ülker, & Koçer, 2021; Y. Li, Wang, & Tian, 2012; F. Wang et al., 2020). The parameters selected and shared by both models include the number of hidden layers (HL), number of iterations (IT), dropout (DO), and learning rate (LR). HL represents all the layers between the input and output layers of the algorithm for processing

the data. IT indicates how many times to repeat the model learning process so it can learn better based on the given input. DO indicates how much of the input dataset is randomly ignored during each learning process to reduce the possibility that one signal data point is picked up several times by the model, which ultimately lowers the chance of data overfitting. Finally, LR is a hyperparameter that controls how much to change the model in response to the estimated error each time the model weights are updated. LR is the parameter that primarily increases the computing time during the training process of the model (Goodfellow et al., 2016; Sarasaen et al., 2021). By optimizing specified parameters in each model, the training and testing processes can be optimized for comparing the CNN and GRU models based on their loss function from the training process and signal and label prediction from the testing process. We used up to seven levels of values for each parameter during the sensitivity analysis: the initial value (0) and three levels of changed values in the positive and negative direction (±1, ±2, and ±3). We assigned all seven levels for HL and IT due to the flexibility of variation, six levels for DO, and three levels for LR due to their available variation ranges.

After conducting the sensitivity analysis, we selected the three parameters that showed the maximum variance over the sensitivity analysis: HL, IT, and DO. We then further optimized these parameters using a response surface methodology (RSM) (Khuri & Mukhopadhyay, 2010). The RSM allows us to optimize the response variable, i.e., the loss or MSE, by finding the relation between the response and the three independent predictor variables or parameters selected through the sensitivity analysis (Myers, Montgomery, & Anderson-Cook, 2016). We chose the Box-Behnken design as postulated by Box and Behnken (Box & Behnken, 1960) for applying the RSM. The Box–Behnken design represents a class of rotatable or almost rotatable second-order design, and for a three-factor system, as in our research, requires a lower number of variable combinations

than a central composite design (Ferreira et al., 2007). For our Box-Behnken design, we had three values for each predictor variable: the initial value (0) and one level in the positive and negative direction (±1). The total number of runs is 15, including 3 center runs. The Box-Behnken RSM results were analyzed statistically by an analysis of variance (ANOVA) at an alpha level of 0.05 to determine the statistically significant terms and estimate the fitness of the regression models described by Equation 4.4.

$$Y_i = \beta_o + \beta_1(HL) + \beta_2(IT) + \beta_3(DO) + \beta_{11}(HL)^2 + \beta_{22}(IT)^2 + \beta_{33}(DO)^2\beta_{12}(HL)(IT) + \beta_{13}(HL)(IT) + \beta_{23}(IT)(DO) + \varepsilon_i \quad (4.4)$$

We analyzed the residuals of the model to ascertain the model's suitability. Finally, we generated response surface plots to examine the individual and combined effects on the parameters on the loss. Based on the response surface plots, a parameter combination with specific values for each parameter is concluded with the lowest MSE value that indicates the deep learning models can have the best training performance when using such parameter combination to tune the model algorithm.

Table 4-1 shows the combinations of the parameters for each run using the Box-Behnken design. We used a second-order regression model for estimating the responses. The model is based on the generalized second-order Taylor series approximation described by Equation 4.3 (Mante & Agblevor, 2011).

$$\begin{aligned} Y_i &= \beta_o + \beta_1 x_{i1} + \beta_2 x_{i2} + \cdots + \beta_k x_{ik} + \beta_{11} x_{i1}^2 + \beta_{22} x_{i2}^2 \ldots + \beta_{kk} x_{ik}^2 + \beta_{12} x_{i1} x_{i2} + \beta_{13} x_{i1} x_{i3} \\ &\quad + \cdots + \beta_{k-1,k} x_{i,k-1} x_{ik} + \varepsilon_i \\ &= \beta_o + \sum_{j=1}^{k} \beta_j x_{ij} + \sum_{j=1}^{k} \beta_{jj} x_{ij}^2 + \sum_{j=1}^{k-1} \sum_{j'>j}^{k} \beta'_{jj} x_{ij} x'_{ij} + \varepsilon_i \,, \end{aligned} \quad (4.3)$$

The Box-Behnken RSM results were analyzed statistically by an analysis of variance (ANOVA) at an alpha level of 0.05 to determine the statistically significant terms and estimate the fitness of the regression models described by Equation 4.4.

$$Y_i = \beta_o + \beta_1(HL) + \beta_2(IT) + \beta_3(DO) + \beta_{11}(HL)^2 + \beta_{22}(IT)^2 + \beta_{33}(DO)^2\beta_{12}(HL)(IT) + \beta_{13}(HL)(IT) + \beta_{23}(IT)(DO) + \varepsilon_i \quad (4.4)$$

We analyzed the residuals of the model to ascertain the model's suitability. Finally, we generated response surface plots to examine the individual and combined effects on the parameters on the loss. Based on the response surface plots, a parameter combination with specific values for each parameter is concluded with the lowest MSE value that indicates the deep learning models can have the best training performance when using such parameter combination to tune the model algorithm.

Table 4-1. Box-Behnken experimental design.

Run	Independent Variables			Design Patterns		
	HL	IT	DO	x_1	x_2	x_3
1	40	20	0.2	-1	-1	0
2	40	80	0.2	-1	1	0
3	160	20	0.2	1	-1	0
4	160	80	0.2	1	1	0
5	40	50	0.1	-1	0	-1
6	40	50	0.3	-1	0	1
7	160	50	0.1	1	0	-1
8	160	50	0.3	1	0	1
9	100	20	0.1	0	-1	-1
10	100	20	0.3	0	-1	1
11	100	80	0.1	0	1	-1
12	100	80	0.3	0	1	1
13	100	50	0.2	0	0	0
14	100	50	0.2	0	0	0
15	100	50	0.2	0	0	0

HL = hidden layers, IT = iterations, and DO = dropout

4.4. Results and Discussions

4.4.1. Clogging Analysis

Figure 4-3 shows the current and vibration signals of three biomass materials and three conveyance statuses. Each conveyance status subplot in Figure 4-3 represents the mean of 20 runs straddled by a plus and minus one standard deviation region. The total observations include 12,000 and 120 data points for the current and vibration signals, respectively. The baseline and normal conveyance status runs are consistent with our results previously presented in Chapter III. During baseline and normal conveyance status runs, the current signal is relatively steady with a mean of 7.78 mA and standard deviation of 0.04 mA. Similarly, the vibration signal is relatively steady with a mean of 1.24 m/s^2 and standard deviation of 0.015 m/s^2 during normal operation. In the abnormal conveyance status runs, a clogging event is guaranteed in each conveyance run since the conveyor has no outlet as previously mentioned. Consequently, after first starting with signal values similar to values observed for the baseline and normal conveyance status, all current signal curves show an obvious increase representative of the clogging formation until reaching its plateau, which is about 16 mA for all three materials. The abnormal conveyance status signals of switchgrass and hybrid poplar showed a large and abrupt shift from the baseline and normal signals at the onset of clogging (~ t >22s), whereas switchgrass showed an earlier shift (~ t >15s). Switchgrass and hybrid poplar had a steeper slope and achieved plateau and minima earlier than loblolly pine for both current and vibration signals, respectively, indicating a faster clogging event development before reaching the full clogging region. Loblolly pine demonstrated a more gradual clogging development compared to switchgrass and hybrid poplar, which resulted in a longer clogging development duration. All behavioral observations on the current plots are also visible in the vibration plots, which suggest that the differences are due to the materials. However,

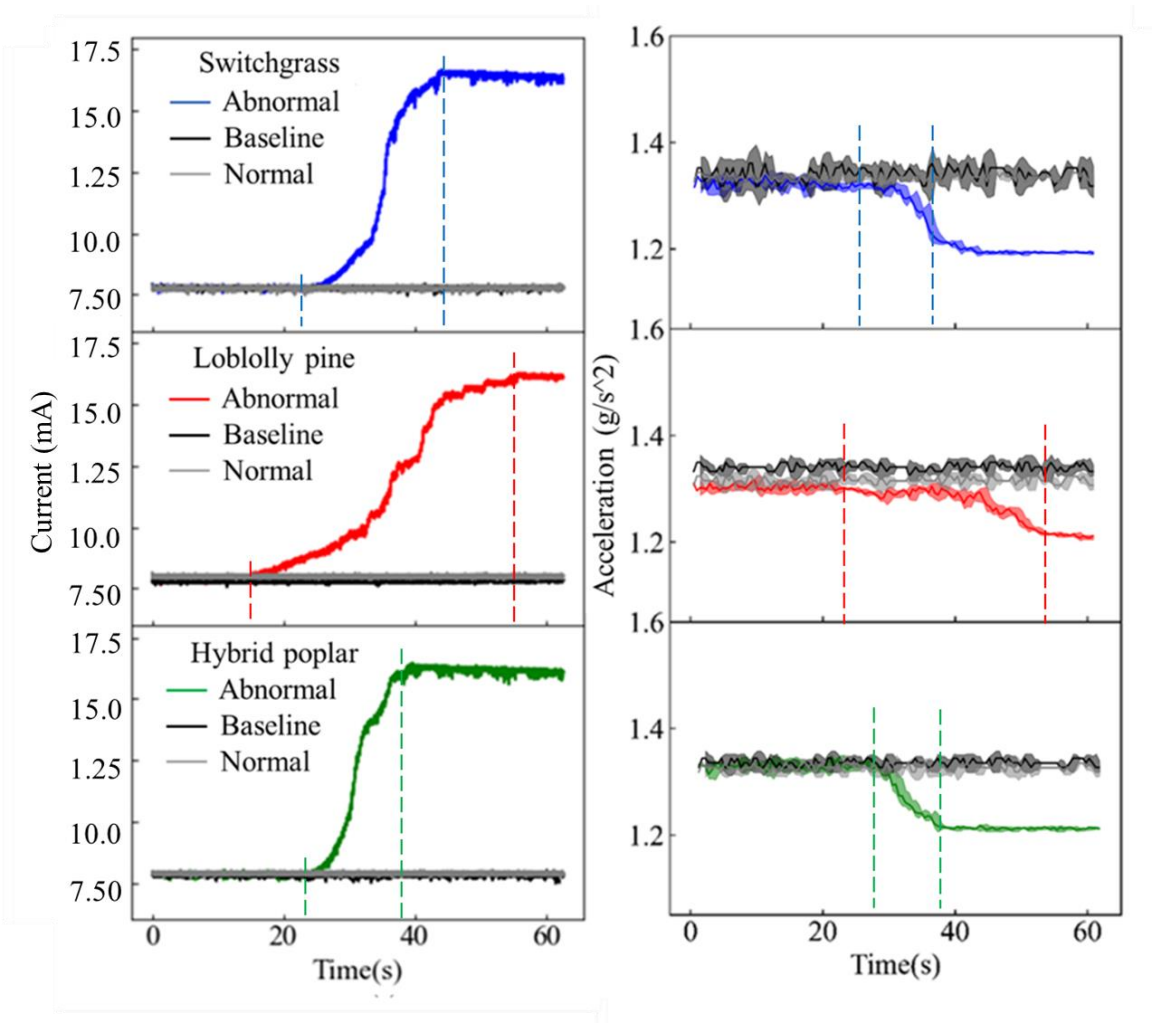

Figure 4-3. Mean results of the current (left) and vibration (right) signatures of three biomass materials and the control group for 20 runs. Each mean is displayed as a thick colored line and was derived from 20 individual runs. The standard deviation region is represented by the overlayed semi-transparent shaded regions with the same color as the mean. Note: On the current signals, the standard deviation regions are plotted but are not easily discerned.

we did not further investigate these differences, given the scope of this project.

4.4.2. Model Training

Figure 4-4 shows the loss functions using the six input datasets we defined in material and methods section for the CNN and GRU models. A total number of 300 epochs or iterative training cycles are conducted to generate the loss function curve. The loss or Mean Squared Error (MSE) is an indicator that shows how well the algorithm has learned from the training data based on predicted labels and actual labels associated with the input training data. The loss decreases during the training process, eventually becoming steady and reaching an asymptotic minimum, which means the model has learned the training data to its best performance capacity, and the training should be stopped to avoid overfitting by further decreasing the loss or MSE (C. Zhang, Vinyals, Munos, & Bengio, 2018). Both algorithms start with a relatively high loss at the first epoch or training cycle that is greater than 1. However, the loss curves of both models converge very fast in the initial five epochs. Subsequently, the loss drops quickly to lower than 0.5 and stays at that level with a relatively steady trend after 10 epochs. This phenomenon appears to be present for both models, indicating that both algorithms learn quickly based on the training dataset (He, Shao, Zhong, & Zhao, 2020; Mao et al., 2021). Additionally, the decrease in the loss curve for all plots slows down significantly after the 10th iteration. This may indicate that overfitting has occurred with repetitive training(Adams et al., 2021; T. Zhang, Liu, Wei, & Zhang, 2021). However, we need further validation data to confirm this theory. We compared the MSE scores of all the sub-datasets when it became steady and observed the following: input sub-datasets (4) showed a much smaller MSE score and was therefore excluded from consideration; On the other hand, input sub-datasets (3) yielded a similar result as sub-dataset (1). However, for sub-dataset (3), the vibration signal has been interpolated to 100 times its original data size to match the current signal, resulting

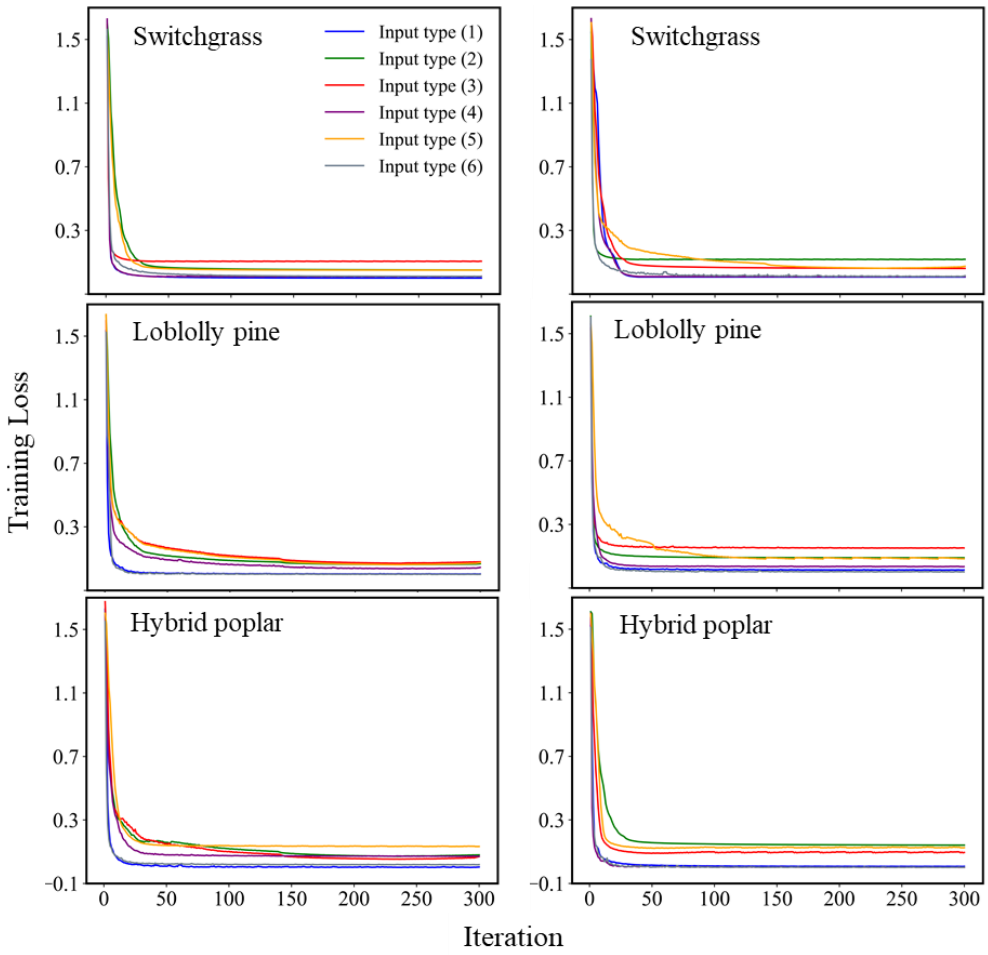

Figure 4-4. Loss functions of the six input datasets using the CNN (left) and GRU (right) models.

in many more simulated data points. Sub-datasets (5) and (6) were also evaluated. Sub-dataset (5) showed slightly higher scores than type sub-dataset (1) using the GRU model, and sub-dataset (6) had lower scores than sub-dataset (1). However, similar to the sub-dataset (3), sub-datasets (5) have an extremely high amount of simulated data due to the interpolation of the vibration signal. Hence, we decided to eliminate sub-datatypes (5) and (6). Consequently, we kept sub-datasets (1) and (2) for further evaluation. Finally, when evaluating sub-datasets (1) and (2) based on the MSE scores, we observed that the highest score occurred for sub-dataset (1), indicating that the deep learning models show the best forecasting performance for the raw current signal, which has not been extrapolated or decimated. Thus, we only use the raw current signal for further analytical procedures.

4.4.3. Model Testing and Clogging Prediction

Figure 4-5 and Figure 4-6 show the forecasted data generated by the CNN and GRU models, respectively. As mentioned previously, forecasting is achieved by taking 20 previous data points to predict the next 10 data points. By comparing the R^2 score of current signals from each material, CNN showed overall higher values than GRU, which indicates a better forecasting capability than GRU model. One particular example is the forecasted current signal of both models using hybrid poplar, which CNN has R^2 score of 0.985 and GRU is 0.747.

Figure 4-7 shows the 2D feature map using the current signal for the CNN and GRU model. We assigned 12,000 total observations with labeling information according to the first derivative transformation method and two criteria that defined in Chapter III to find the precise data point that separates normal region and clogging status, the two criteria are: (1) a threshold first-derivative value of 0.05 mA/s and -0.02 m/s^2 for the current and vibration signals, respectively (criteria #1);

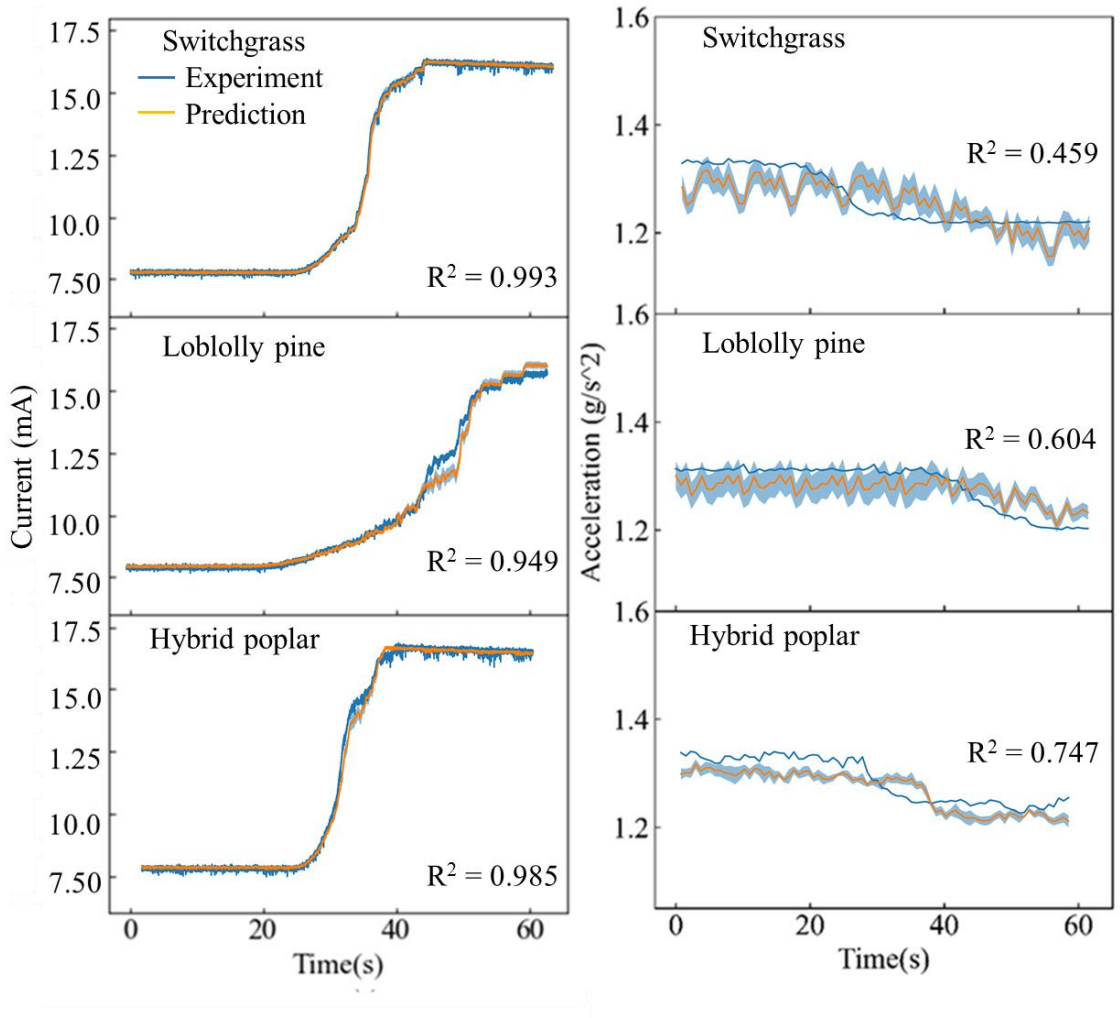

Figure 4-5. CNN model: predicted signal using current (left) and vibration (right) signals for three biomass materials.

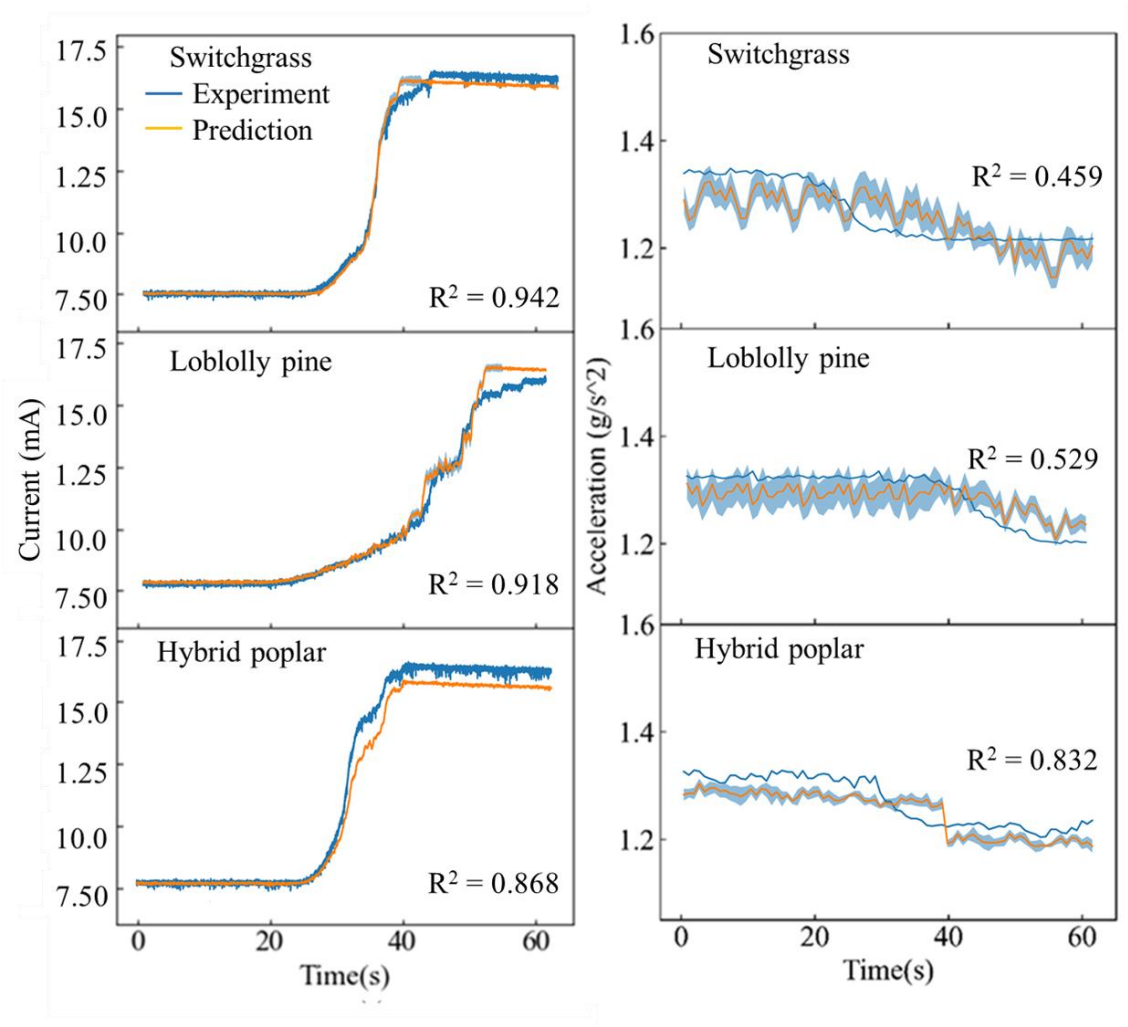

Figure 4-6. GRU model: predicted signal using current (left) and vibration (right) signals for three biomass materials. *Note*: Figure 4-5 presents the predicted signal using 1 run of current or vibration signal from the total 20 runs of each material.

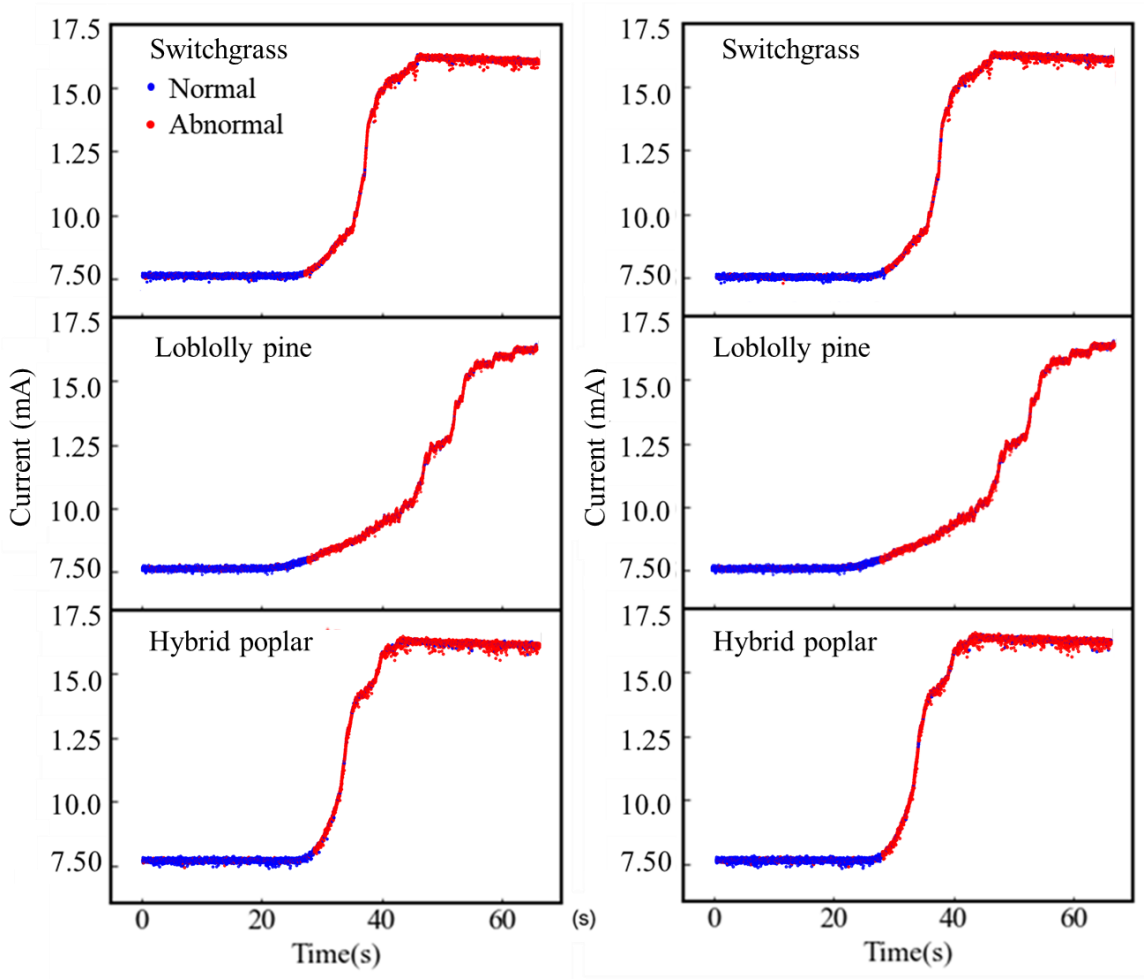

Figure 4-7. Feature maps for predicted data using the current signal dataset are based on the CNN (left) and GRU (right) approaches.

and (2) 90% of signal data points maintaining the selected threshold values over a 5 s window (criteria #2). This labeling information is added to the original input dataset as associated information for models to output predicted labeling information based on assigned labels. Therefore, the data points with different colors in the feature map represent the original signals with predicted labels for each status. Generally, the labeling technique is useful to better visualize the model prediction on each status (Bianchini, Maggini, Sarti, & Scarselli, 2005), and the predicted labels can be utilized to compare with the original labels and yield labeling accuracy by calculating the percentage of correctly predicted labels using deep learning models (T. Zhang et al., 2021). According to the figures, both CNN and GRU models are sensitive to recognizing the status changes in current signals, which means they are able to predict the abnormal behavior in the current signal. Overall, both the CNN and GRU models were able to correctly predict whether a point was a normal operation or a clogging event. However, it is important to note that there is a non-negligible number of incorrect predictions. This phenomenon can negatively affect the model prediction performance by generating mistaken clogging recognition decisions due to "wrongly labeled" data points. However, it is possible to refine this shortcoming by optimizing the deep learning model parameters discussed in the later section.

Table 4-2 shows the percentage accuracy for such classification using predicted labels and original labels discussed above. Based on the accuracy results, GRU has an overall higher prediction accuracy of clogging events than CNN. Similarly to forecasted data, the prediction accuracies using the raw current signal and a combination of current and vibration vector sum signals are indistinguishable. However, considering that the vibration signal has been interpolated 100 times to match the population of the current signal, we suspect the vibration signal to be different from the original vibration signal. This might have contributed to a less convincing result

Table 4-2. Percentage accuracy of the clogging prediction using raw current signal by the deep learning network models.

	Mean (standard deviation)		
	SG	PI	PO
CNN	80.51(±1.42)	82.24(±1.67)	81.67(±1.15)
GRU	82.49(±0.98)	81.99(±1.01)	83.98(±0.88)

Note: SG = switchgrass, PI = loblolly pine, PO = hybrid poplar.

than the results using the current signal only. Therefore, we concluded that the current signal is more beneficial than other types of input datasets for clogging prediction. By comparing the prediction accuracy values, the GRU model showed overall consistent clogging prediction performance by having lower standard deviation results. Additionally, the GRU model showed higher mean prediction accuracies using switchgrass and hybrid poplar data and only slightly lower using loblolly pine data. Overall, the GRU model showed slightly better prediction performance compared to the CNN model.

4.4.4. Model Optimization

We selected four parameters, namely the number of hidden layers (HL), number of iterations (IT), dropout (DO), and learning rate (LR), for optimizing our CNN and GRU algorithms for the raw current signal data. These parameters can affect mean square error, representing the loss of the predicted signals (Yanming Guo et al., 2016; Lee, Jo, & Hwang, 2017). We take each parameter and vary their values at each level while keeping the rest of the parameters fixed. We used seven levels of values for numbers of hidden layer and iteration, six levels for drop out, and three levels for learning rate. The levels selected are common values used for the tuning procedure (Gao et al., 2020; Y. Wang, Zhang, & Zhang, 2019): the initial value (0) and three levels of changed values in the positive and negative direction (±1, ±2, and ±3). Table 4-3 shows the different values of the tuning parameters.

Figure 4-8 shows the results of the optimization of the CNN and the GRU algorithms using the current signal data. At their initial values, the parameters provided poor forecasting with obvious fluctuations in both the normal operation status and the clogging event status. However, as we continue the parameter tuning process, the fluctuations reduce significantly and accurately

Table 4-3. Tuning parameter values for optimizing CNN and GRU algorithms.

Level	Loss							
	HL		IT		DO		LR	
	CNN	GRU	CNN	GRU	CNN	GRU	CNN	GRU
-3	0.794	0.917	0.923	1.648	-	-	-	-
-2	0.552	0.634	0.652	0.953	0.325	0.163	0.114	0.137
-1	0.348	0.428	0.405	0.563	0.182	0.103	0.145	0.148
0	0.230	0.226	0.313	0.373	0.094	0.097	0.158	0.152
+1	0.199	0.115	0.123	0.175	0.115	0.163	-	-
+2	0.070	0.125	0.118	0.102	0.167	0.197	-	-
+3	0.099	0.117	0.108	0.109	0.269	0.260	-	-

Note: HL = # of hidden layers, IT = iteration, DO = dropout.

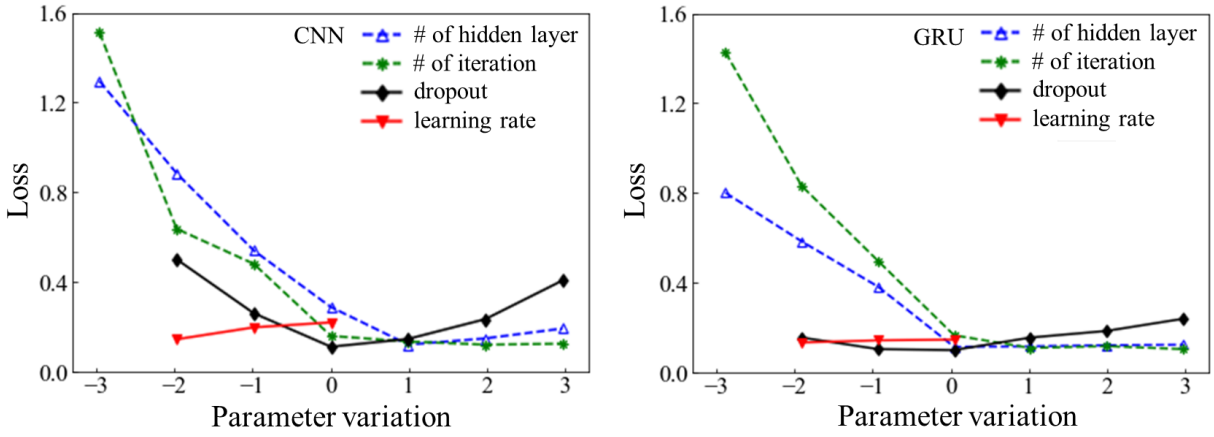

Figure 4-8. Optimized model parameters for predicted data using the current signal dataset based on the CNN (left) and GRU (right) approach.

fit the original data. We can also see that both models obtain excellent forecasting on the timing of the clogging event regardless of the fluctuation severity(Gao et al., 2020; Y. Wang et al., 2019).

Additionally, we performed the Box-Behnken test to determine representative parameter combinations that need to be studied to find the optimal combination with the lowest loss(Nekkaa, Benaissa, Lalaouna, Mutelet, & Canabady-Rochelle, 2021). Since the learning rate did not show obvious changes in loss response during the previous tuning process, we performed a Box-Behnken design based on the other three parameters. Figure 4-9 shows the surface plots for each parameter examined with the Box-Behnken test design combinations. Based on the Box-Behnken three factorial design, the surface plots show the correlated effect on loss of every two parameters together and result in the hold value that is the optimal condition for each parameter. As a result, the optimal combination for both CNN and GRU models is 100 hidden layers, 50 iterations, and a dropout rate of 0.2. The associated losses by employing the optimal parameter combination for CNN and GRU model are 0.052 and 0.032, respectively.

By employing the optimal parameter combination for both CNN and GRU models, we regenerated the forecasted current signals with R^2 value calculated to compare the prediction performance to unoptimized models prior to the optimization process. Figure 4-10 shows the forecasted current signal generated by optimized CNN and GRU models, respectively. Based on the R^2 values between unoptimized models and optimized models using same materials, both optimized models showed higher R^2 values compared to unoptimized models, which indicates that the optimization of selected parameters has a positive effect on improving the model forecasting ability.

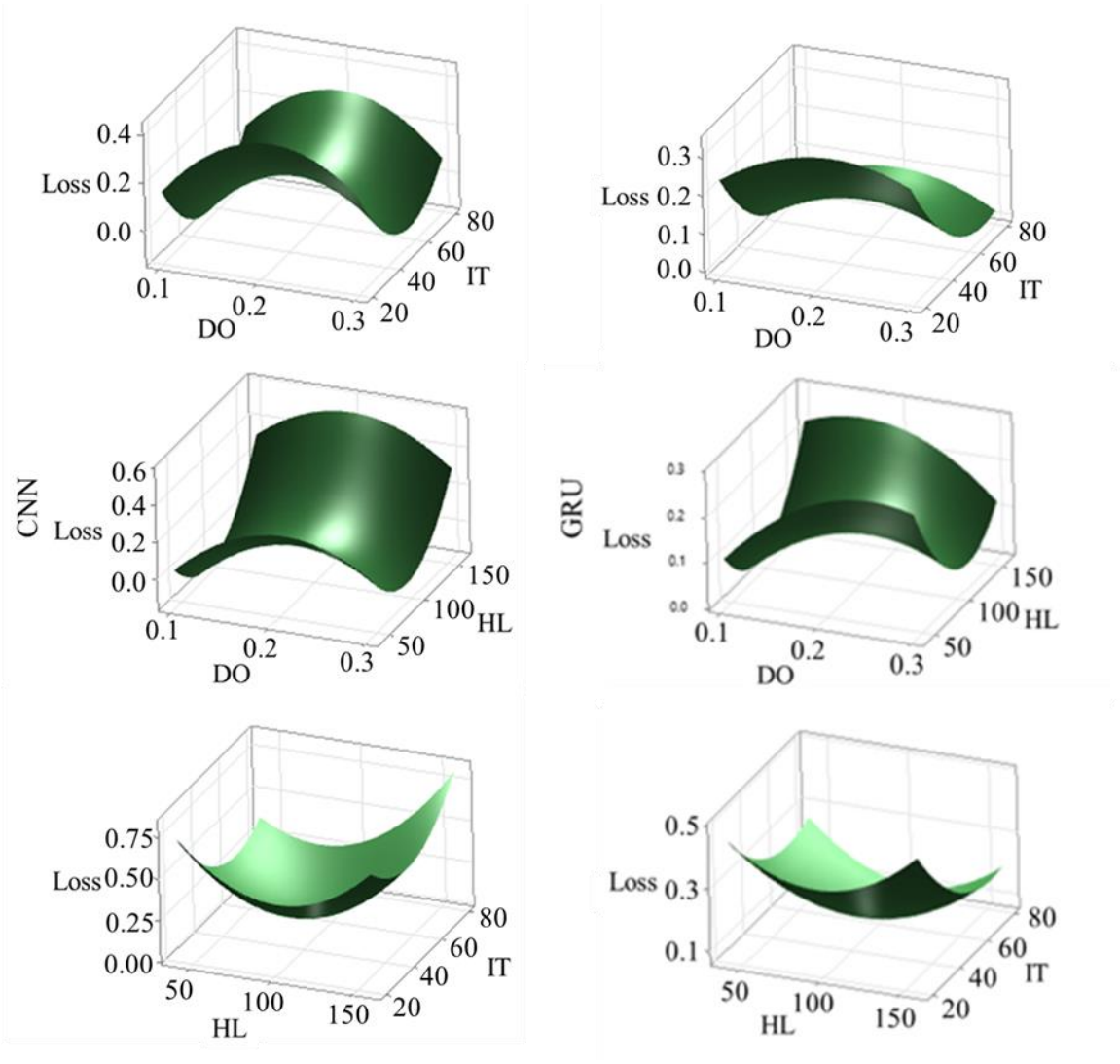

.

Figure 4-9. Surface plots by Box-Behnken design for optimal parameter combination selection.

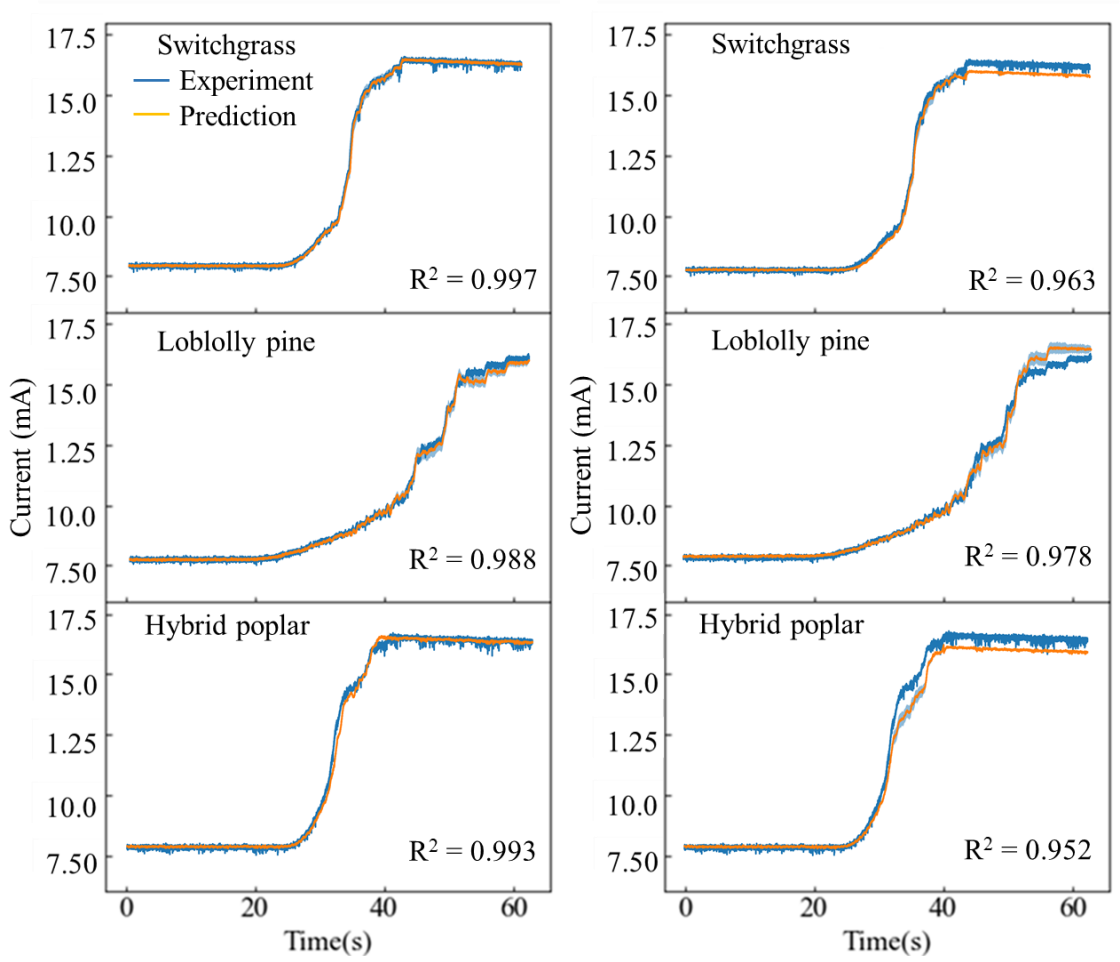

Figure 4-10. Predicted current signal using optimal model parameter combination that determined from Box-Behnken design.

4.5. Conclusions

This paper presents a deep learning-based framework for clogging prediction in screw conveyors using CNN and GRU models. Each proposed model consists of the data transformation module, the deep learning algorithmic module, and the optimization module. We validated the performance of each proposed model by clogging simulations in a custom lab-scale screw conveyor for metering different biomass materials. In addition, we provided various scenarios of input datasets into the models to verify the stability and potential of the proposed deep learning models. According to the results, the proposed GRU and CNN models showed similar performances in labeling accuracy that we experimented with, and the GRU model showed lower clogging prediction performance among all input datasets from switchgrass, loblolly pine, and hybrid poplar. Finally, the model optimization results show that by further tuning the model parameters and using the Box-Behnken design to find local or global optimal parameter combinations, we can potentially improve the accuracy and stability of the model even further.

References

Adams, M. P., Rahmim, A., & Tang, J. (2021). Improved motor outcome prediction in Parkinson's disease applying deep learning to DaTscan SPECT images. *Computers in Biology and Medicine, 132*, 104312. doi:https://doi.org/10.1016/j.compbiomed.2021.104312

Al-Saffar, A. A. M., Tao, H., & Talab, M. A. (2017, 2017). *Review of deep convolution neural network in image classification*.

Aloysius, N., & Geetha, M. (2017, 2017). *A review on deep convolutional neural networks*.

Altug, S., Mo-Yuen, C., & Trussell, H. J. (1999). Fuzzy inference systems implemented on neural architectures for motor fault detection and diagnosis. *IEEE Transactions on Industrial Electronics, 46*(6), 1069-1079. doi:10.1109/41.807988

Alzubaidi, L., Zhang, J., Humaidi, A. J., Al-Dujaili, A., Duan, Y., Al-Shamma, O., . . . Farhan, L. (2021). Review of deep learning: Concepts, CNN architectures, challenges, applications, future directions. *Journal of big Data, 8*(1), 1-74.

Avci, O., Abdeljaber, O., Kiranyaz, S., Hussein, M., Gabbouj, M., & Inman, D. J. (2021). A review of vibration-based damage detection in civil structures: From traditional methods to Machine Learning and Deep Learning applications. *Mechanical Systems and Signal Processing, 147*, 107077. doi:https://doi.org/10.1016/j.ymssp.2020.107077

Azamfar, M., Singh, J., Bravo-Imaz, I., & Lee, J. (2020). Multisensor data fusion for gearbox fault diagnosis using 2-D convolutional neural network and motor current signature analysis. *Mechanical Systems and Signal Processing, 144*, 106861. doi:https://doi.org/10.1016/j.ymssp.2020.106861

Bianchini, M., Maggini, M., Sarti, L., & Scarselli, F. (2005). Recursive neural networks for processing graphs with labelled edges: Theory and applications. *Neural networks, 18*(8), 1040-1050.

Box, G. E. P., & Behnken, D. W. (1960). Some new three level designs for the study of quantitative variables. *Technometrics, 2*(4), 455-475.

Butzer, P. L., Fischer, A., & Stens, R. L. (1990). Generalized sampling approximation of multivariate signals; theory and some applications. *Note di Matematica, 10*(suppl. 1), 173-191.

Chow, M., Sharpe, R. N., & Hung, J. C. (1993). On the application and design of artificial neural networks for motor fault detection. II. *IEEE Transactions on Industrial Electronics, 40*(2), 189-196. doi:10.1109/41.222640

Chung, J., Gulcehre, C., Cho, K., & Bengio, Y. (2014). Empirical evaluation of gated recurrent neural networks on sequence modeling. *arXiv preprint arXiv:1412.3555*.

Deng, Y., Wang, L., Jia, H., Tong, X., & Li, F. (2019). A sequence-to-sequence deep learning architecture based on bidirectional GRU for type recognition and time location of combined power quality disturbance. *IEEE Transactions on Industrial Informatics, 15*(8), 4481-4493.

Dutta, A., Sahir, A., Tan, E., Humbird, D., Snowden-Swan, L. J., Meyer, P. A., . . . Lukas, J. (2015). *Process design and economics for the conversion of lignocellulosic biomass to hydrocarbon fuels: Thermochemical research pathways with in situ and ex situ upgrading of fast pyrolysis vapors*. Retrieved from

El-Kenawy, E.-S. M., Mirjalili, S., Ibrahim, A., Alrahmawy, M., El-Said, M., Zaki, R. M., & Eid, M. M. (2021). Advanced Meta-Heuristics, Convolutional Neural Networks, and Feature

Selectors for Efficient COVID-19 X-Ray Chest Image Classification. *IEEE Access, 9*, 36019-36037.

Falcon, A. J., Lupon, M., Abellanas, E. H., Lopez, P., Latorre, F., Pratas, F. C., & Tournavitis, G. (2016). Weight-shifting mechanism for convolutional neural networks. In: Google Patents.

Ferreira, S. L. C., Bruns, R. E., Ferreira, H. S., Matos, G. D., David, J. M., Brandão, G. C., . . . Souza, A. S. (2007). Box-Behnken design: an alternative for the optimization of analytical methods. *Analytica chimica acta, 597*(2), 179-186.

Fuessel, D., & Isermann, R. (2000). Hierarchical motor diagnosis utilizing structural knowledge and a self-learning neuro-fuzzy scheme. *IEEE Transactions on Industrial Electronics, 47*(5), 1070-1077. doi:10.1109/41.873215

Gao, S., Huang, Y., Zhang, S., Han, J., Wang, G., Zhang, M., & Lin, Q. (2020). Short-term runoff prediction with GRU and LSTM networks without requiring time step optimization during sample generation. *Journal of Hydrology, 589*, 125188. doi:https://doi.org/10.1016/j.jhydrol.2020.125188

Garcia-Ramirez, A. G., Morales-Hernandez, L. A., Osornio-Rios, R. A., Benitez-Rangel, J. P., Garcia-Perez, A., & Romero-Troncoso, R. d. J. (2014). Fault detection in induction motors and the impact on the kinematic chain through thermographic analysis. *Electric Power Systems Research, 114*, 1-9. doi:https://doi.org/10.1016/j.epsr.2014.03.031

Glowacz, A., Glowacz, W., Glowacz, Z., & Kozik, J. (2018). Early fault diagnosis of bearing and stator faults of the single-phase induction motor using acoustic signals. *Measurement, 113*, 1-9. doi:https://doi.org/10.1016/j.measurement.2017.08.036

Goodfellow, I., Bengio, Y., & Courville, A. (2016). *Deep learning*: MIT press.

Guimarães, L. N. F., & Shiguemori, E. H. (2019). Hybrid adaptive computational intelligence-based multisensor data fusion applied to real-time UAV autonomous navigation. *Inteligencia Artificial, 22*(63), 162-195.

Guo, Y., Liu, Y., Oerlemans, A., Lao, S., Wu, S., & Lew, M. S. (2016). Deep learning for visual understanding: A review. *Neurocomputing, 187*, 27-48. doi:https://doi.org/10.1016/j.neucom.2015.09.116

Guo, Y., Zhou, Y., & Zhang, Z. (2021). Fault diagnosis of multi-channel data by the CNN with the multilinear principal component analysis. *Measurement, 171*, 108513. doi:https://doi.org/10.1016/j.measurement.2020.108513

He, Z., Shao, H., Zhong, X., & Zhao, X. (2020). Ensemble transfer CNNs driven by multi-channel signals for fault diagnosis of rotating machinery cross working conditions. *Knowledge-Based Systems, 207*, 106396. doi:https://doi.org/10.1016/j.knosys.2020.106396

Hochreiter, S., & Schmidhuber, J. (1997). Long short-term memory. *Neural computation, 9*(8), 1735-1780.

Hou, Q. F., Dong, K. J., & Yu, A. B. (2014). DEM study of the flow of cohesive particles in a screw feeder. *Powder Technology, 256*, 529-539. doi:https://doi.org/10.1016/j.powtec.2014.01.062

Hu, Q., Si, X.-S., Zhang, Q.-H., & Qin, A.-S. (2020). A rotating machinery fault diagnosis method based on multi-scale dimensionless indicators and random forests. *Mechanical Systems and Signal Processing, 139*, 106609. doi:https://doi.org/10.1016/j.ymssp.2019.106609

Ince, T., Kiranyaz, S., Eren, L., Askar, M., & Gabbouj, M. (2016). Real-time motor fault detection by 1-D convolutional neural networks. *IEEE Transactions on Industrial Electronics, 63*(11), 7067-7075.

İnik, Ö., Altıok, M., Ülker, E., & Koçer, B. (2021). MODE-CNN: A fast converging multi-objective optimization algorithm for CNN-based models. *Applied Soft Computing, 109*, 107582. doi:https://doi.org/10.1016/j.asoc.2021.107582

Jha, S. K., Bilalovic, J., Jha, A., Patel, N., & Zhang, H. (2017). Renewable energy: Present research and future scope of Artificial Intelligence. *Renewable and Sustainable Energy Reviews, 77*, 297-317.

Johanson, K. (2004). Rathole stability analysis for aerated powder materials. *Powder technology, 141*(1-2), 161-170.

Kalchbrenner, N., Grefenstette, E., & Blunsom, P. (2014). A convolutional neural network for modelling sentences. *arXiv preprint arXiv:1404.2188*.

Khuri, A. I., & Mukhopadhyay, S. (2010). Response surface methodology. *Wiley interdisciplinary reviews: computational statistics, 2*(2), 128-149.

Konar, P., & Chattopadhyay, P. (2011). Bearing fault detection of induction motor using wavelet and Support Vector Machines (SVMs). *Applied Soft Computing, 11*(6), 4203-4211. doi:https://doi.org/10.1016/j.asoc.2011.03.014

Lawrence, S., Giles, C. L., Tsoi, A. C., & Back, A. D. (1997). Face recognition: A convolutional neural-network approach. *IEEE transactions on neural networks, 8*(1), 98-113.

Lee, Y. O., Jo, J., & Hwang, J. (2017, 11-14 Dec. 2017). *Application of deep neural network and generative adversarial network to industrial maintenance: A case study of induction motor fault detection.* Paper presented at the 2017 IEEE International Conference on Big Data (Big Data).

Li, X., Li, J., Qu, Y., & He, D. (2019). Gear Pitting Fault Diagnosis Using Integrated CNN and GRU Network with Both Vibration and Acoustic Emission Signals. *Applied Sciences, 9*(4), 768.

Li, Y., Wang, L., & Tian, W. (2012). *The Optimization of Weighing and Feeding System for Powder in Mixer Feeding System.* Paper presented at the Key Engineering Materials.

Lu, N., Li, T., Ren, X., & Miao, H. (2016). A deep learning scheme for motor imagery classification based on restricted boltzmann machines. *IEEE transactions on neural systems and rehabilitation engineering, 25*(6), 566-576.

Mante, O. D., & Agblevor, F. A. (2011). Parametric study on the pyrolysis of manure and wood shavings. *Biomass and Bioenergy, 35*(10), 4417-4425.

Mao, X., Zhang, F., Wang, G., Chu, Y., & Yuan, K. (2021). Semi-random subspace with Bi-GRU: Fusing statistical and deep representation features for bearing fault diagnosis. *Measurement, 173*, 108603. doi:https://doi.org/10.1016/j.measurement.2020.108603

Miao, Z., Grift, T. E., Hansen, A. C., & Ting, K. C. (2014). Flow performance of ground biomass in a commercial auger. *Powder technology, 267*, 354-361.

Minglani, D., Sharma, A., Pandey, H., Dayal, R., Joshi, J. B., & Subramaniam, S. (2020). A review of granular flow in screw feeders and conveyors. *Powder Technology, 366*, 369-381. doi:https://doi.org/10.1016/j.powtec.2020.02.066

Mutlu, A. Y., & Yucel, O. (2018). An artificial intelligence based approach to predicting syngas composition for downdraft biomass gasification. *Energy, 165*, 895-901.

Myers, R. H., Montgomery, D. C., & Anderson-Cook, C. M. (2016). *Response surface methodology: process and product optimization using designed experiments*: John Wiley & Sons.

Mysior, M., Koziołek, S., & Rusiński, E. (2018). Problem formulation of screw feeding system of fibrous materials using TRIZ. In *Advances and Impacts of the Theory of Inventive Problem Solving* (pp. 57-64): Springer.

Nachenius, R. W., van de Wardt, T. A., Ronsse, F., & Prins, W. (2015). Residence time distributions of coarse biomass particles in a screw conveyor reactor. *Fuel Processing Technology, 130*, 87-95. doi:https://doi.org/10.1016/j.fuproc.2014.09.039

Nekkaa, A., Benaissa, A., Lalaouna, A. E. D., Mutelet, F., & Canabady-Rochelle, L. (2021). Optimization of the extraction process of bioactive compounds from Rhamnus alaternus leaves using Box-Behnken experimental design. *Journal of Applied Research on Medicinal and Aromatic Plants, 25*, 100345. doi:https://doi.org/10.1016/j.jarmap.2021.100345

Nguyen, Q. H., Ly, H.-B., Ho, L. S., Al-Ansari, N., Le, H. V., Tran, V. Q., . . . Pham, B. T. (2021). Influence of Data Splitting on Performance of Machine Learning Models in Prediction of Shear Strength of Soil. *Mathematical Problems in Engineering, 2021*, 4832864. doi:10.1155/2021/4832864

Nhuchhen, D. R., Basu, P., & Acharya, B. (2014). A comprehensive review on biomass torrefaction. *International Journal of Renewable Energy & Biofuels, 2014*, 1-56.

OSMAN, H. B. (2012). *Granular flow and heat transfer in a screw conveyor heater: a discrete element modeling study*.

Ouamane, A., Boutellaa, E., Bengherabi, M., Taleb-Ahmed, A., & Hadid, A. (2017). A novel statistical and multiscale local binary feature for 2D and 3D face verification. *Computers & Electrical Engineering, 62*, 68-80.

Patel, J. N., Patel, S. P., & Patel, S. S. (2013). Productivity Improvement of Screw Conveyor by Modified Design. *International Journal of Emerging Technology and Advanced Engineering, 3*(1), 492-496.

Pezo, L., Jovanović, A., Pezo, M., Čolović, R., & Lončar, B. (2015). Modified screw conveyor-mixers – Discrete element modeling approach. *Advanced Powder Technology, 26*(5), 1391-1399. doi:https://doi.org/10.1016/j.apt.2015.07.016

Prescott, J. K., & Barnum, R. A. (2000). On powder flowability. *Pharmaceutical technology, 24*(10), 60-85.

Qiu, X., Ren, Y., Suganthan, P. N., & Amaratunga, G. A. J. (2017). Empirical mode decomposition based ensemble deep learning for load demand time series forecasting. *Applied Soft Computing, 54*, 246-255.

Roberts, A. W. (2001). Design considerations and performance evaluation of screw conveyors. *Proceedings of the BELTCON, 11*(11), 263-270.

Sarasaen, C., Chatterjee, S., Breitkopf, M., Rose, G., Nürnberger, A., & Speck, O. (2021). Fine-tuning deep learning model parameters for improved super-resolution of dynamic MRI with prior-knowledge. *Artificial Intelligence in Medicine, 121*, 102196. doi:https://doi.org/10.1016/j.artmed.2021.102196

Selvin, S., Vinayakumar, R., Gopalakrishnan, E. A., Menon, V. K., & Soman, K. P. (2017, 13-16 Sept. 2017). *Stock price prediction using LSTM, RNN and CNN-sliding window model.* Paper presented at the 2017 International Conference on Advances in Computing, Communications and Informatics (ICACCI).

Sencer, B., Dumanli, A., & Yamada, Y. (2018). Spline interpolation with optimal frequency spectrum for vibration avoidance. *CIRP annals, 67*(1), 377-380.

Shi, H., Xu, M., & Li, R. (2017). Deep learning for household load forecasting—A novel pooling deep RNN. *IEEE Transactions on Smart Grid, 9*(5), 5271-5280.

Sievers, D. A., Kuhn, E. M., Thompson, V. S., Yancey, N. A., Hoover, A. N., Resch, M. G., & Wolfrum, E. J. (2020). Throughput, reliability, and yields of a pilot-scale conversion process for production of fermentable sugars from lignocellulosic biomass: a study on feedstock ash and moisture. *ACS Sustainable Chemistry & Engineering*, *8*(4), 2008-2015.

Simard, P. Y., Steinkraus, D., & Platt, J. C. (2003). *Best practices for convolutional neural networks applied to visual document analysis.* Paper presented at the Icdar.

Sokolovic, M., Jovanovic, B., & Damnjanovic, M. (2004, 2004). *Decimation filter design*.

Voulodimos, A., Doulamis, N., Doulamis, A., & Protopapadakis, E. (2018). Deep learning for computer vision: A brief review. *Computational intelligence and neuroscience, 2018*.

Wang, F., Liu, R., Hu, Q., & Chen, X. (2020). Cascade Convolutional Neural Network With Progressive Optimization for Motor Fault Diagnosis Under Nonstationary Conditions. *IEEE Transactions on Industrial Informatics, 17*(4), 2511-2521.

Wang, L., Gong, G., Shi, H., & Liu, H. (2010). *Rotation and gate movement compound control of screw conveyor hydraulic system with disturbance compensation.* Paper presented at the International Conference on Intelligent Robotics and Applications.

Wang, Y., Zhang, H., & Zhang, G. (2019). cPSO-CNN: An efficient PSO-based algorithm for fine-tuning hyper-parameters of convolutional neural networks. *Swarm and Evolutionary Computation, 49*, 114-123. doi:https://doi.org/10.1016/j.swevo.2019.06.002

Yamak, P. T., Yujian, L., & Gadosey, P. K. (2019). *A Comparison between ARIMA, LSTM, and GRU for Time Series Forecasting*. Paper presented at the Proceedings of the 2019 2nd International Conference on Algorithms, Computing and Artificial Intelligence, Sanya, China. https://doi.org/10.1145/3377713.3377722

Yan, J., Oyedeji, O., Leal, J. H., Donohoe, B. S., Semelsberger, T. A., Li, C., . . . Zeng, Y. (2020). Characterizing variability in lignocellulosic biomass-A review. *ACS Sustainable Chemistry & Engineering*.

Yang, Q., Li, X., Wang, Y., Ainapure, A., & Lee, J. (2020). Fault Diagnosis of Ball Screw in Industrial Robots Using Non-Stationary Motor Current Signals. *Procedia Manufacturing, 48*, 1102-1108. doi:https://doi.org/10.1016/j.promfg.2020.05.151

Ye, Z., & Wu, B. (2000, 15-18 Aug. 2000). *A review on induction motor online fault diagnosis.* Paper presented at the Proceedings IPEMC 2000. Third International Power Electronics and Motion Control Conference (IEEE Cat. No.00EX435).

Yu, S., Liu, D., Zhu, W., Zhang, Y., & Zhao, S. (2020). Attention-based LSTM, GRU and CNN for short text classification. *Journal of Intelligent & Fuzzy Systems, 39*(1), 333-340.

Zhang, C., Vinyals, O., Munos, R., & Bengio, S. (2018). A study on overfitting in deep reinforcement learning. *arXiv preprint arXiv:1804.06893*.

Zhang, T., Liu, S., Wei, Y., & Zhang, H. (2021). A novel feature adaptive extraction method based on deep learning for bearing fault diagnosis. *Measurement, 185*, 110030. doi:https://doi.org/10.1016/j.measurement.2021.110030

Zhong, Z., & O'Callaghan, J. (1990). The effect of the shape of the feed opening on the performance of a horizontal screw conveyor. *Journal of Agricultural Engineering Research, 46*, 125-128.

Zhu, Q., Du, B., Turkbey, B., Choyke, P. L., & Yan, P. (2017). *Deeply-supervised CNN for prostate segmentation.* Paper presented at the 2017 international joint conference on neural networks (IJCNN).

Zhu, Z., Su, J., & Zhou, Y. (2019). Improving distantly supervised relation classification with attention and semantic weight. *IEEE Access, 7*, 91160-91168.

CHAPTER V

THE EFFECTS OF MOISTURE CONTENT AND PARTICLE SIZE DISTRIBUTION ON PREDICTING A CLOGGING EVENT

Abstract

The particle size and moisture content in biomass are important factors that affect particle flowability and clogging formation. Smaller particle size and high moisture content add particle internal friction and lockability that diminish the flowability of the feedstock and elevate the possibility of a clogging event. It is valuable to investigate the influence of these two properties on clogging occurrence as well as associated motor current signals and testify the capability of applying the deep learning model for clogging prediction that proposed in Chapter IV to feedstocks that have varied particle size and moisture content.

First, we chose hammermilled switchgrass with particle size greater than 1 mm as the starting feedstock for this study and selected three levels for moisture content and particle size: 5, 10, and 15 wt. % wet basis for moisture content and particle size fractions between 1 and 0.850 mm (i.e., particles retained on a sieve with mesh 20, particle size fraction 1), 0.850 and 0.425 mm (i.e., particles retained on a sieve with mesh 40, particle size fraction 2), and 0.425 to 0.180 mm (i.e., particles retained on a sieve with mesh 60, particle size fraction 3) for particle size variation. Then a fractional factorial design was employed for dividing switchgrass into several samples with varied moisture content or particle size. Each sample was fed into the bench-scale screw conveyor used in Chapter III, and clogging data was collected in the same manner as conducted in Chapter III. We evaluated the effect of moisture content and particle size fractions on the current signal and observed the following: (i) increasing moisture contents result in an increase in the rate of formation of clogging once started and lower moisture content decreases the starting time of clogging; and (ii) as the mean particle size of a biomass fraction increases, clogging occurs more rapidly. Additionally, we evaluated the performance of a trained and optimized Convolutional Neural Networking (CNN) developed in Chapter IV in predicting the current signals of switchgrass

samples with varying moisture contents and particle size fractions. We achieved R^2 prediction accuracies between 0.926 and 0.963 and 0.834 and 0.963 for materials with varying moisture contents and particle sizes, respectively, without additional training. This outcome suggests that the CNN model is capable of predicting eminent clogging events over the varying moisture content and particle size range evaluated in this study.

5.1 Introduction

Biomass feedstocks vary by species (e.g., herbaceous and woody), geographical locations, climate (e.g., warm and cold climate), and harvesting and collection methods (Oyedeji, Daw, Labbe, Ayers, & Abdoulmoumine, 2017). These factors translate to varying compositions in cellulose, hemicellulose, lignin, and ash (Downing et al., 2011; Ray et al., 2020). The differences in composition have consequences on the flow properties. For example, cellulose and hemicellulose affect the plant cell wall's elastic modulus in the longitudinal and transverse directions, respectively (Bergander & Salmén, 2002; Yildiz, Gezer, & Yildiz, 2006). Hemicellulose affects the crosswise elastic modulus in the wood cell wall (Bergander & Salmén, 2002), and the removal of hemicellulose enhances the tensile strength in lignocellulosic jute fibers (Saha et al., 2010). Lignin has been shown to influence the axial stiffness of poplar microfibril with higher lignin contents and densities, resulting in higher elastic modulus (Özparpucu et al., 2019). Additionally, other properties relevant to flow are altered during preprocessing in lignocellulosic biorefineries. For example, the moisture content is intentionally altered through drying in biorefineries to bring the materials within specifications tolerable for the conversion operations. However, the moisture content in biomass is directly related to the physical and morphological properties of particle solids (Faqih, Mehrotra, Hammond, & Muzzio, 2007; Pachón-Morales et al., 2020). For example, the higher moisture content in biomass increases particle cohesiveness, which negatively affects their

flowing behavior (Faqih et al., 2007; Pachón-Morales et al., 2020). Higher moisture content also produces higher particle density, and cell wall properties of biomass were correlated to water resistance that slows the moisture absorption of the biomass (Bergander & Salmén, 2002; Ewanick & Bura, 2011; Mani, Tabil, & Sokhansanj, 2006). Size reduction is typically performed to modify the morphological properties of biomass by decreasing the particle size and increasing its specific surface area, which improves heat and mass transfer as well as chemical reactivity (Tripathi, Arya, & Ciolkosz, 2021). Changes in morphological properties such as size, shape, and roughness are known to influence flow significantly. For example, smaller particles have inferior flowability than larger particles due to increased particle-particle surface area that causes rising in surface interactions, cohesive forces, and internal friction between particles (Juliano & Barbosa-Cánovas, 2010), the irregular or elongated shapes of biomass particles after hammermilling show poorer flowability compared to spherical particles due to higher degrees of mechanical interlocking and hence more friction during conveyance (Hou & Sun, 2008; Mattsson & Kofman, 2002), and the particle surface roughness also impacts the particle interaction to each other and housing inner wall, which means higher roughness also leads to higher friction and interlocking with the consequence of disturbing feeding and flowability (Dai, Cui, & Grace, 2012).

In this objective, we examine the effect of varying particle size distribution and moisture content on the current signal following the approach used in Chapter III. These properties have been shown to affect clogging in screw conveyors (Miao, Grift, Hansen, & Ting, 2014). Additionally, we evaluate the performance of our Convolutional Neural Networking (CNN) deep learning (DL) prediction model developed in Chapter IV in predicting a clogging event. We use the CNN model pretrained and optimized in Chapter IV to predict new data generated in this chapter on switchgrass with varying moisture content and particle size distribution. The goal of

the study in this chapter is to evaluate the robustness and ability of the CNN model to predict clogging events on biomass materials with varying moisture and particle distribution properties.

5.2 Materials and Methods

5.2.1 Material Preparation and Characterization

Raw switchgrass (*Panicum Virgatum* L.) was hammermilled and size reduced to less than 1mm and used as a starter batch. The testing materials with variable particle size was generated as described next. Samples were collected from the starter batch and sieved into three fractions using sieves with 20, 40, and 60 mesh openings (Hames et al., 2008). The first fraction consisted of particles retained on the sieve with mesh opening 20 and included material with sizes between 1 and 0.850 mm. The first fraction is denoted PSF(+1), where PSF stands for Particle Size Fraction and +1 represents the “high” particle size level. The second fraction consisted of particles that passed through the previous sieve with a 20 mesh opening but were retained on sieve with a 40 mesh opening. The second fraction included material with sizes between 0.850 and 0.425 mm and is denoted PSF(0) henceforth, where 0 represents the “middle” particle size level. The third and last fraction consisted of particles that passed through the previous sieve with a 40 mesh opening but were retained on a sieve with a 60 mesh opening. The third fraction included material with sizes between 0.425 and 0.180 mm and is denoted PSF(-1) henceforth, where -1 represents the “low” particle size level. Each sieved fraction is further characterized by particle size image analysis using a Microtrac analyzer (PARTAN 3D) to determine the mean particle diameter, expressed in millimeters.

The switchgrass starter batch had a moisture content of around 10 wt. %, wet basis. Therefore, we used a wetting and drying procedure to generate switchgrass samples with varying moisture contents, as described next. Two samples were collected from the starter batch and were

submerged in deionized water for 48 hours in a 5 l borosilicate glass bottle (Ewanick & Bura, 2011). Each soaked sample was then filtered with a polypropylene Büchner funnel with a 42.5 mm plate diameter to remove as much excess water as possible. The filtered samples were placed on aluminum foil sheets and air-dried under a laboratory fume hood over 48 hours. At 24, 36, and 48h, approximately 1g of each sample was collected and transferred to 2.5 cm porcelain crucibles for moisture content analysis following American Society for Testing and Materials (ASTM) standards, ASTM E871-82 (Özsin & Pütün, 2017). During moisture content analysis, the remaining materials of each fraction were stored in sealed plastic bags at room temperature to prevent moisture loss, and the air-drying process was resumed after each moisture analysis test was completed. After completing all drying experiments and moisture content analyses for the samples collected at the three timestamps (i.e., 24, 36, and 48h), drying curves were produced using the experimental data. These drying curves were then used to determine the drying times required to generate test samples with 5 and 15 wt. %, wet basis moisture content for each fraction. The soaking and drying experiments were then repeated to generate two batches denoted MC(+1) and MC(-1), where MC stands Moisture Content, +1 represents the "high" moisture content level, and -1 represents the "low" moisture content level. The MC(0) batch with the "middle" moisture content level, i.e., 10 wt. % wet basis, was generated by collecting a representative sample of the starter batch, which had an approximate moisture content of 10 wt. %, wet basis as mentioned earlier. In total, five switchgrass samples with three particle size fractions and three moisture contents were generated. Figure C-1 in Appendix C shows the different levels of switchgrass for testing purposes.

5.2.2 Experimental Setup, Data Collection, and Clogging Analysis

The experimental setup is the same as in Chapter III. Similarly, the data collection and analysis steps outlined in Chapters III and IV will be followed in this chapter. Each sample generated following the procedure described in the previous sections is fed into the bench-scale screw conveyor used in Chapter III following the identical methodology described earlier to simulate clogging occurrence and extract current and vibration data. Then, all datasets are processed and analyzed following the procedure used in Chapter IV for data transformation and interpretation.

5.2.3. Deep Learning Model Evaluation and Clogging Prediction

The deep learning model used in this chapter is the optimized CNN model developed in Chapter IV. Although the GRU model produced slightly higher labeling accuracy, the CNN model showed a higher R^2 score in predicting the current signals compared to GRU. Therefore, we selected the CNN model in this study. Similar procedures defined in Chapter IV are used in this chapter for testing the performance of the CNN model. It is noteworthy to point out that the CNN model was intentionally not re-trained in this study to evaluate its predictive robustness on data that vary in moisture content and particle size properties from its original training data. The ability of the pretrained CNN's model to accurately label the data points were evaluated using the feature map following the same approach used in Chapter IV. Similarly, the CNN model's Mean Squared Error (MSE) was calculated as a loss function as described in Chapter IV, Section 4.3.3.2. Finally, the effects of moisture content at three levels (MC(-1), MC(0), and MC(+1)) and the particle size fraction at three levels (PSF(-1), PSF(0), and PSF(+1)) on the CNN clogging prediction accuracies were analyzed using the coefficient of determination (R^2) using only the current signal.

5.3. Results and Discussions

5.3.1. Material Preparation and Characterization

Based on the property variation, proximate analysis is performed on each biomass sample to quantify the moisture, ash, volatile, and fixed carbon contents for all the materials, as shown in Table 5-1. Each analysis was performed in triplicate. Although we targeted 5, 10, and 15 wt. % moisture contents, we achieved experimental moisture contents slightly different from our targeted values as shown in Table 5-1. The experimental moisture content values are 6.57, 10.86, and 16.68 wt. %, wet basis. The deviation from our targeted values was expected based on our moisture content alternation procedure because it is difficult to dry each material to a specific moisture content without dynamically measuring the moisture content during the experiments. Nonetheless, the experimental moisture content values were close to our original experimental plan, and the materials were therefore used in the rest of the study.

Figure 5-1 shows the particle size distribution of the three material fractions generated for this study. The shape of the particle size distribution of the fractions was similar. However, the mean size of particles in PSF(+1), PSF(0), and PSF(-1) were 1.239 mm, 0.580, and 0.379 mm. For PSF (+1), the targeted particle size range was 1 – 0.850 mm, which is less than what we obtained in experiments. This phenomenon is caused by the natural non-spherical shape of the switchgrass particles that is usually needle-like. The particles have a low width/length ration with a mean value of 0.342 and a standard deviation of 0.022, which allows the particles to pass through the 1 mm screen on the narrower side yet the particle size is larger than 1 mm.

5.3.2. Clogging Analysis

Switchgrass samples of varying moisture contents and particle sizes are used for conveyance status

Table 5-1. Proximate analysis of switchgrass at various properties.

	Mean (SD)		
Wt. %, dry basis	**Low (-1)**	**Middle (0)**	**High (+1)**
Material with varying moisture content			
Moisture[a]	6.57 (0.18)	10.86 (0.33)	16.68 (0.22)
Ash	1.04 (0.06)	0.79 (0.14)	0.92 (0.04)
Volatile Matter	85.21 (0.49)	88.56 (0.22)	86.62 (0.29)
Fixed Carbon	12.76 (0.42)	10.27 (0.34)	13.16 (0.19)
Material with varying particle size fraction			
Moisture[a]	10.86 (0.33)	10.86 (0.33)	10.86 (0.33)
Ash	1.47 (0.019)	0.79 (0.14)	0.52 (0.04)
Volatile Matter	88.38 (0.46)	88.56 (0.22)	86.73 (0.12)
Fixed Carbon	10.16 (0.19)	10.27 (0.34)	11.75 (0.26)

SD stands for standard deviation of three replicates per sample. [a]Moisture content is reported on a wet basis.

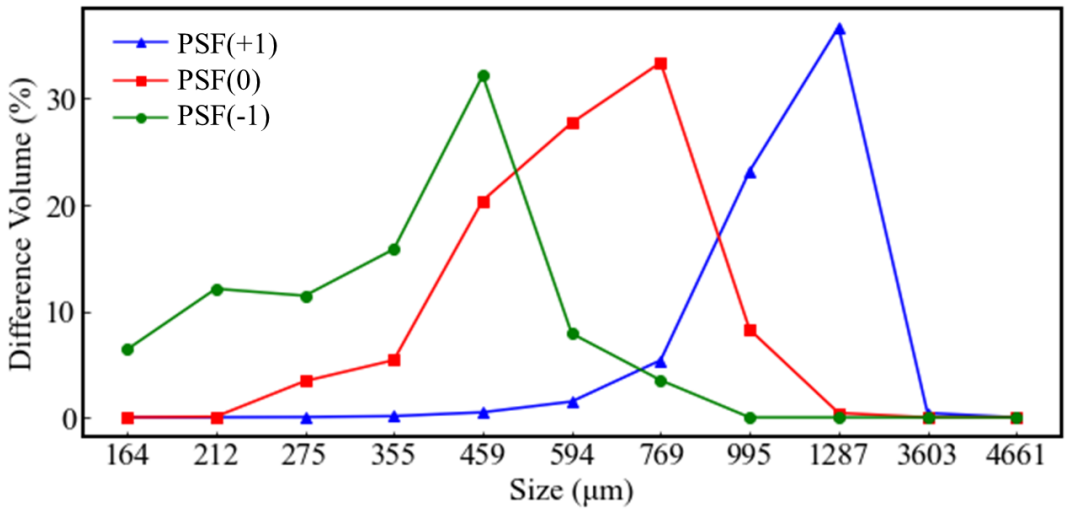

Figure 5-1. Particle size distribution of the switchgrass particle fraction 1 which includes material with sizes between 1 and 0.850 mm (PSF(+1)), particle fraction 2 which includes material with sizes between 0.850 and 0.425 mm (PSF(0)), and particle fraction 3 which includes material with sizes between 0.425 and 0.180 mm (PSF(-1). All fractions have the same mean moisture content of 10.86 wt. %, wet basis.

runs with 20 replications for each material following the same methodology used in Chapter III. However, in this chapter, only the current signal was used based on our findings and conclusions from Chapters III and IV, which showed that the current signal alone is sufficient for our subsequent analyses. Figure 5-2 shows the mean current signals of the particle size levels on the left side of the figure, whereas the right side of the figure shows the moisture content levels. In the figure, we observed no obvious changes with varying particle size for the raw current signal during normal operation and clogging events. However, when varying the moisture content in switchgrass materials, current signals have noticeable differences in the signal-increasing region. As the moisture content increased from the low to the high levels, we observed a steeper slope in the region where the current signals increase in Figure 5-2. The steepness of the slope is more pronounced and more easily discerned visually with the high moisture content level (Figure 5-2, MC (+)). The relationship between the steepness of the slope and increasing moisture content is also observed in Figure 5-3, where dmA/dt was the lowest and highest at the low and high moisture content levels, respectively. Figure 5-3 shows the first derivative transformation using the same datasets as in Figure 5-2 and the data transformation procedure discussed in Chapter III. Figure 5-3 provides better visualization of the signal increasing region, which represents the clogging event under development. Our observation on the relationship between the steepness of the current slope and increasing moisture contents suggests that as moisture content increases, clogging occurs more rapidly. This finding is consistent with expectation since higher moisture content in biomass has been linked to higher particle cohesiveness, which negatively affects the flow behavior of this material (Faqih et al., 2007; Pachón-Morales et al., 2020). The start of the current signal increase is indicative of when clogging begins, as discussed in Chapter III. The start time or onset of clogging appears to also be affected by moisture content, with high and middle moisture content

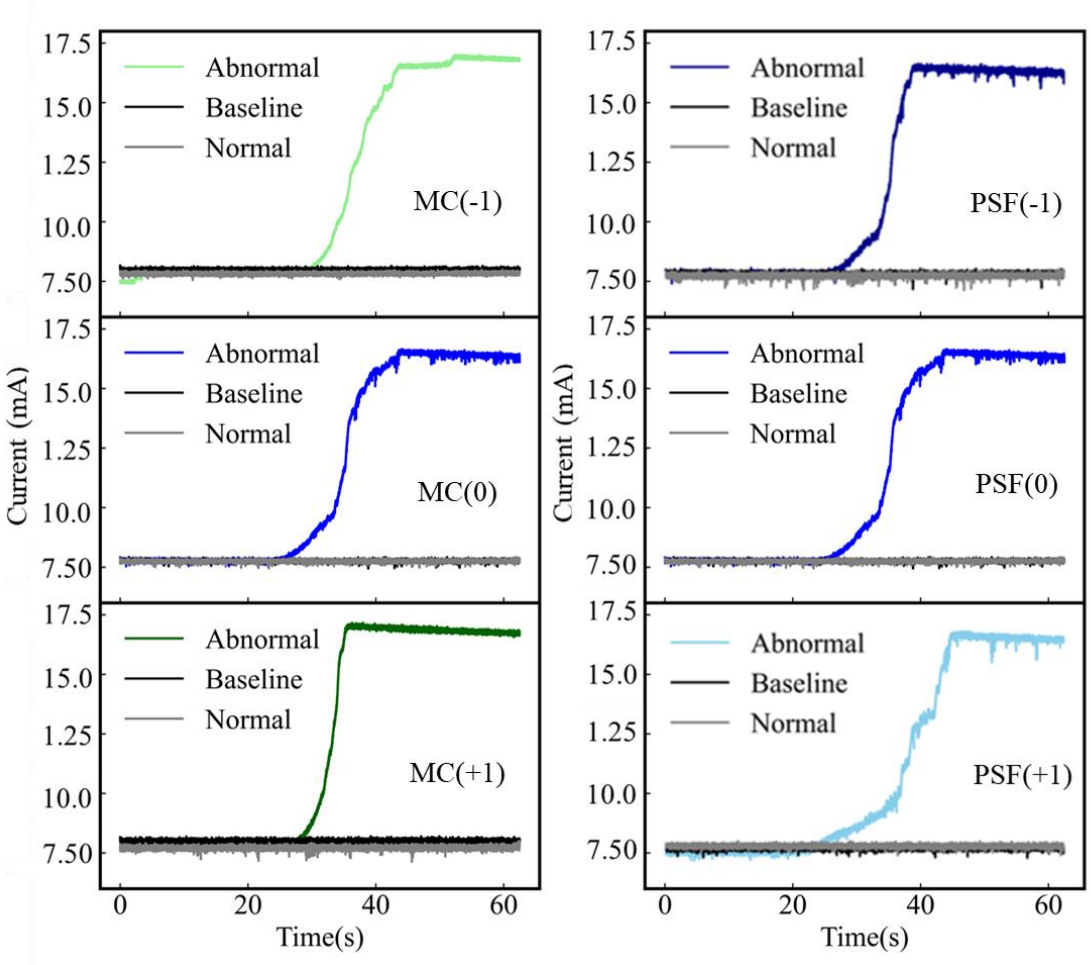

Figure 5-2. Raw current signal with three levels of moisture content (MC(-1) = 6.47 wt. %, wet basis, MC(0) = 10.86 wt. % wet basis, MC(+1) = 16.68 wt. % wet basis from top to bottom in the left column) and particle size (PSF(-1) = particle size fraction with mean of 0.379 mm, PSF(0) = particle size fraction with mean of 0.580 mm, and PSF(+) = particle size fraction with mean of 0.939 mm from left to right).

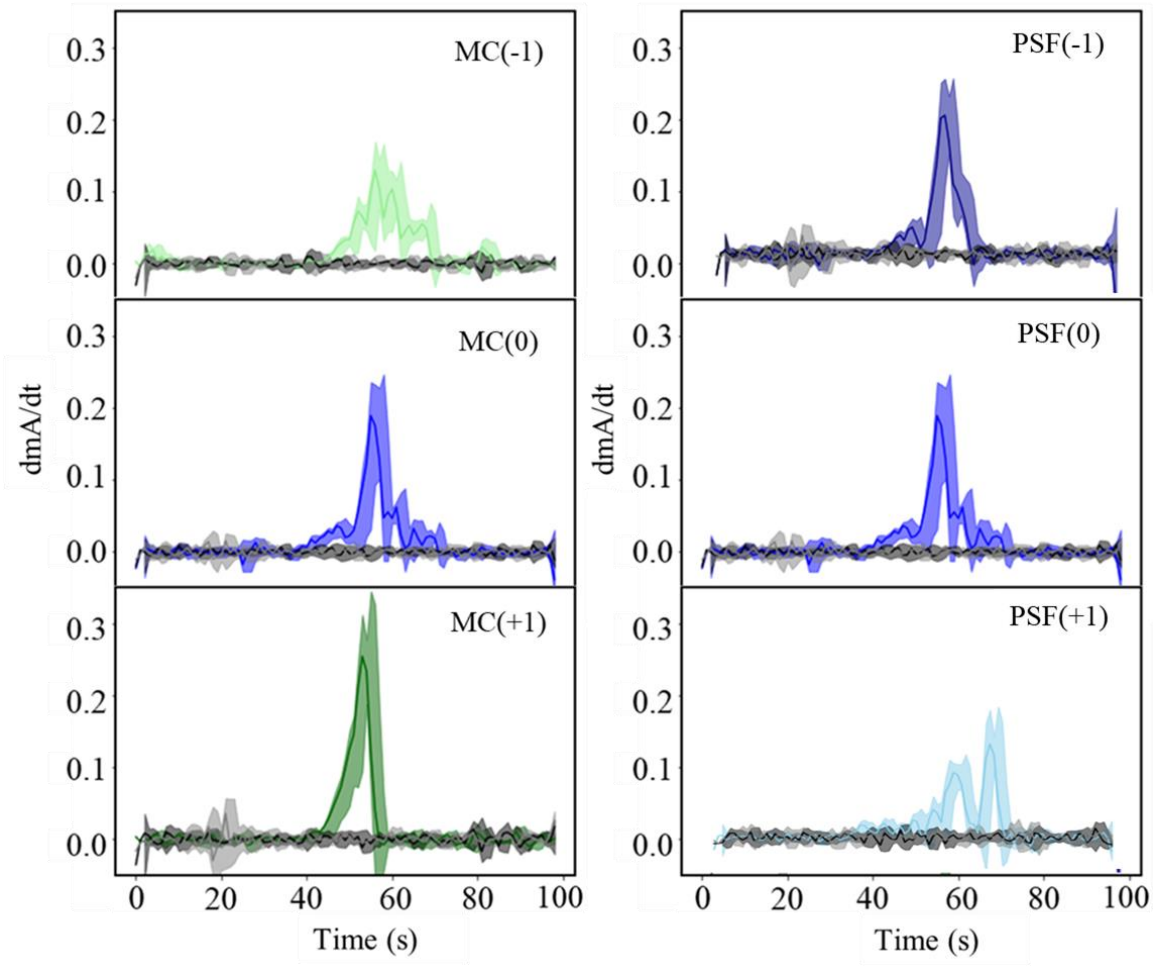

Figure 5-3. First derivative transformation of the current signal of materials with varying moisture content (left side) at three levels (MC(-1) = 6.47 wt. %, wet basis, MC(0) = 10.86 wt. % wet basis, MC(+1) = 16.68 wt. % wet basis from top to bottom) and varying particle size fractions (right side) with three levels (FSP(-1) = 0.379 mm, PSF(0) = 0.580 mm, and PSF(+1)= 0.839 mm from top to bottom).

levels showing a similar onset around t = 22.5s while the low moisture content level had an onset around t = 25s. This observation suggests that clogging will start sooner as moisture content increases when a clogging event is likely to occur.

Samples with varying particle sizes exhibited different behaviors at different levels. As the mean particle size decreased, the steepness of the slope increased in the region where the current signal increased. This observation suggests that as the mean particle size of a biomass particulate assembly becomes smaller, clogging occurs more rapidly. However, we did not observe obvious differences in the onset of clogging between the three particle size fractions.

5.3.4. Model Testing and Clogging Prediction

Figure 5-4 shows the 2D feature map using the current signal for the CNN model. We assigned 12,000 total observations with labeling information according to the first derivative transformation method and the two criteria defined in Chapter III to find the precise data point that separates normal and clogging data regions. The two criteria are: (1) a threshold first-derivative value 0.05 mA/s and -0.02 m/s^2 for the current and vibration signals, respectively (criteria #1); and (2) 90% of signal data points maintaining the selected threshold values over a 5 s window (criteria #2). This labeling information is added to the original input dataset as associated information for models to output predicted labeling information based on assigned labels.

Therefore, the data points in Figure 5-4 with different colors represent the current signals and their predicted labels assigned internally by the CNN model. Generally, the labeling technique is useful to better visualize the model prediction on each status (Bianchini, Maggini, Sarti, & Scarselli, 2005), and the predicted labels can be compared with the original labels to assess the model's labeling performance by calculating the percentage of correctly predicted labels (Zhang, Liu, Wei, & Zhang, 2021).

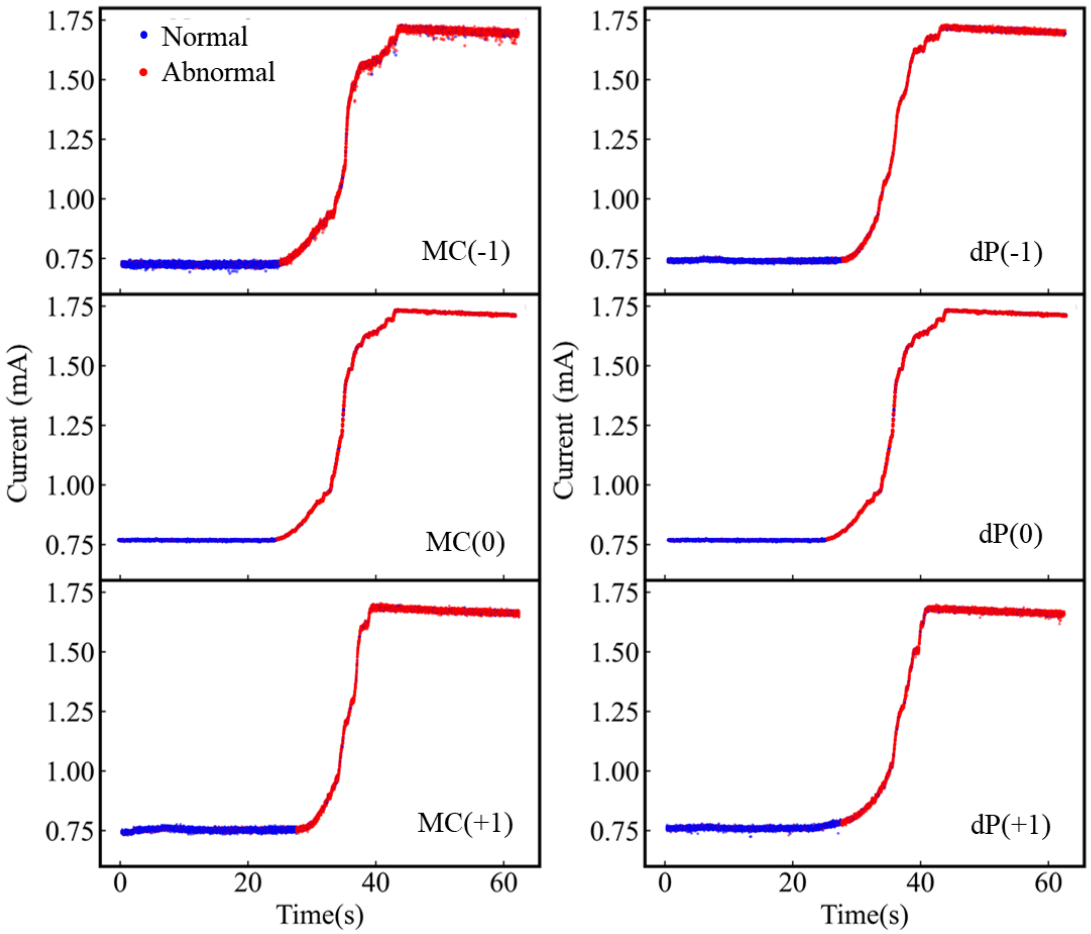

Figure 5-4. Feature map of the predicted labels of the current signal of materials with varying moisture content (left side) at three levels (MC(-1) = 6.47 wt. %, wet basis, MC(0) = 10.86 wt. % wet basis, MC(+1) = 16.68 wt. % wet basis from top to bottom) and varying particle size fractions (right side) with three levels (FSP(-1) = 0.379 mm, PSF(0) = 0.580 mm, and PSF(+1)= 0.839 mm from top to bottom).

Table 5-2 shows the percentage accuracy for such classification using the predicted labels and original labels assigned to the data points. The highest and lowest labeling accuracies are 80.51 and 76.44 % for all materials. The highest labeling accuracies were recorded for the middle levels, i.e., MC(0) and PSF(0). The lower labeling accuracies at MC(+1) and MC(-1) and PSF(+1) and PSF(-1) suggest performance decrease when using the previously trained CNN model. However, the lower labeling accuracies at MC(+1), MC(-1), PSF(+1), and PSF(-1) are not unexpected because the CNN model was trained datasets in Chap IV with similar characteristics as MC(0) and PSF(0) for moisture content and particle size fractions. Therefore, the lower labeling accuracies at MC(+1), MC(-1), PSF(+1), and PSF(-1) could be interpreted as the CNN model performing less well on datasets not included in its training.

Figure 5-5 shows the predicted current signals of switchgrass samples with varying moisture contents and particle sizes. We observe the previously trained CNN model from Chapter IV performed well for all materials with the highest and lowest R^2 values of 0.963 and 0.834. The highest R^2 values were recorded for the middle levels, i.e., MC(0) and PSF(0). The lower predictions at MC(+1) and MC(-1) and PSF(+1) and PSF(-1) indicate a performance loss when using the previously trained CNN model. Since the training datasets in Chap IV were collected on materials with similar characteristics as MC(0) and PSF(0), the lower R^2 predictions could be interpreted as the CNN model performing less well on datasets not included in its training. The prediction R^2s of 0.942 and 0.926 on MC(-1) and MC(+1), respectively, and 0.834 and 0.937 on PSF(-1) and PSF(+1), respectively, are notable. The low moisture content level's current signal fluctuated more than the middle and the high moisture levels. Moreover, the onset of clogging occurred at different times. The material with high moisture content level, i.e., (MC+1), had the earliest onset of clogging, followed by the materials with the middle and low moisture content

Table 5-2. Percentage accuracy of the clogging prediction using trained CNN model.

Factors	**Mean (SD)**		
Levels	*Low (-1)*	*Middle (0)*	*High (+1)*
Moisture content	76.44(±2.06)	80.51(±1.42)	78.26(±1.17)
Particle size fractions	77.92(±1.56)	80.51(±1.42)	78.48(±1.41)

SD stands for standard deviation

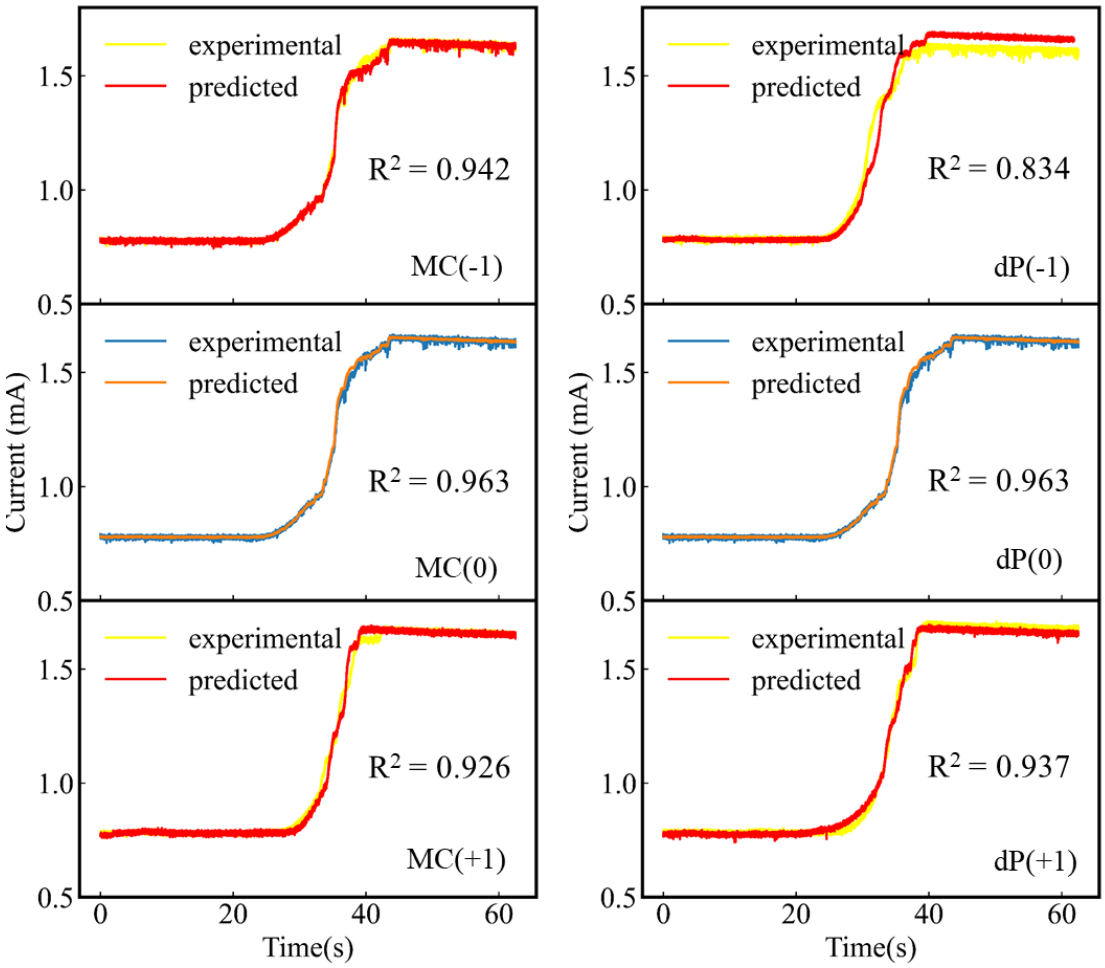

Figure 5-5. The CNN trained model's prediction of the current signal on materials with varying moisture content (left side) at three levels (MC(-1) = 6.47 wt. %, wet basis, MC(0) = 10.86 wt. % wet basis, MC(+1) = 16.68 wt. % wet basis from top to bottom) and varying particle size fractions (right side) with three levels (FSP(-1) = 0.379 mm, PSF(0) = 0.580 mm, and PSF(+1)= 0.839 mm from top to bottom).

levels, respectively. This observation suggests that a clogging event tends to initiate faster when switchgrass samples have a higher moisture content. Additionally, when a clogging event is starting to form, i.e., an increase in current caused by increased resistance to the motor shaft, high moisture material tends to cause a more steady and firm clogging event until the motor fully stops and the current reaches its peak value. Furthermore, the predicted signal shows consistent predictability regardless of property variation. This indicates a clogging event can be well predicted using the selected deep learning algorithm and proposed methodology over a variety of switchgrass properties.

5.4. Conclusions

This chapter investigates the effect of moisture content and particle size on clogging events and the performance of a pretrained CNN for predicting the current signals during the clogging events in a biomass screw conveyor. We evaluated the effect of moisture content and particle size fractions on the current signal and observed the following: (i) increasing moisture contents result in increases in the rate of formation of clogging once started and lower moisture content decreases the starting time of clogging; and (ii) as the mean particle size of a biomass fraction decreases, clogging occurs more rapidly. Additionally, we evaluated the ability of a CNN model to predict the current signal for materials with varying moisture contents and particle sizes and achieved R^2 prediction accuracies between 0.926 and 0.963 and 0.834 and 0.963 for materials with varying moisture contents and particle sizes, respectively. This outcome suggests that the CNN model can predict eminent clogging events over the varying moisture content and particle size range evaluated in this study.

References

Bergander, A., & Salmén, L. (2002). Cell wall properties and their effects on the mechanical properties of fibers. *Journal of materials science, 37*(1), 151-156.

Bianchini, M., Maggini, M., Sarti, L., & Scarselli, F. (2005). Recursive neural networks for processing graphs with labelled edges: Theory and applications. *Neural networks, 18*(8), 1040-1050.

Dai, J., Cui, H., & Grace, J. R. (2012). Biomass feeding for thermochemical reactors. *Progress in Energy and Combustion Science, 38*(5), 716-736.

Downing, M., Eaton, L. M., Graham, R. L., Langholtz, M. H., Perlack, R. D., Turhollow Jr, A. F., . . . Brandt, C. C. (2011). *US billion-ton update: Biomass supply for a bioenergy and bioproducts industry*. Retrieved from

Ewanick, S., & Bura, R. (2011). The effect of biomass moisture content on bioethanol yields from steam pretreated switchgrass and sugarcane bagasse. *Bioresource Technology, 102*(3), 2651-2658. doi:https://doi.org/10.1016/j.biortech.2010.10.117

Faqih, A. M. N., Mehrotra, A., Hammond, S. V., & Muzzio, F. J. (2007). Effect of moisture and magnesium stearate concentration on flow properties of cohesive granular materials. *International Journal of Pharmaceutics, 336*(2), 338-345. doi:https://doi.org/10.1016/j.ijpharm.2006.12.024

Hames, B., Ruiz, R., Scarlata, C., Sluiter, A., Sluiter, J., & Templeton, D. (2008). Preparation of samples for compositional analysis. *Laboratory Analytical Procedure (LAP), 1617*, 65-71.

Hou, H., & Sun, C. C. (2008). Quantifying effects of particulate properties on powder flow properties using a ring shear tester. *Journal of pharmaceutical sciences, 97*(9), 4030-4039.

Juliano, P., & Barbosa-Cánovas, G. V. (2010). Food powders flowability characterization: theory, methods, and applications. *Annual review of food science and technology, 1*, 211-239.

Mani, S., Tabil, L. G., & Sokhansanj, S. (2006). Effects of compressive force, particle size and moisture content on mechanical properties of biomass pellets from grasses. *Biomass and Bioenergy, 30*(7), 648-654. doi:https://doi.org/10.1016/j.biombioe.2005.01.004

Mattsson, J. E., & Kofman, P. D. (2002). Method and apparatus for measuring the tendency of solid biofuels to bridge over openings. *Biomass and Bioenergy, 22*(3), 179-185.

Miao, Z., Grift, T. E., Hansen, A. C., & Ting, K. C. (2014). Flow performance of ground biomass in a commercial auger. *Powder Technology, 267*, 354-361.

Oyedeji, O., Daw, C. S., Labbe, N., Ayers, P., & Abdoulmoumine, N. (2017). Kinetics of the release of elemental precursors of syngas and syngas contaminants during devolatilization of switchgrass. *Bioresource Technology, 244*, 525-533. doi:https://doi.org/10.1016/j.biortech.2017.07.167

Özparpucu, M., Gierlinger, N., Cesarino, I., Burgert, I., Boerjan, W., & Rüggeberg, M. (2019). Significant influence of lignin on axial elastic modulus of poplar wood at low microfibril angles under wet conditions. *Journal of experimental botany, 70*(15), 4039-4047.

Özsin, G., & Pütün, A. E. (2017). Insights into pyrolysis and co-pyrolysis of biomass and polystyrene: Thermochemical behaviors, kinetics and evolved gas analysis. *Energy Conversion and Management, 149*, 675-685.

Pachón-Morales, J., Perré, P., Casalinho, J., Do, H., Schott, D., Puel, F., & Colin, J. (2020). Potential of DEM for investigation of non-consolidated flow of cohesive and elongated biomass particles. *Advanced Powder Technology, 31*(4), 1500-1515. doi:https://doi.org/10.1016/j.apt.2020.01.023

Ray, A. E., Williams, C. L., Hoover, A. N., Li, C., Sale, K. L., Emerson, R. M., . . . Donohoe, B. S. (2020). Multiscale Characterization of Lignocellulosic Biomass Variability and Its Implications to Preprocessing and Conversion: a Case Study for Corn Stover. *ACS Sustainable Chemistry & Engineering*, *8*(8), 3218-3230. doi:10.1021/acssuschemeng.9b06763

Saha, P., Manna, S., Chowdhury, S. R., Sen, R., Roy, D., & Adhikari, B. (2010). Enhancement of tensile strength of lignocellulosic jute fibers by alkali-steam treatment. *Bioresource Technology*, *101*(9), 3182-3187.

Tripathi, J., Arya, A., & Ciolkosz, D. (2021). Switchgrass as oil and water-spill sorbent: Effect of particle size, torrefaction, and regeneration methods. *Journal of Environmental Management, 281*, 111908. doi:https://doi.org/10.1016/j.jenvman.2020.111908

Yildiz, S., Gezer, E. D., & Yildiz, U. C. (2006). Mechanical and chemical behavior of spruce wood modified by heat. *Building and Environment*, *41*(12), 1762-1766. doi:https://doi.org/10.1016/j.buildenv.2005.07.017

Zhang, T., Liu, S., Wei, Y., & Zhang, H. (2021). A novel feature adaptive extraction method based on deep learning for bearing fault diagnosis. *Measurement, 185*, 110030. doi:https://doi.org/10.1016/j.measurement.2021.110030

CHAPTER VI

CONCLUSION

6.1 Thesis Conclusion

In this thesis, we studied using deep learning models to predict clogging occurrences during lignocellulosic biomass feeding in screw conveyors using CNN and GRU models and two mechanical signals extracted from the motor, which functions as the power source of the conveyor. The two mechanical signals are current and vibration and extracted using sensors with different data capture frequencies. In Chapter III, the clogging event is monitored and investigated by using vibration and the current measurements, respectively. All of the flowing conditions defined in the study can be diagnosed via both signals analyses. The time-varying motor current and vibration signals are derived, showing that clogging events in screw conveyors can be diagnosed by detecting a series of abnormal current and vibration signal sidebands around the power supply frequency component in the time-frequency domain. Besides, we defined two criteria that successfully recognized the clogging region based on the two signals, which is helpful for predicting a clogging event using deep learning approaches in next chapter. In Chapter IV, we presented a deep learning-based framework for clogging prediction in screw conveyors using CNN and GRU models. Each proposed model consists of the data transformation module, the deep learning algorithmic module, and the optimization module. We validated the performance of each proposed model by clogging simulations in a custom lab-scale screw conveyor for metering different biomass materials. In addition, we provided various scenarios of input datasets into the models to verify the stability and potential of the proposed deep learning models. According to the results, the proposed GRU and CNN models showed similar performances in labeling accuracy that we experimented with, and the GRU model showed lower clogging prediction performance among all input datasets from switchgrass, loblolly pine, and hybrid poplar. Finally, the model optimization results show that by further tuning the model parameters and using the Box-Behnken

design to find local or global optimal parameter combinations, we can potentially improve the accuracy and stability of the model even further. In Chapter V, we investigated the effect of moisture content and particle size on clogging events and the performance of a pretrained CNN for predicting the current signals during the clogging events in a biomass screw conveyor. We evaluated the effect of moisture content and particle size fractions on the current signal and observed the following: (i) increasing moisture contents result in increases in the rate of formation of clogging once started and lower moisture content decreases the starting time of clogging; and (ii) as the mean particle size of a biomass fraction decreases, clogging occurs more rapidly. Additionally, we evaluated the ability of a CNN model to predict the current signal for materials with varying moisture contents and particle sizes and achieved R^2 prediction accuracies between 0.926 and 0.963 and 0.834 and 0.963 for materials with varying moisture contents and particle sizes, respectively. This outcome suggests that the CNN model can predict eminent clogging events over the varying moisture content and particle size range evaluated in this study.

6.2 Future Work

The results of this study provide evidence that a logging event can be predicted using deep learning models. In the future, we want to expand the scope of this study with additional research objectives. First, we plan to investigate the effect of different feedstocks and mechanical properties that influence the flowing behavior on the current and vibration signals. Second, to verify the generalizability of our selected deep learning model, we will expand the input data to include all current data from each feedstock into one input dataset for the model training process and evaluate the performance based on model testing and clogging prediction using randomly selected sub datasets from each feedstock. Third, we realize that the sampling frequency of vibration data in this study is comparably low to current signal sampling frequency. We plan to reperform the

clogging experiments with new vibration sensor that also able to capture high frequency vibration data and analyze the deep learning model performance using high frequency vibration data. Last, a new signal can be introduced to the system to enhance the independence of the inputs and outputs of the deep learning model. For example, infrared imaging technique is valuable to capture the motor temperature maps that related to conveyor flowing condition. Using current or vibration signal as input datasets and temperature as output dataset can eliminate any possible correlation between inputs and outputs when using the same data for both.

VITA

Originally from China, Yang Li grew up in Songyuan, Jilin. After high school, he attended the Tennessee Technological University and received a Bachelor of Science degree in Agricultural Engineering Technology. Before graduating with his undergraduate degree, he already decided to attend graduate school. He chose to attend the University of Tennessee, Knoxville to pursue a master's degree in Biosystems Engineering Technology. His research interest includes predicting a clogging event in a screw conveyor based on deep learning algorithms. After graduation, he will begin his PhD program at the University of Tennessee. He is incredibly grateful for all the support from his friends, colleagues, and mentors as he begins his new program.